Safe Interaction Between Lateral and Longitudinal Adaptive Cruise Control in Autonomous Vehicles

ADEM F. IDRIZ

Master of Science Thesis

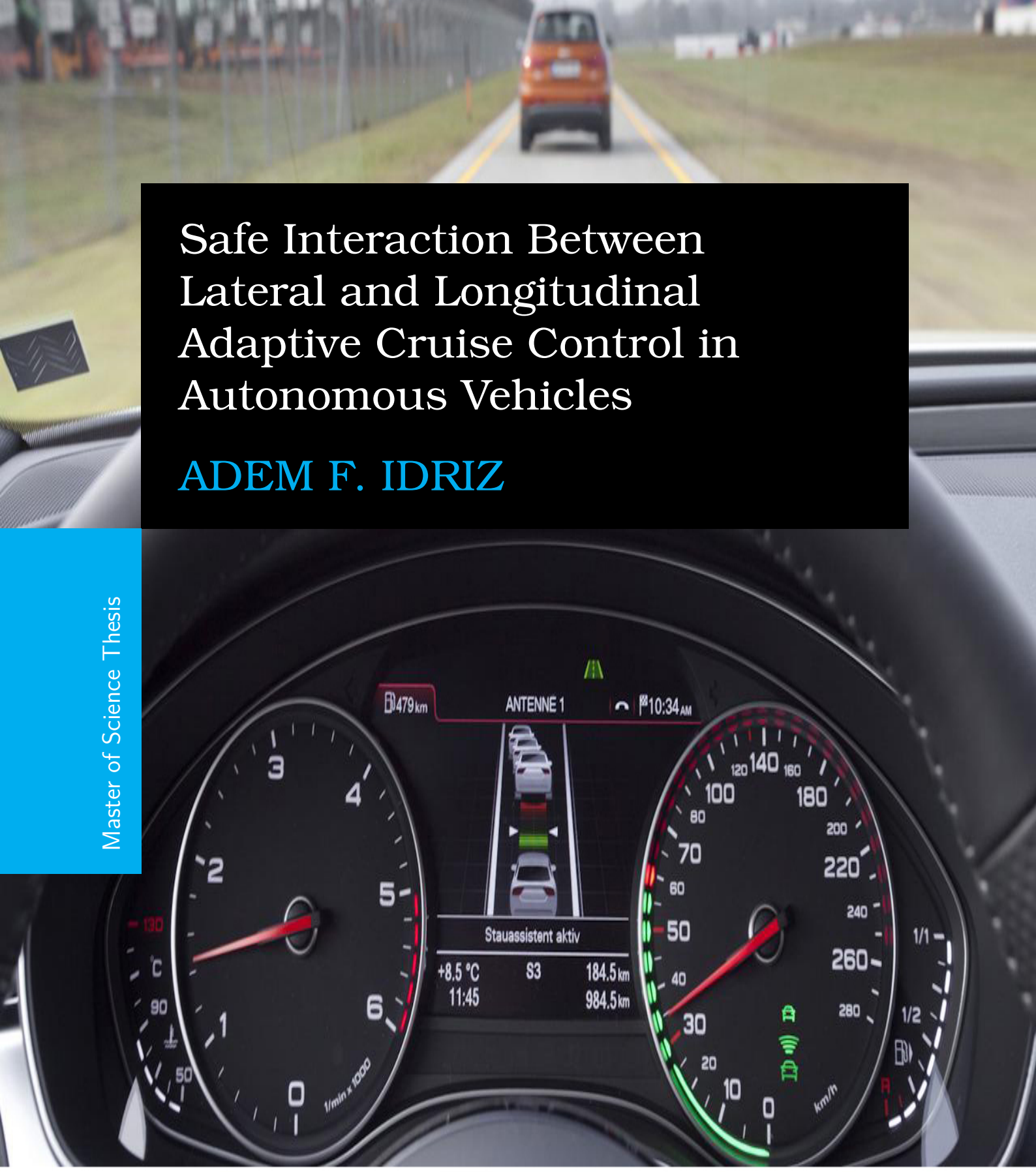

TU Delft Delft University of Technology

Delft Center for Systems and Control

Safe Interaction Between Lateral and Longitudinal Adaptive Cruise Control in Autonomous Vehicles

Master of Science Thesis

For the degree of Master of Science in Systems and Control at Delft University of Technology

ADEM F. IDRIZ

August 18, 2015

Faculty of Mechanical, Maritime and Materials Engineering (3mE) · Delft University of Technology

Delft University of Technology
Department of

The undersigned hereby certify that they have read and recommend to the Faculty of Mechanical, Maritime and Materials Engineering (3mE) for acceptance a thesis entitled

Safe Interaction Between Lateral and Longitudinal Adaptive Cruise Control in Autonomous Vehicles

by

ADEM F. IDRIZ

in partial fulfillment of the requirements for the degree of

Master of Science Systems and Control

Dated: August 18, 2015

Supervisor(s): _____

Reader(s): _____

Abstract

According to the statistics, driver error is the main reason for the road accidents: this has motivated an intensive research on intelligent vehicles equipped with automated driving technology, active safety and driver-assistance systems so as to enhance the safety of drivers, facilitate vehicle controllability and stability, and improve driving comfort.

One of the driver assistant systems currently under development by most automotive manufacturers is the Adaptive Cruise Control (ACC) system. The ACC system, which is an extension of the classic Cruise Control (CC) system, controls both speed and distance to preceding vehicles: the aim of ACC is not only provide the drivers with comfort and safety during driving, but also increase the capacity of roads and reduce fuel consumption.

One of the major drawbacks of ACC system solutions commercially available in the automotive industry is the limited performance in cornering situations, where the road presents current/future curvatures. In particular, the interaction between longitudinal and lateral controller systems has not been deeply studied. Moreover, in order to obtain both lateral stability and safe clearance to avoid rear end collisions in critical driving situations, coordinated control of the actuators is necessary without avoiding conflicts caused by the coupling of vehicle dynamics. Summarizing, an implementation of an integrated vehicle dynamics control is far from definiteness.

A part of this thesis concerns the parametric vehicle model which is based on a set of vehicle parameters (mass, maximum torque etc.) with realistic nonlinearities in longitudinal and lateral dynamics of vehicle. The longitudinal and lateral control systems are designed to fulfill the objectives and requirements. Since driver acceptance of the proposed control systems is crucial, practical constraints are determined via experimental studies on human driving. Furthermore, in order to allow the driver to personalize the control system in a desired manner, parameterization of control system is provided.

An appropriate control structure is adopted to create synergies and safe interaction between longitudinal and lateral controllers, taking into account the previous mentioned aspects, compromising between comfort and safety for various driving situations, in order to obtain both lateral stability and safe clearance of advanced autonomous driving vehicle. This MSc thesis mainly focuses on the design of an Integrated Vehicle Dynamics Control (IVDC) strategy for

Adaptive Cruise Control with auto steering application intended to decrease driver's workload. In severe driving situations, the proposed control strategy is designed based on indexes for driving situations to optimally coordinate the brake and steering actuators to avoid rear-end collision danger and unstable lateral motion of the vehicle.

Afterwards, the implementation of the designed controllers has been carried out. Simulations are conducted in Matlab/Simulink by using a set of traffic scenarios which are likely to occur in reality. From simulation results, the performances of designed controllers are evaluated with respect to determined performance specifications. Simulation results have shown that the proposed integrated controller satisfies the performance in terms of autonomous driving, path tracking and collision avoidance for a complete envelope of working conditions.

Table of Contents

List of Figures

List of Tables

Acknowledgements

I am delighted to be involved in such a cutting edge and challenging topic for my MSc thesis. I would like to express my gratitude to many people that have helped to make this thesis possible. Firstly, I would like thank to Dimitrios Kotiadis for pointing me towards this prospective project in Adaptive Cruise Control. Especially I would like to thank my supervisor Dr.ir. Simone Baldi for his invaluable guidance and direction during the developmental process of my thesis. I am also appreciated by assistance of Dr. Barys Shyrokau in vehicle dynamics section. Thanks to their assistance, some moments became easier to deal with and overcome.

Eventually, I would like to thank my parents for their love and confidence in me. They have been a tremendous support to me throughout my studies and for that I will always be eternally grateful. I sincerely believe that this work would not exist without their guidance and support.

Delft, University of Technology ADEM F. IDRIZ
August 18, 2015

"Imagination is everything. It is the preview of life's coming attractions."
— *Albert Einstein*

Chapter 1

Introduction

The automotive community is achieving substantial progress in the development of automated vehicles. Many definitions of automated driving are currently in use (e.g., autopilot, autonomous vehicles, automatic vehicles, etc.). In this context, we distinguish driver assistance (i.e., ADAS) from partial, high and full automation. In Figure 1-1 these different concepts are explained along with respect to complexity of technology and time. The different stages are overlapping in time and manually driven vehicles will be present in mixed traffic with automated vehicles with varying levels of automation. This is referred to as the penetration level, a critical factor in the beneficial introduction of automation.

Currently we find ourselves in the stage of driver assistance as shown in Figure 1-1. Many systems, such as Adaptive Cruise Control (ACC), have already been commercially available. Partial and high automation is a subject of intensive R&D projects. Fully automated experimental vehicles have already been developed in the USA. Other countries have already been using automated vehicles based on dedicated and restricted infrastructures. Although automated driving tests are presently being conducted worldwide, the question of when automation will be available in consumer vehicles still remains unanswered. In order to have automated vehicles drive safely and efficiently on public roads, numerous challenges have to be resolved.

Automated driving can be assumed to offer unique possibilities to improve traffic flow efficiency, traffic safety and reduce greenhouse gas emissions. In this context, the following improvements are envisaged:

- Assuming the current levels of traffic flow, it seems realistic to expect that automated driving may reduce congestion by 50%. We envisage that this improvement follows from better anticipation towards the traffic conditions downstream, thereby reducing the probability of a traffic breakdown, and acceleration of the clearance of congestion by increasing the outflow from a queue.
- Automated driving aims at a 100% reduction of accidents involving vehicles. Via advanced technology, automated vehicles will be able to detect and respond to hazards

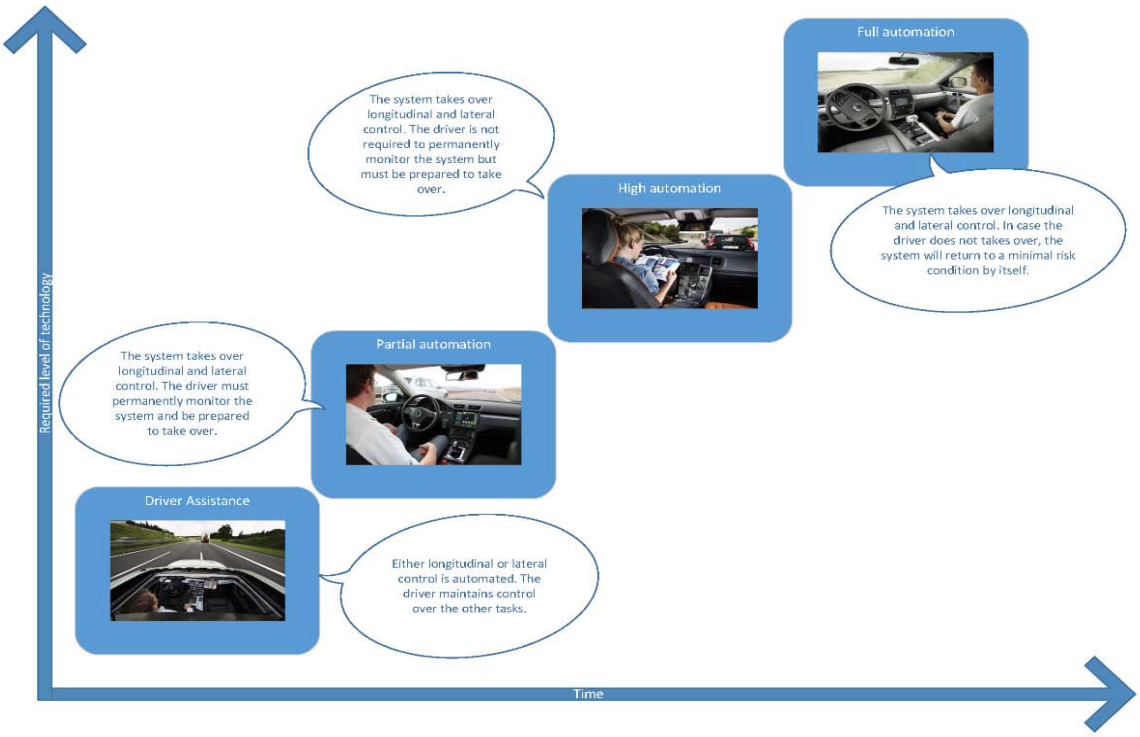

Figure 1-1: A visual representation of the evolution of automated vehicles

and vulnerable road users (i.e. cyclist, pedestrians etc) faster and more adequately than the human driver.

- Automated driving is expected to improve energy efficiency by approximately 20% through efficient and precise speed control. The reduction in congestion also leads to an improvement in the energy efficiency through a reduction in the variation of speed. Finally, platooning with small time headways substantially improves energy efficiency through a reduction in the aerodynamic drag (i.e. trucks etc).
- Besides these benefits to society, automated driving will lead to an improved travel experience, as in fully automated vehicles drivers will have the freedom to spend their time on other activities during a long trip as well [1].

Every year merely in Europe, more than 40 000 casualties and 1.4 million injuries are caused by vehicle-related accidents. Although advances in passive safety, as illustrated in Figure 1-2, have made passenger cars safer than ever; the safety potential of further improvements in passive safety (which reduce fatalities in case of an accident) features is limited. However, active safety (which assist in avoiding an accident) systems offer possibilities for improving traffic safety by assisting the driver in his driving task. In addition, Advanced Driver Assistance System (ADAS) have the potential to significantly reduce the number of road accidents. An ADAS is a vehicle control system that uses environment sensors (e.g. radar, laser, vision) to improve driving comfort and traffic safety by assisting the driver in recognizing and reacting to potentially dangerous traffic situations. Since an ADAS can even autonomously intervene, an ADAS-equipped vehicle is popularly referred to as an 'intelligent vehicle'.

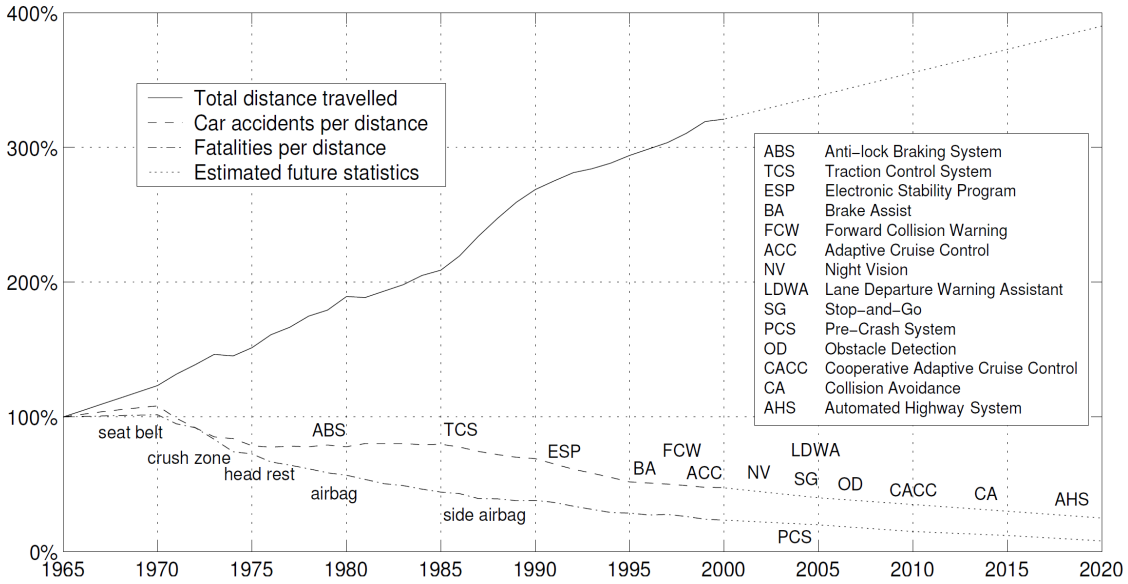

Figure 1-2: Total number of road accidents and fatalities with passive and active safety systems

As explained in more detail in several surveys, the following types of intelligent vehicle systems can be distinguished;

- Driver information systems increase the driver's situation awareness, e.g. advanced route navigation systems
- Driver warning systems actively warn the driver of a potential danger, e.g. lane departure warning, blind spot warning, and forward Collision Warning (CW) systems. This warning then allows the driver to take appropriate corrective actions in order to mitigate or completely avoid the event
- Intervening systems provide active support to the driver, e.g. ACC system. ACC is a comfort system that maintains a set cruise control velocity, unless an environment sensor detects a slower vehicle ahead. The ACC then controls the vehicle to follow the slower vehicle at a safe distance. ACC is intended for speeds above 30 km/h, but is currently being extended to a Stop-and-Go application for automated longitudinal control in low-speed complex environments, such as traffic jams and urban areas.
- Integrated passive and active safety systems. In addition to passive safety systems that are activated during the crash, a pre-crash system can mitigate the crash severity by deploying active and passive safety measures before a collision occurs. Pre-crash safety measures, such as brake assist and seat belt pre-tensioners, have recently been introduced on the market.
- Fully automated systems are the next step beyond driver assistance, and operate without a human driver in the control loop. Automated highway systems, using fully automated passenger cars, are expected to significantly benefit traffic safety and throughput, but are not considered for short-term introduction.

According to several surveys, ADAS can prevent up to 40% of traffic accidents, depending on the type of ADAS and the type of accident scenario. Despite this safety potential, market penetration of ADAS has gone slow. Main challenges in this respect are customer acceptance and understanding of the added value, liability exposure, and regulatory issues. Drivers also expect an ADAS to meet high requirements in terms of (subjective) performance, reliability (low rate of false alarms), and safety (low rate of missed detections). Therefore, the ADAS must be tested for the wide variety of complex traffic situations that the system should be able to recognize and handle [2].

1-1 Adaptive Cruise Control

Adaptive Cruise Control (also called autonomous cruise control or radar cruise control) is an optional cruise control system for road vehicles that automatically adjusts the vehicle speed to maintain a safe distance from vehicles ahead. It makes no use of satellite or roadside infrastructures nor of any cooperative support from other vehicles. Hence control is imposed based on sensor information from on-board sensors only. Current commercial ACC has following modes;

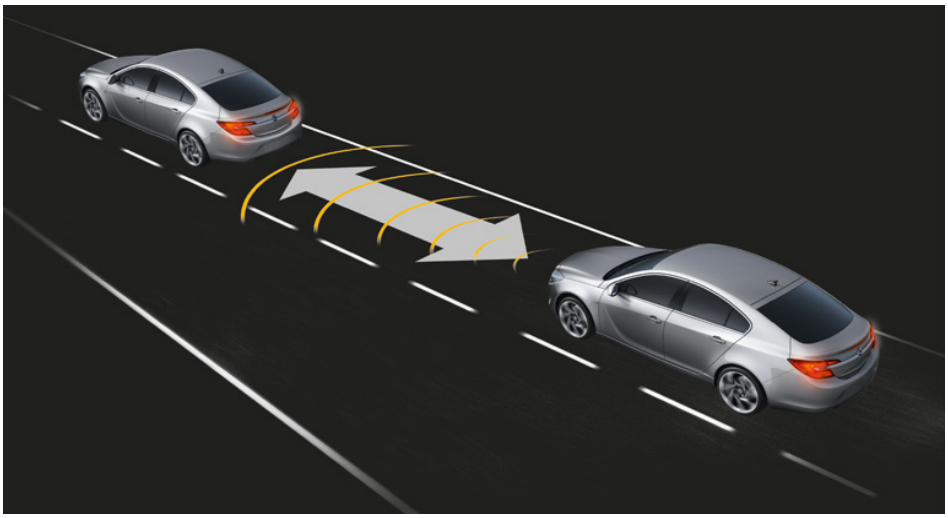

Figure 1-3: Adaptive Cruise Control

Velocity Control (CC) Mode: The system operates in this Cruise Control (CC) mode when the distance between vehicles is greater than the desired distance. Also, the system can enter this mode, if the target vehicle speed becomes higher than the cruising speed which is set by user.

Space Control (ACC) Mode: The system operates in the Adaptive Cruise Control (ACC) mode, when the vehicle approaches the vehicle traveling (slower)in front of it. Then, the distance between vehicles is maintained.

Stop and Go (SG) Mode: This situation occurs when the vehicle has to frequently stop and move, depending on the behavior of other vehicles in the traffic. When the traffic slows down and comes to standstill, the vehicle equipped with ACC needs to slowdown and stop for a while, until the vehicle in front starts moving.

Collision Avoidance (CA) Mode: A Collision Avoidance system is an automobile safety system designed to reduce the severity of an accident. Also known as pre-crash system, forward Collision Warning system or collision mitigating system, it uses radar (all-weather) and sometimes laser and camera (both sensor types are ineffective during bad weather) to detect an imminent crash. Once the detection is done, these systems either provide a warning to the driver when there is an imminent collision or take action autonomously without any driver input (by braking or steering or both). Cars with Collision avoidance are also equipped with adaptive cruise control, and use the same sensors like ACC.

1-2 Problem Statement

The ACC controller detects a target vehicle in different situations and determines when a vehicle ceases to be a target. Note that an ACC-equipped vehicle refers to the host vehicle. The ACC presented in this section uses seven different scenarios and switches the controller between its different modes of operation based on the scenarios listed below and illustrated in Figure 1-4.

These scenarios are the modes of operation of the ACC system. During operation the ACC system switches among these scenarios based on the relative position and speed of the surrounding vehicles.

Scenario 1: Velocity Control (CC)
In the CC scenario, there is no vehicle in front of the host vehicle within the radar sensor range. Thus, the host vehicle is under CC only. Accordingly, the host vehicle travels in CC mode with the cruise speed set by the driver. This scenario ends when the radar on the host vehicle detects a vehicle in front as a target. The ACC controller intervenes and switches from CC to ACC mode in that case.

Scenario 2: Appearance of a Slower Vehicle in Front (ACC+CW/CA)
In this scenario, a slower preceding vehicle is detected by the radar and is chosen as the target vehicle. The host vehicle speed is reduced to that of the preceding vehicle, and the distance between the vehicles is controlled automatically. The following mode is reached when the two vehicles travel at the same speed and the appropriate inter-vehicle distance.

Scenario 3: Target Vehicle Speeds Up (ACC/CC)
In this scenario, while the following mode continues, the target vehicle begins to speed up. The speed of the host vehicle also increases. After the transient period, the host vehicle's speed reaches that of the target vehicle.

Scenario 4: Target Vehicle Slows Down (ACC+CW/CA/SG)
In this scenario, the target vehicle slows down during the following mode. The host vehicle also slows down, decreasing its speed to that of the target vehicle. After the transient period, the host vehicle's speed decreases to that of the target vehicle, and this scenario ends in the following mode.

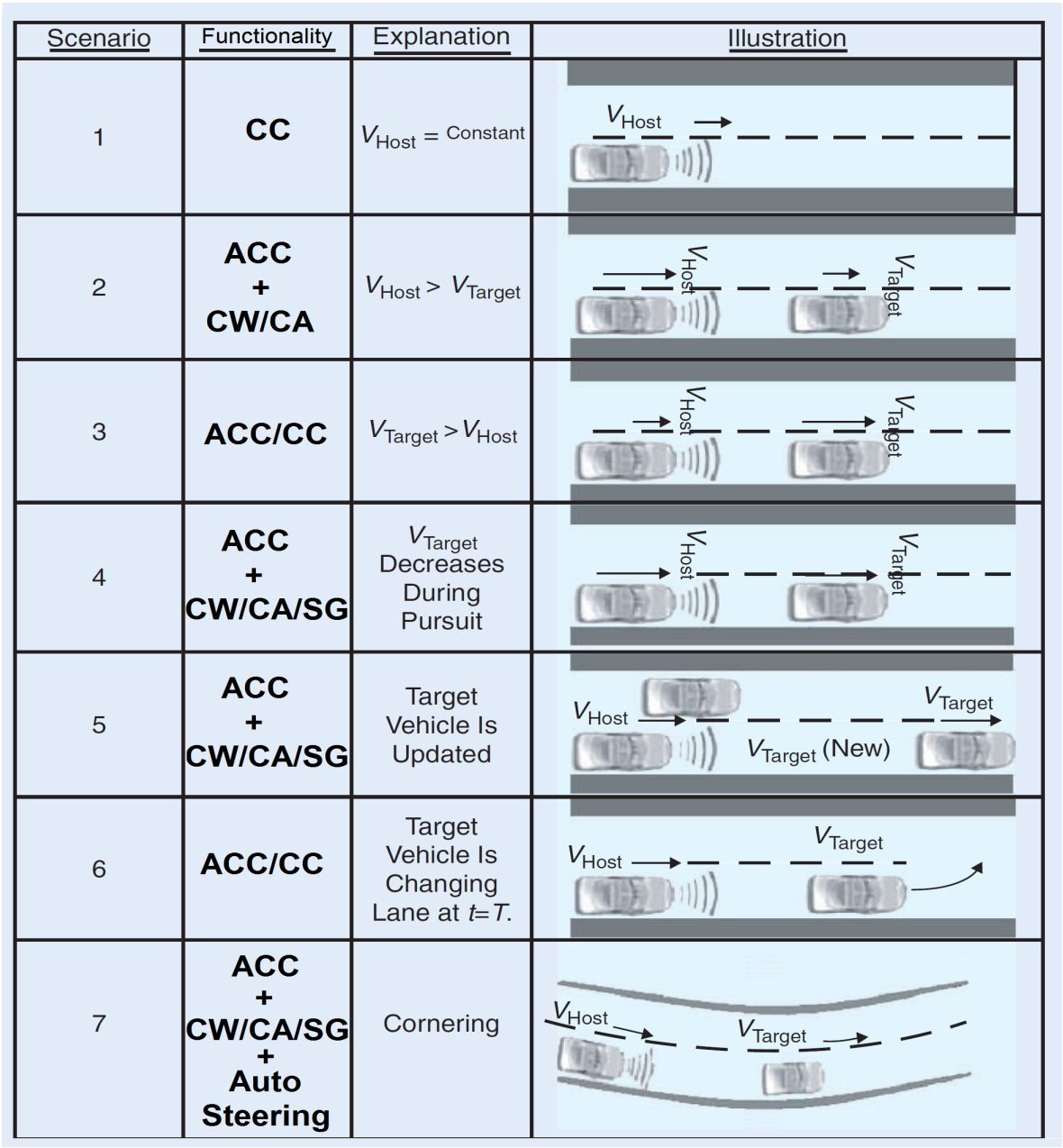

Figure 1-4: ACC Scenarios

Scenario 5: Appearance of a Cutting-In Vehicle (ACC+CW/CA/SG)
In this scenario, during the following mode, a third vehicle suddenly cuts in between the host and current target vehicles. In this situation, the host vehicle chooses the cutting-in vehicle as the new target vehicle. The host vehicle decreases its speed according to the new target vehicle with an appropriate distance, which is controlled automatically. Three vehicle models run in this scenario.

Scenario 6: Target Vehicle Changes Lane (ACC/CC)
In this scenario, while two vehicles cruise in the following mode in the same lane, the target vehicle changes its lane. The host vehicle's radar detects that there is no vehicle in front. After waiting for a set amount of time, the host vehicle changes its speed to the set speed of the CC mode. If the target vehicle returns to its former lane before the host vehicle passes by, the radar of the host vehicle again detects it as the target vehicle and switches from CC mode to Scenario 2 [7].

Scenario 7: Cornering (ACC + CW/CA/SG + Auto Steering)
Cornering is a difficult maneuver for the ACC system. In addition, all emergency situations have to be handled while cornering. First of all, the system must be aware of the fact that a curved part of the road is being approached and distinguished from a cornering target vehicle in front. Today, the trend is to increase the effectiveness of active safety interventions by additional actuator types such as active steering, active suspensions, or active differentials, and also by additional sensor information, such as the increased inclusion of on-board cameras, as well as infrared and other sensor alternatives. All these will be further complemented by GPS information including pre-stored mapping.

The steering control for an autonomous driving vehicle deals with the path tracking problem. In the case of an autonomous vehicle driving along a given path, the main goal of the lateral control is tracking the reference path while maintaining the stability of the vehicle in the center of the desired path using the appropriate control inputs. This constraint can be generalized as the minimization of the vehicle's lateral distance and heading angle error with respect to the desired trajectory.

The research on integrated vehicle dynamics control has become focused and attracted much attention. The co-existence of several control subsystems can cause two main problems. First, the design of software and hardware will become more complicated due to the dramatically increased number of sensors and signal cables. Second, because of the possible function overlapping among these systems, their conflicts of control objectives and actions will inevitably occur. Without coordination, the dynamic performance of these systems could be worse than that of an individual system or even worse than a passive system without any active control. Therefore, the two key problems of integrated vehicle dynamics control to be solved are:

- to avoid the conflicts and interventions among different subsystems;
- to exploit the potentials of each subsystems by communication and coordination among the sub-systems since different system has different action domain.

Although many relevant researches have been published recently, the definition of Integrated Vehicle Dynamics Control (IVDC) is still not very definitive. However, its attribution is obvious, i.e. it needs to coordinate two or more subsystems systematically according to control objectives and actions in terms of both software and hardware, rather than simply put the subsystems altogether. Hence, overall vehicle dynamics performances, in directions of longitudinal and lateral, can be improved [31].

The development of advanced autonomous driving technology requires an efficient combination of complicated state-of-the-art technologies such as those for vision, obstacle detection, sensor fusion, localization and mapping, path generation, path planning, modeling, and lateral and longitudinal control. Among these, the optimized control of the steering input and

longitudinal velocity is one of the most important to ensure the performance and dynamic stability of an autonomous vehicle. Optimized lateral and longitudinal control is especially critical for the roads with curvatures.

1-3 Aims and Objectives

The main aim of this MSc thesis is to create synergies and safe interactions in Integrated Controller in order to obtain both lateral stability and safe clearance of advanced autonomous driving vehicle.

The following objectives can be drawn up to realize the above-mentioned aim:

- The development of a parametric vehicle model which is based on a set of vehicle parameters (mass, maximum torque etc.) with realistic nonlinearities in longitudinal and lateral dynamics of vehicle.
- The design of the longitudinal and lateral controllers.
- The tuning of designed controller in compliance with experimental studies on human driving.
- The control concept including parameterization that allows the driver to personalize the control system in a desired manner in terms of comfort and safety.
- The integration of the longitudinal and lateral controllers with an efficient control structure in order to ensure the enhanced overall performance.
- The implementation of developed vehicle model and designed controllers in Matlab/Simulink environment.
- The performance evaluation of vehicle model and controllers with respect to determined performance specifications via simulations by using a set of traffic scenarios which are likely to occur in reality.

1-4 Contributions of Thesis

This thesis offers the following contributions to the field of vehicle control:

- The longitudinal weight transfer is taken into account in vehicle model. Hereby, the control system can accomplish safety in the strict sense especially in severe braking situations since load transfer can not be neglected in these circumstances.
- The customizable integrated vehicle dynamics control concept in terms of comfort and safety intends to enhance driver acceptance of the proposed control system.
- A new lateral index is determined based on experimental study on human driving which primarily concerns lateral acceleration in highways. It has been used to evaluate lateral motion of the vehicle in integrated vehicle dynamics control system.

- In case of unstable lateral motion of the vehicle, the integrated vehicle dynamics control system determines desired longitudinal acceleration based on physical limitation in braking with cornering situations.

1-5 Outline

The remaining chapters of this thesis are structured in the following manner. Chapter 2 introduces vehicle dynamics. The longitudinal and lateral controller designs are presented in Chapter 3 and 4, respectively. Chapter 5 describes the integrated control structure. Simulations for the evaluation of the designed controllers are conducted in Chapter 6. Finally, conclusions regarding the work and some suggestions for the future work are presented in Chapter 7.

The parameters used in the vehicle model and the design of controllers are provided in Appendix A. The implementation outcomes of developed vehicle model and designed controllers in Simulink are displayed in Appendix B.

Chapter 2

Vehicle Dynamics

When considering Cruise Control (CC) in highways, it is not necessary to model the interaction between the road and the tire as soon as the longitudinal slip is small. In addition there is no mass transferred between the axles (front axle and rear axle) under this condition. However when considering other control problems such as Adaptive Cruise Control (ACC), a more sophisticated dynamic model of a vehicle is necessary. Such a model will be developed in this chapter.

The model consists two major components: the dynamics of vehicle which considers also the external forces acting on the vehicle and the dynamics of powertrain. In the following of this chapter, the different components of the model are studied in detail. This chapter is organized as follows: terminology related to vehicle dynamics, vehicle chassis model, tire model, powertrain model, brake model, wheel dynamics, steering dynamics and simulations results of vehicle model.

2-1 Vehicle Dynamics Terminology

2-1-1 Coordinate System

The system of coordinates and major forces affecting a vehicle are shown in Figure 2-1. It is in accordance to the ISO standards, as described in ISO 8855 [14]. Using this coordinate system, the forward movement of the vehicle is described in the positive X-axis, the lateral movement is described by the Y-axis, being positive when oriented to the left (from the driver position) and the vertical movement is represented in the Z-axis. The rotations of the vehicle cabin are also included in this system of coordinates. The roll rotation is defined around the X-axis, the pitch rotation around the Y-axis and the yaw rotation around the Z-axis [14].

2-1-2 Centripetal Force

Any motion in a curved path causes an acceleration, and requires a force directed toward the center of curvature of the path. This force is called the centripetal force, which is described

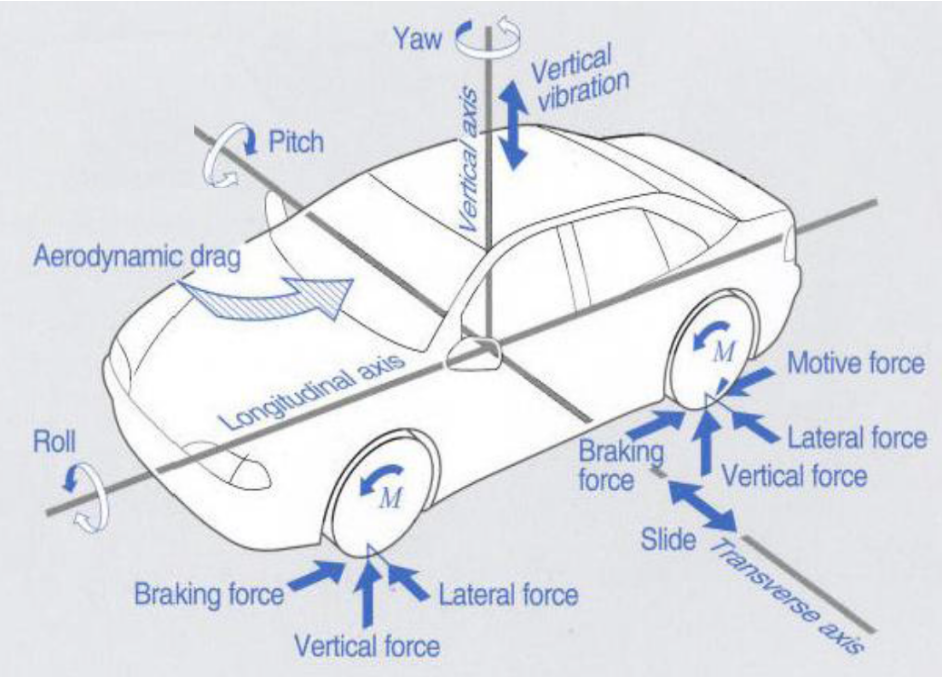

Figure 2-1: The system of coordinates and forces affecting a vehicle

by

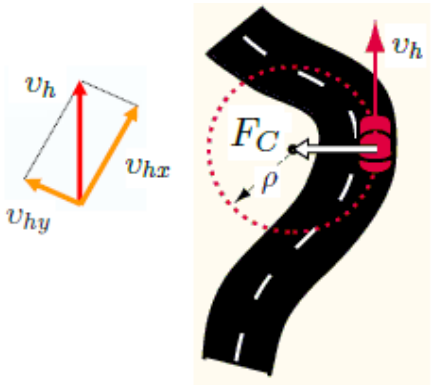

Figure 2-2: Speed vector and centripetal force

$$F_C = m\frac{v_h^2}{\rho} \tag{2-1}$$

$$v_h = \sqrt{v_{h_x}^2 + v_{h_y}^2} \tag{2-2}$$

where F_C is the centripetal force, m is the total mass of the vehicle, ρ is the radius of curvature, v_h is the absolute velocity of the host vehicle or ACC-equipped vehicle; v_{h_x}, v_{h_y} are longitudinal and lateral velocity of the host vehicle. The maximum speed for which the centripetal force equals the force of static friction in case of flat roadway;

$$v_{h,limit} = \sqrt{\rho g \mu} \tag{2-3}$$

where $v_{h,limit}$ is the maximum allowable velocity of the host vehicle in curve, g is the gravitational acceleration, μ is the friction coefficient.

Friction is defined as the resistance to motion between two surfaces that impedes vehicle motion. Average values of tire friction coefficient μ for different road conditions are given in Table 2-1.

Table 2-1: Average values of the tire friction coefficient

Road Surface	μ - Value
Dry Asphalt	0.80 - 0.90
Wet Asphalt	0.50 - 0.70
Gravel	0.60
Dry Earth Road	0.68
Wet Earth Road	0.55
Snow	0.20
Ice	0.10

In addition, following assumptions have been made under environment conditions: perfect weather (no rain, snow, ice etc.) and highway road with high friction coefficient. Thus, it has been concentrated on a dry asphalt coefficient $\mu = 0.9$.

2-1-3 Aerodynamic Resistance

Aerodynamic resistance is composed of turbulent air flow around vehicle body, friction of air over vehicle body and vehicle component resistance, from radiators and air vents etc. As the aerodynamic drag force is a function of the square of the speed, thus it has a significant impact on the performance of the vehicle only at speeds greater than 48 km/h [4].

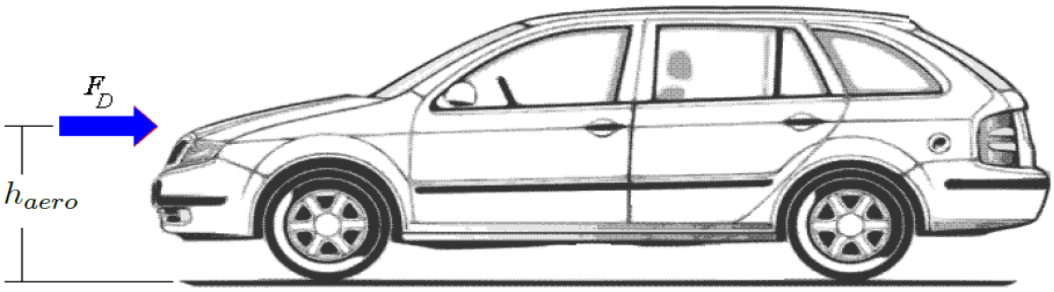

Figure 2-3: Aerodynamic drag force

The drag force, acting at height h_{aero} above the ground as depicted in Figure 2-3, can be expressed as

$$F_D = \frac{1}{2} C_D A_h \varrho (v_{h_x} + v_{wind})^2 \tag{2-4}$$

where C_D is the drag factor, A_h is the area of the host vehicle frontal projection, ϱ is the atmospheric air density, v_{wind} is the wind velocity [10]. It is assumed that no wind blows.

An approximated relationship for the area of the host vehicle frontal projection A_h has been determined as a function of the vehicle mass m in the range of 800-2000 kg [4] given by

$$A_h = 1.6 + 0.00056(m - 765) \tag{2-5}$$

2-1-4 Gravitational Resistance

Gravitational force acts on a vehicle going uphill and downhill: the sign of this force depends on whether the vehicle is going up or downhill. In particular, it is negative when the vehicle goes uphill and positive otherwise:

$$F_g = \pm mg \sin\theta \tag{2-6}$$

where θ varies depending on inclination of the road and it is so-called road slope as depicted in Figure 2-4 [5]. It is assumed that vehicle runs on a road with no slope.

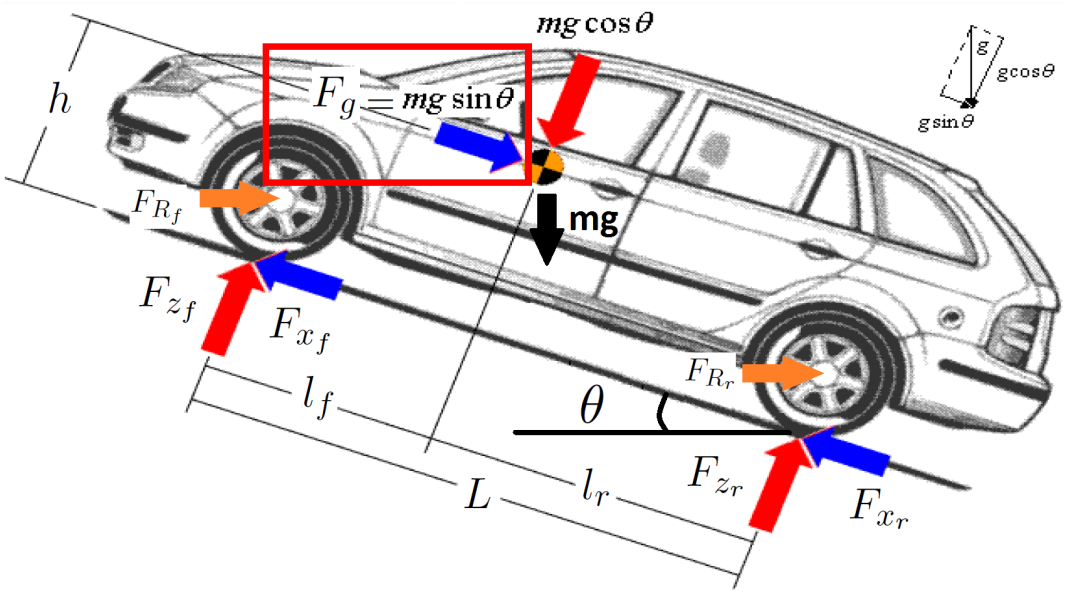

Figure 2-4: Longitudinal force exerting on vehicle when traveling on the inclined road

2-1-5 Rolling Resistance

The rolling resistance forces produced due to the deflection of the tires while rotating on the road are created at the contact point of the tires and the road interface. These longitudinal forces are translated into center of rotation as displayed in Figure 2-4. The rolling resistance forces depend on several factors, mainly the tire shoulder temperature, the ambient temperature, the tire diameter, the road conditions, the inflation pressure of the tire and the type of tire [4]. The effect of all these factors is lumped into a coefficient of rolling resistance C_R and total rolling resistance force F_R can be expressed simply as

$$F_R = F_{R_f} + F_{R_r} = C_R mg \cos\theta \tag{2-7}$$

2-1-6 Vehicle Load Distribution

In wheeled vehicles, load transfer is the measurable change of Center of Gravity (CoG) location and change of load borne by different wheels of even perfectly rigid vehicles during acceleration and braking as visualized in Figure 2-5. Load transfer is a crucial concept in understanding vehicle dynamics and it can not be neglected. The same is also valid for bikes and bicycles, though only longitudinally. Weight transfers occur as a result of the chassis twisting around the vehicle's roll center. When you accelerate, the weight of the vehicle is thrown backwards. This causes the rear suspension to compress slightly and increases the available grip at the rear tires. Weight transfers under braking are thus more likely to affect the balance of the vehicle [5].

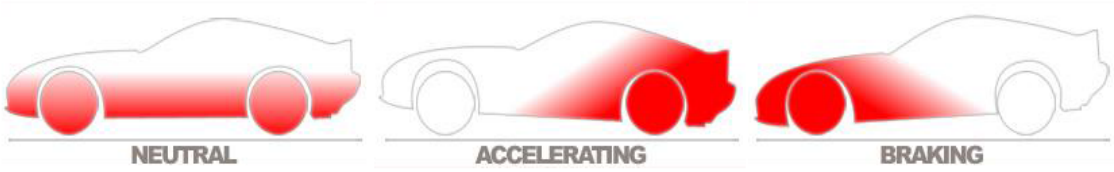

Figure 2-5: Vehicle load distribution during accelerating and braking

The static load distribution is simply a function of vehicle geometry and the inclination of the road, and is obtained by summing the forces at each contact point. There is, however, a dynamic load distribution that can transfer load between the front and rear wheels as the vehicle accelerates and brakes. Examining the geometry, the following two equations may be formulated to describe the front and rear normal forces:

$$F_{z_f} = F_{z_{f,static}} + F_{z_{f,dynamic}} = mg(\frac{l_r}{L}\cos\theta + \frac{h}{L}\sin\theta) - ma_{h_x}\frac{h}{L} \tag{2-8}$$

$$F_{z_r} = F_{z_{r,static}} + F_{z_{r,dynamic}} = mg(\frac{l_f}{L}\cos\theta - \frac{h}{L}\sin\theta) + ma_{h_x}\frac{h}{L} \tag{2-9}$$

where l_f, l_r are respectively the distance from the vehicle center of gravity to the front and the rear wheel axle of the vehicle, L is the distance between the front and the rear wheel axle of the vehicle, h is the height of center of gravity relative to the road surface a_{h_x} is the longitudinal acceleration of the host vehicle.

The first terms on the right of these equations are the static load terms, while the second, acceleration dependent terms, are the dynamic loading terms. In agreement with intuition, while the vehicle is accelerating in longitudinal direction, the load is transferred to the rear wheels, and during braking it is transferred to the front wheels.

2-2 Vehicle Chassis Model

There are a lot of different ways of representing a vehicle chassis and its equations of motion, mainly depending on the desired level of detail. Some of those models consider complex issues, such as the impact of the tire on the vehicle performance, the load transfer between the front

and rear axles during braking and acceleration etc. Some others are based on simplified equations. Although a four wheeled model can capture the most relevant dynamics of the vehicle, the comparison between the different models demonstrated that similar results could be obtained when the vehicle drives at high speed and there are no adverse road conditions, e.g. ice. Therefore, the simple model is opted for the control design generally [13].

The simplest approach to the vehicle motion is to consider a vehicle moving on a horizontal plane with 3 Degree of Freedom (DOF), the two displacements on the plane (longitudinal and lateral) and the rotation around an axis normal to that plane (yaw rotation). By controlling these 3 DOF over time, the vehicle's trajectory will be known, so the path described by the vehicle can be studied. If additional simplifications are made, considering that the vehicle travels at constant speed and the trajectory radius when turning is much larger than the vehicle's track width, this model can be represented by a two-wheeled vehicle model, usually known as Single-track or Bicycle model, as shown in Figure 2-6 [14].

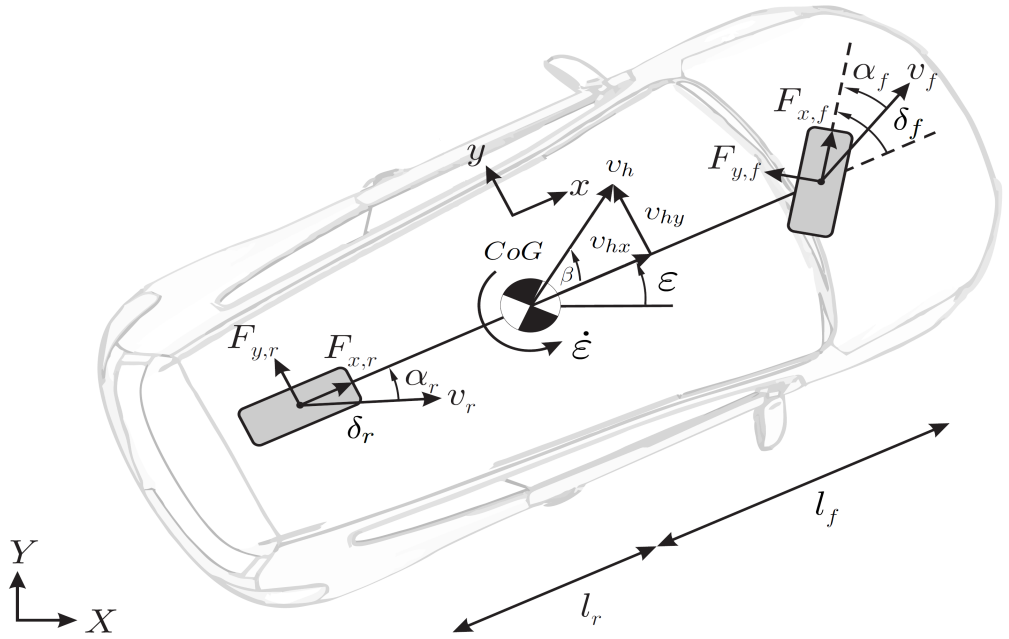

Figure 2-6: Nonlinear single-track vehicle chassis model

The bicycle model is usually the first approach to vehicle dynamics studies due to its easy understanding and simplicity. Moreover it is an appropriate model to study vehicle response in steady-state conditions and the stability of the resulting motion. The vertical dynamics of the vehicle and its pitch and roll motions do not affect performance significantly and, thus, are not included in the model [7].

The summation of forces $\sum F_x$ and $\sum F_y$ along the vehicles X and Y axes and summation of Z-axis moment $\sum M_z$ about the vehicle's center of gravity and the steering angle of each tire can be expressed as

$$\sum F_x = \cos\delta_f F_{x_f} + \cos\delta_r F_{x_r} - \sin\delta_f F_{y_f} - \sin\delta_r F_{y_r} - F_D - F_R \pm F_g \tag{2-10}$$

$$\sum F_y = \cos\delta_f F_{y_f} + \cos\delta_r F_{y_r} + \sin\delta_f F_{x_f} + \sin\delta_r F_{x_r} \tag{2-11}$$

$$\sum M_z = l_f \cos\delta_f F_{y_f} - l_r \cos\delta_r F_{y_r} + l_f \sin\delta_f F_{x_f} - l_r \sin\delta_r F_{x_r} \tag{2-12}$$

where F_{x_i} and F_{y_i} are the longitudinal and lateral tire forces respectively for front and rear wheels, δ_f and δ_r are the front and rear wheel steering angles. For the vehicle motion in the plane, applying Newton's equations for equilibrium of forces and momentum, the vehicle velocities and accelerations can be calculated. As shown in Figure 2-6, the main external (longitudinal and lateral) forces on the vehicle are generated by the tire-road contact and must be balanced with the vehicle inertial forces. The Newton-Euler equations for the vehicle become as [7], [14]

$$ma_{h_x} = mv_{h_y}\dot{\varepsilon} + \sum F_x \tag{2-13}$$

$$ma_{h_y} = -mv_{h_x}\dot{\varepsilon} + \sum F_y \tag{2-14}$$

$$I_z\ddot{\varepsilon} = \sum M_z \tag{2-15}$$

where I_z is the mass moment of inertia with respect to a vertical axis, ε and $\dot{\varepsilon}$ are yaw angle and yaw rate of the host vehicle. The vehicle's equations of motion in an absolute inertial frame are

$$\dot{X} = v_{h_x}\cos\varepsilon - v_{h_y}\sin\varepsilon \tag{2-16}$$

$$\dot{Y} = v_{h_x}\sin\varepsilon + v_{h_y}\cos\varepsilon \tag{2-17}$$

where X, Y are absolute vehicle position in global coordinates [9].

2-3 Tire Model

During the last 60 years an impressive amount of research has been done regarding tire behavior and modeling, ending up with several different types of tire models with different characteristics [14]. An extended classification of tire models is based on the different approaches used to develop the models, which can go from a completely empiric view, mainly fitting full scale tire test data by regression techniques, to fully theoretical tire models, usually based on its structural behavior study through finite element simulations. Between these two extremes, a bunch of models combining theoretical solutions with empirical measurements in different levels have been developed. Typically, empirical models are over parameterized and as a consequence it is hard to use them in domains where there are no measurements available, e.g. when using in combined slip situation a tire model fitted with pure lateral and longitudinal measurement data. On the other hand, these models are often very compact,

usually some analytical equations, and computationally fast, which can be a great advantage for real-time simulation. Theoretical models describe the tire behavior in great detail, usually including most of the steady-state and transient phenomenon affecting the tire response, but this level of detail means that simulating these models is a computational heavy task. Full theoretical models are often used to develop new tires but they have no practical application for complete vehicle simulation. Finally, one can identify the middle ground in the so-called Semi-empirical tire models, which include tire models specially developed to represent the tire as a component of a vehicle in a simulation environment. These models are based on measured data but also may contain structures and strategies used in theoretical models, presenting a good balance between accuracy and computation speed [14].

Tires are one of the most important components of vehicles, since they are the only component keeping the vehicle in contact with the ground. The primary force generated between the tire and the road interface push the vehicle forward during acceleration(traction force) and reduces the speed of the vehicle during braking (braking effort). This force is known as the longitudinal force. Except for aerodynamic, gravity and rolling resistance forces, all of the other forces which affect vehicle handling are produced by the tires as depicted in Figure 2-7 and appear in vehicle dynamic Equations (2-10) - (2-15).

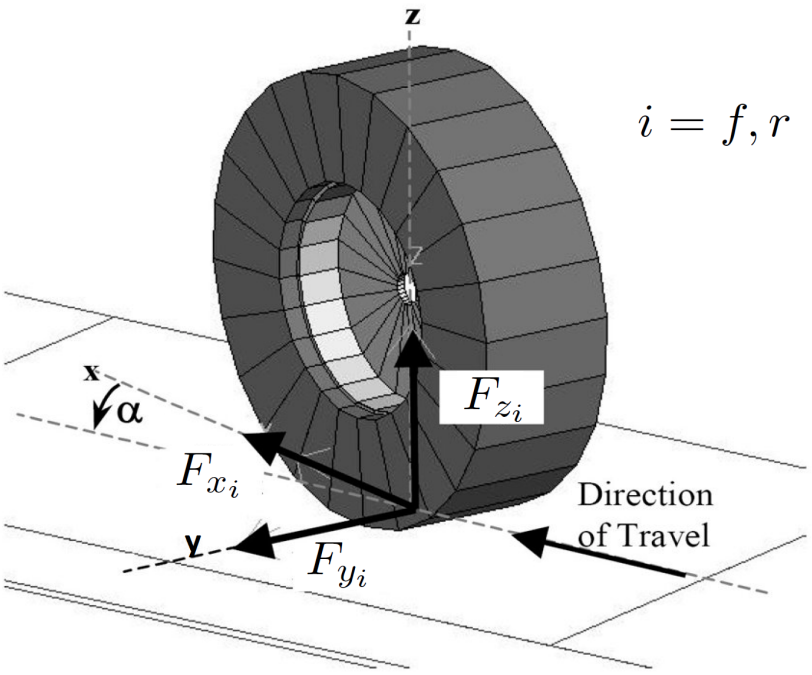

Figure 2-7: Illustration of the tire model

Before introducing sophisticated tire model, firstly some terms related to tire model have been defined in following. The front and rear tire speeds along x-axis and y-axis are calculated as below

$$v_{x_i} = v_i \cos \alpha_i \tag{2-18}$$

$$v_{y_i} = v_i \sin \alpha_i \tag{2-19}$$

where v_f and v_r are the front and rear tire speed, α_f and α_r are the front and rear tire slip angle. The correlation between tire speeds and host vehicle speed is given below

$$v_{x_f} = v_{h_x} \tag{2-20}$$

$$v_{x_r} = v_{h_x} \tag{2-21}$$

$$v_{y_f} = v_{h_y} + l_f\dot{\varepsilon} \tag{2-22}$$

$$v_{y_r} = v_{h_y} - l_r\dot{\varepsilon} \tag{2-23}$$

The slip angle represents the angle between the wheel velocity and the direction of the wheel itself [6]. Then tire side-slip angles are computed as

$$\alpha_f = \delta_f - \arctan(\frac{v_{y_f}}{v_{x_f}}) \tag{2-24}$$

$$\alpha_r = \delta_r - \arctan(\frac{v_{y_r}}{v_{x_r}}) \tag{2-25}$$

The tire forces depend on the tire side-slip values and on the friction characteristics between the road and the tires. The longitudinal wheel-slip ratio, which refers to the difference in angular speed between a purely rolling wheel and a wheel that also slides, is defined for each tire as

$$s_i = \begin{cases} \frac{r\omega_i - v_{x_i}}{v_{x_i}} & r\omega_i < v_{x_i} \quad \text{Braking} \\ \frac{r\omega_i - v_{x_i}}{r\omega_i} & r\omega_i > v_{x_i} \quad \text{Driving} \end{cases} \qquad where \quad i = f, r \tag{2-26}$$

where ω_f and ω_r are the angular velocities of front and rear tires, r is the radius of wheels.

The maximum function in the denominator of the above equation allows its use for both acceleration and braking models. A slip ratio equal to zero means that the forward velocity and tire rolling speed are equal, which implies an absence of either engine or brake torque. A positive slip ratio implies that the tire has a positive finite rolling velocity, and the vehicle posses a greater finite forward velocity. A negative slip ratio implies that the vehicle has a finite forward velocity and the tire has a greater equivalent positive rolling velocity. At each extreme, i.e. +1 and - 1, the wheel is either "locked" at zero speed, or "spinning" with the vehicle at zero speed. When both tire and vehicle velocity are equal to zero, the slip is mathematically undefined, and is taken to be zero for simulation purposes. Experimental studies have produced several clearly defined friction/slip characteristics between the tire and road surface for a variety of different driving surfaces and conditions [11].

It is important to use a realistic nonlinear tire model for longitudinal direction especially. Therefore, the model for tire tractive forces used are described by a Pacejka model which is a complex semi-empirical one. The longitudinal forces are assumed to depend on the normal force, surface friction, and longitudinal slip ratio as shown below;

$$F_{x_i} = f_x(s_i, \mu, F_{z_i}) \tag{2-27}$$

Note that with this model, weight transfer can be considered during severe acceleration or braking situations. The Pacejka model calculates the friction coefficient as a function of slip ratio:

$$\mu(s_i) = D_P \sin(C_P \arctan(B_P s_i - E_P(B_P s_i - \arctan(B_P s_i)))) \tag{2-28}$$

The value of B_P, C_P, D_P, E_P for different road types are shown in Table 2-2. The model defines in excess of 40 constants that are determined from the given set of experimental data, and the overall model coefficients B_P, C_P, D_P, E_P are then calculated from a combination of these constants.

Table 2-2: Coefficients of the Pacejka model for different road conditions

Road Surface	B_P	C_P	D_P	E_P
Dry Tarmac	10	1.9	1	0.97
Wet Tarmac	12	2.3	0.82	1
Snow	5	2	0.3	1
Ice	4	2	0.1	1

Note that it has been concentrated on dry tarmac (asphalt) coefficients $B_P = 10$, $C_P = 1.9$, $D_P = 1$, $E_P = 0.97$ in compliance with previously made assumptions. Having the friction coefficient $\mu(s_i)$ and the normal force F_{z_i} exerting on the wheel, the longitudinal traction force F_{x_i} is then calculated as follows [4]:

$$F_{x_i} = \mu(s_i) F_{z_i} \tag{2-29}$$

Highly nonlinear behavior of tire forces cause the large variation in vehicle handling properties throughout the longitudinal and lateral maneuvering range. Lateral tire forces which are crucial for maneuvering capability of the vehicle are assumed to depend on the normal force, surface friction, and slip angle as

$$F_{y_i} = f_y(\alpha_i, \mu, F_{z_i}) \tag{2-30}$$

Sample plots of predicted longitudinal and lateral force versus longitudinal slip ratio and slip angle are shown in Figure 2-8. These plots are shown for the front tire of the "bicycle" model, which represents the two front tires of the actual vehicle [9]. Furthermore, Figure 2-9 indicates that the lateral and longitudinal motions of the vehicle are strongly coupled through the tire forces, and large values of longitudinal slip and slip angle can occur simultaneously. However in order to simplify control problem, it will be considered as that lateral and longitudinal tire forces are decoupled.

Since maneuvering capability of the vehicle is limited at high speed in highways and slip angle commutes in linear region as shown in Figure 2-10, lateral tire forces are linear functions of slip angles, cornering stiffnesses of the tire for the sake of simplification [6]:

$$F_{y_i} = 2C_{y_i}\alpha_i \tag{2-31}$$

where C_{y_i} are the cornering stiffness. The factor 2 in Equation (2-31) accounts for the fact that there are 2 tires per axle in the bicycle model adopted [18].

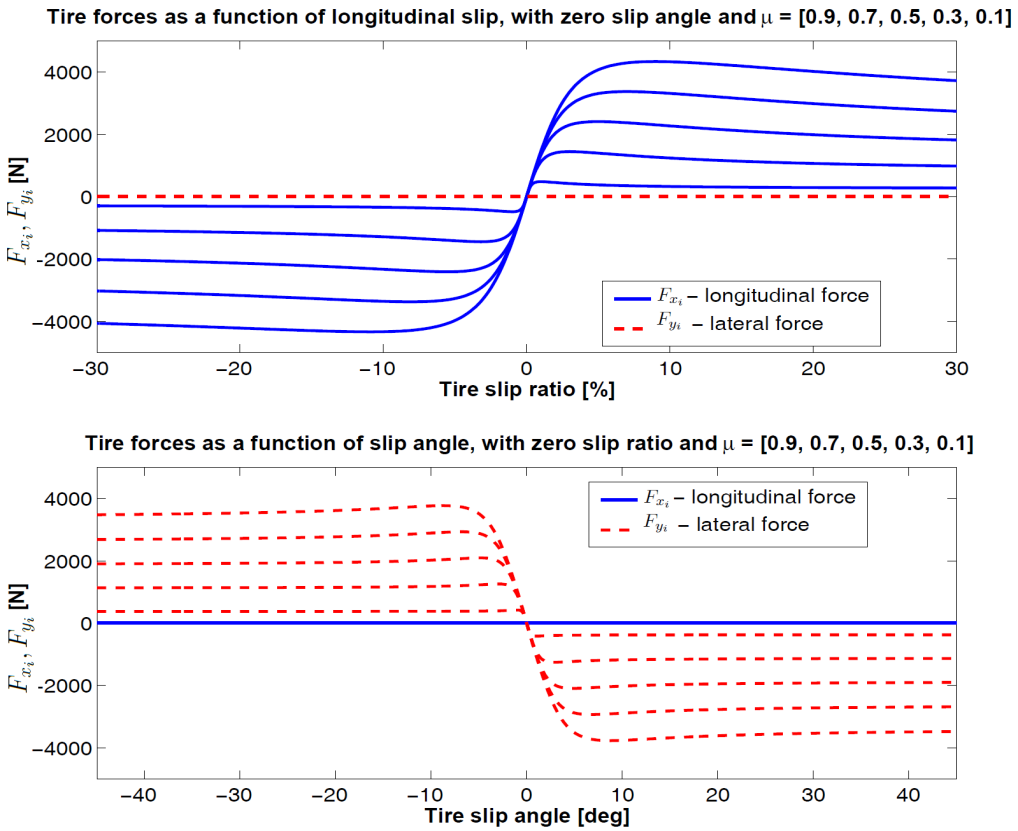

Figure 2-8: Longitudinal and lateral tire forces with different μ coefficient values

The cornering stiffness are defined for the front and rear tires based on the static distribution of weight between the front and rear axles as [15]

$$C_{y_i} = C_s \frac{F_{z_{i,static}}}{2} \tag{2-32}$$

where C_s is the cornering stiffness coefficient. Generally, typical values for the cornering stiffness coefficient C_s varies between 0.12/deg - 0.16/deg according to type of tires [37].

The longitudinal and lateral tire force F_{x_i}, F_{y_i} are limited physically by the adhesion limit between tire and road [18]. Because the forces are transmitted by friction as shown as in Figure 2-11. Therefore, during combined slip conditions the maximum transferred force is defined by Kamm circle as given

$$\sqrt{F_{y_i}^2 + F_{x_i}^2} \leq \mu F_{z_i} \tag{2-33}$$

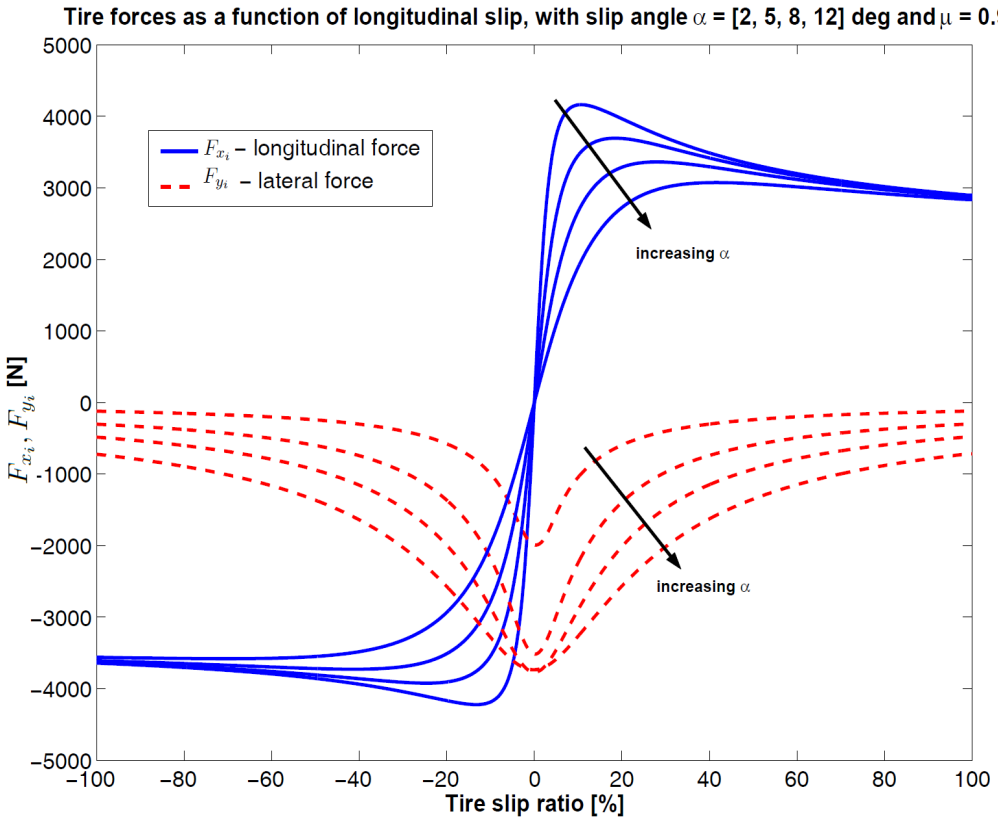

Figure 2-9: Longitudinal and lateral tire forces with combined braking and cornering

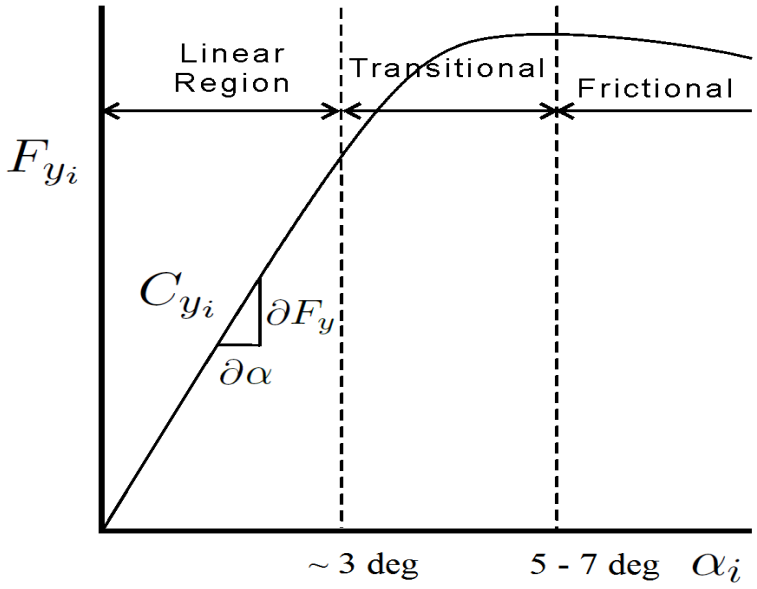

Figure 2-10: Lateral tire force regions

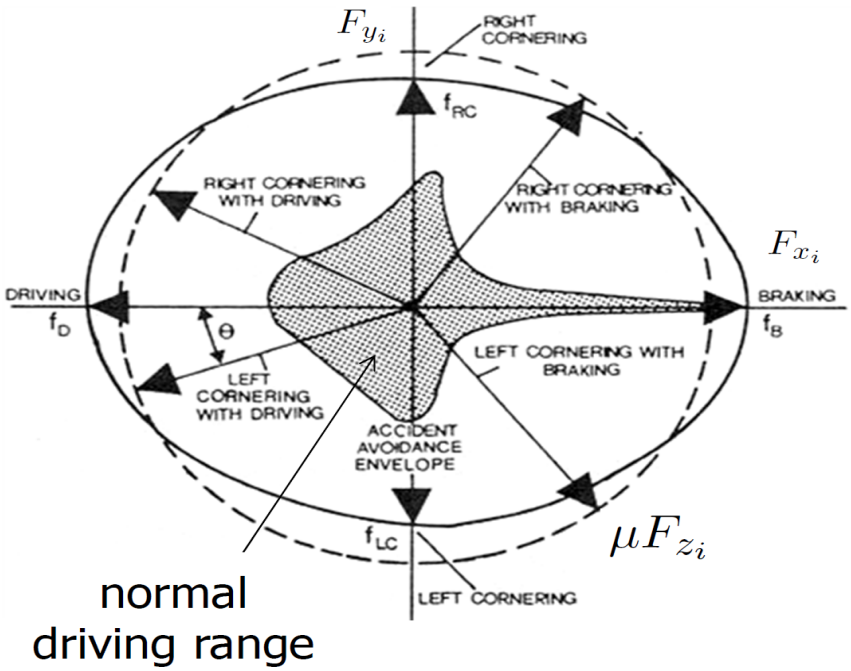

Figure 2-11: Kamm circle of friction forces

2-4 Powertrain Model

The vehicle powertrain includes the engine itself, the torque converter, gearbox and final drive differential to deliver the torque to wheels.

2-4-1 Engine Model and Engine Dynamics

The adaptive cruise controller can specify vehicle speed, engine throttle, and brake commands. While brake commands reduce speed directly, engine throttle commands involve engine, driveline, and wheel dynamics. The engine is modeled as a static map from throttle input and engine speed to engine torque. The lookup table shown in Figure 2-12, which corresponds to a diesel mid-sized passenger car, is used in the Simulink implementation of the engine map. The engine look-up table has two inputs, namely, throttle in terms of percentage (u_t), which is constrained to a value between 0-100%, and engine speed (N_e) in terms of rotations per minute. The output of the model is the engine torque subject to control (T_{ec}) in $N\,m$. Modeling an engine as a lookup table is standard practice in vehicle dynamics control. Switching to a different engine model is easily accomplished by modifying the lookup table. The ACC law specifies a desired acceleration and it is transformed into a corresponding engine torque. An inverse of the engine lookup table with engine torque and engine speed as inputs and throttle command as output is created off-line. This inverse model is used to generate the required throttle command input, which is supplied to the host vehicle model [4].

Under assumption that the conversion of chemical energy into output torque by the engine may be described by a first order time lag, and the throttle is actuated by a servo with an associated time lag, these lags may be lumped together into a single equivalent lag τ_e. The

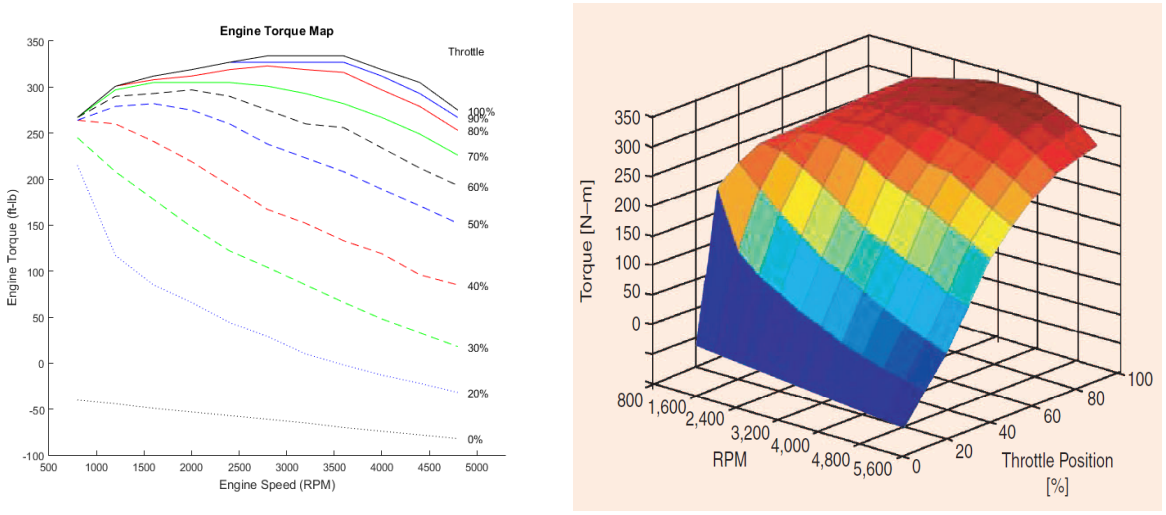

(a) 2-dimensional view **(b)** 3-dimensional view

Figure 2-12: Static engine torque map

torque function can be used in the form of a transfer function in Simulink model as given below [11]

$$T_e(u_t, N_e) = \frac{T_{ec}}{1 + \tau_e s} \tag{2-34}$$

where T_e is the engine torque. The engine torque calculated from static map is transmitted by the driveline to the wheels.

2-4-2 Driveline

Figure 2-13 illustrates the schematic diagram of a powertrain which demonstrates the transmission of the torque and velocity from the engine to the wheels. The torque produced by the engines is transmitted to the gearbox through the torque converter. The torque converter consists of three essential parts i.e. the impeller, the turbine and the reactor. The impeller is connected to the crankshaft that transmits the power of the engine to the turbine by the hydraulic oil inside the torque converter. In turn the turbine is connected to the output shaft of the converter which is coupled to the input shaft of the gearbox. The torque getting through the gearbox varies depending on the gear ratio. Finally the output torque from the gearbox is transmitted to the wheels after passing through the final drive [4].

The torque and the angular velocity of the wheel are effected by the brake torque applied on the wheel and other forces exerted on the wheel resulted from the interaction of the tire and road (rolling resistance and tractive force). The modeling of the powertrain follows the approach adopted by MathWorks [4]. The equation determining the difference between engine torque and impeller torque is defined as

$$I_{ei}\dot{N}_e = T_e(u_t, N_e) - T_i \tag{2-35}$$

where N_e is the engine speed, I_{ei} is the summation of engine and impeller moment of inertia, T_e is the engine torque as a function of engine speed and percentage throttle input, and T_i is

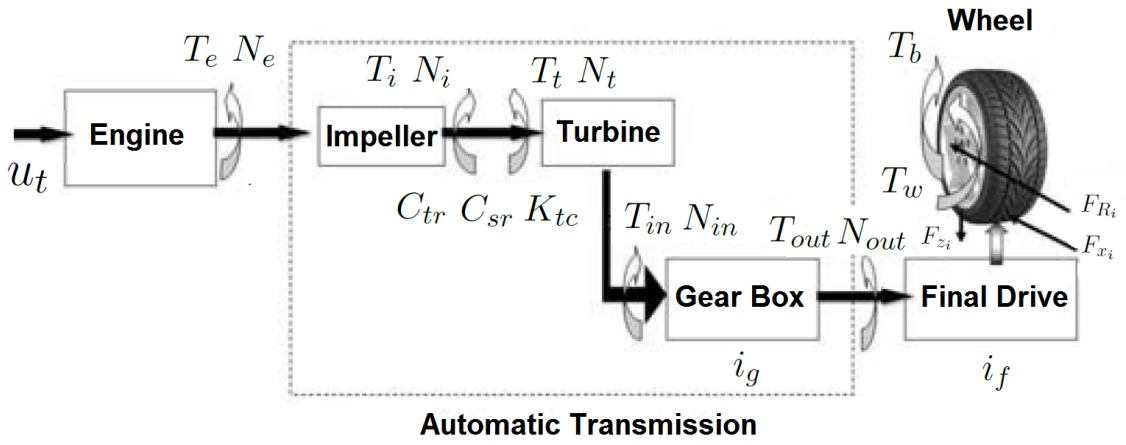

Figure 2-13: Transmission of the torque and speed from the engine to the wheel

the impeller torque. The engine is connected to the impeller of the torque converter which couples it to the transmission. The input-output characteristics of the torque converter can be expressed as functions of the engine speed and the turbine speed. Note that the direction of power flow is always assumed to be from the impeller to the turbine. Parameters playing an important role on the performance of a torque converter are the speed ratio C_{sr}, the torque ratio C_{tr} and the capacity factor $K_{tc} = f(N_i/N_e)$ which is function of the impeller speed (converter input speed) N_i and the engine speed N_e that shows the ability of the converter to absorb or transmit the torque. The input torque of the converter can be defined as

$$T_i = \frac{N_i^2}{K_{tc}^2} \tag{2-36}$$

where T_i is the impeller torque (converter input torque). The engine and the converter should have the same range of capacity factors ($K_{tc} = K_e$) to achieve a proper matching. Assuming that the velocity of the impeller N_i equals to the engine speed N_e, Equation (2-36) is then rewritten as

$$T_i = \frac{N_e^2}{K_{tc}^2} \tag{2-37}$$

Knowing C_{sr} and C_{tr} enables us to find the output characteristic of the torque converter:

$$\begin{aligned} T_t &= C_{tr} T_i \\ N_t &= C_{sr} N_i \end{aligned} \tag{2-38}$$

where T_t is the turbine torque and N_t is the turbine angular velocity. Knowing that the torque and speed outputs from the torque converter equal to the input characteristics of the gearbox ($T_t = T_{in}$, $N_t = N_{in}$) help us to find the outputs of the gearbox [11]:

$$T_{out} = i_g T_{in} \tag{2-39}$$

$$N_{out} = \frac{N_{in}}{i_g} \tag{2-40}$$

where T_{in} and T_{out} , N_{out} and N_{in} are the transmission input and output torques, transmission output and input speeds respectively. i_g is the transmission ratio which varies with the gear setting. Multiplying the transmission output torque by the final drive ratio i_f determines the wheel torque as given

$$T_w = i_f T_{out} \tag{2-41}$$

where T_w indicates the wheel torque. The relation between transmission output speed and wheel speed is determined as follows

$$\omega_r = \frac{N_{out}}{i_f} \tag{2-42}$$

The final element of the powertrain that requires a description is the automatic gearbox, which decides the current gear and consequently the value of i_g [11].

2-4-3 Gearbox Model

In practice, many commercially available passenger vehicles now have automatic gearboxes. Many of the modern gearbox are connected to the vehicle communications network, and run sophisticated adaptive algorithms involving many instrumented variables such as engine speed, vehicle speed, driving wheel speed and throttle setting. An automatic gearbox is best described in terms of a shift-map, that relates the threshold for changing each gear up or down as a function of throttle setting and wheel speed [11]. Figure 2-14 shows the simplified shift map for the 4-speed gearbox.

In the model of powertrain, implementation of the gear shift is done through the shift logic based on the threshold calculated by the respective block for up-shift and down-shift. The model programs the shift points for the transmission according to the schedule shown in Figure 2-14. For a given throttle in a given gear, there is a unique vehicle speed at which an up-shift takes place. It operates similarly for a down-shift [16].

The transmission ratio block determines the ratio shown in Table 2-3 and computes the transmission output torque and input speed [16].

Table 2-3: Transmission gear ratios

Gear	Transmission Ratio
1	$i_g = 2.393$
2	$i_g = 1.450$
3	$i_g = 1.000$
4	$i_g = 0.677$

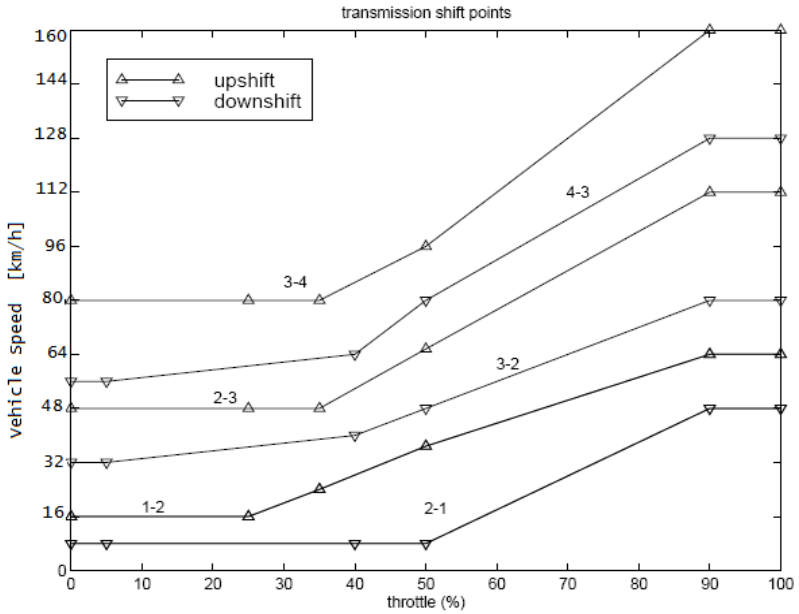

Figure 2-14: Gear shift schedule

2-5 Brake System Model

The brake system model is based around a servo-valve actuate system. Although some systems under development allow a purely servo-actuated brake for each wheel, a more common current implementation is to be used. In this system, an engine-mounted hydraulic pump generates a hydraulic pressure of 150 Bar, which is fed to one of four servo-actuated proportional valves to modulate the brake line pressure delivered to each wheel. Since the model under development here is only a two wheel traction model, only two valves and braking systems are under consideration: the front and rear. Figure 2-15 shows a schematic of this braking system [11].

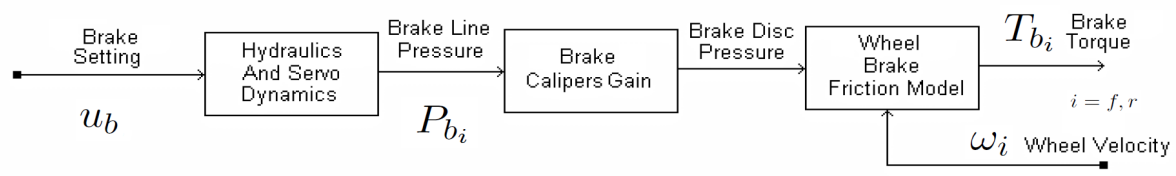

Figure 2-15: Brake system block diagram

A simple model to present a brake system that feed the braking torque as function of the brake pedal into the vehicle model is used. The amount of the braking torque is varied in order to control the performance of the vehicle in various situations. According to this model of brake system, the braking torque is obtained by finding out the amount of pressure produced behind the brake disk P_{b_i} while applying the brake pedal. The brake line pressure is defined as [4]

$$P_{b_i} = 1.5K_{c_i}u_b - \tau_b\dot{P}_{b_i} \qquad i = f, r \tag{2-43}$$

where τ_b is the lumped lag obtained by combining two lags relating to the dynamic of the servo valve and the hydraulic system, K_{c_i} is the pressure gain and the notations of r and f denote the rear and front wheel, respectively. In this model, the value of u_b is varied between 0-100% which indicates the position of the brake pedal. The pressure function can be used in the form of a transfer function in Simulink model. For doing so the Laplace transform is taken of the pressure equation as

$$P_{b_i}(s) = \frac{1.5 K_{c_i} u_b}{1 + \tau_b s} \tag{2-44}$$

This brake line pressure is then converted into a braking torque T_{b_i} via a friction relationship that varies with vehicle speed, temperature and several other parameters. However, a quasi-linear relationship may be assumed and a simplified friction characteristic is utilized [11]:

$$T_{b_i} = P_{b_i} K_{b_i} \min(1, \frac{\omega_i}{0.001}) \qquad i = f, r \tag{2-45}$$

where K_{b_i} is a pressure/torque conversion constant for each brake system. The brake torque being applied for each of the front and the rear wheel are different because of the load transfers during braking. This behavior is introduced by determining a different value of K_{b_i} for each axle. In a typical passenger vehicle, the front brakes tend to have a larger capacity than the rear brakes due to the effects of dynamic load transfer and suspension. It can be seen that as the wheel speed ω_i approaches zero, the effective brake torque also approaches zero.

2-6 Wheel Dynamics

Rear-wheel drive (RWD) typically places the engine in the front of the vehicle and the driven wheels are located at the rear, a configuration known as front-engine, rear-wheel drive layout (FR layout) in Figure 2-16. Nearly all motorcycles and bicycles use rear-wheel drive as well. This traditional automobile layout has been chosen for its simple design and good handling characteristics. In addition, it benefits from weight transfer during acceleration and braking of vehicle. While the vehicle is accelerating, the load is transferred to the rear wheels and it improves traction. On the other hand, weight distribution helps prevent lockup from the rear wheels becoming unloaded under severe braking situations and provides better braking performance.

Developing the gross equations of motion for the rear-wheel-driven vehicle body, summing the torques about each wheel enables the following equation for wheel acceleration to be written as [4]

$$I_w \dot{\omega}_f = -T_{b_f} - r(\cos\delta_f F_{x_f} - \sin\delta_f F_{y_f}) \tag{2-46}$$

$$I_w \dot{\omega}_r = T_w - T_{b_r} - r(\cos\delta_r F_{x_r} - \sin\delta_r F_{y_r}) \tag{2-47}$$

where I_w is moment of inertia of the wheels, $\dot{\omega}_i$ is the angular acceleration of the wheel which by integration, the rotational velocity of each set of wheels can be obtained, T_w is the wheel torque and T_{b_f}, T_{b_r} are braking torques. The subscript f and r denote the front and rear wheel respectively. The last terms at right hand side of equations are the reaction torque on each wheel due to the tire tractive force where r denotes radius of wheels.

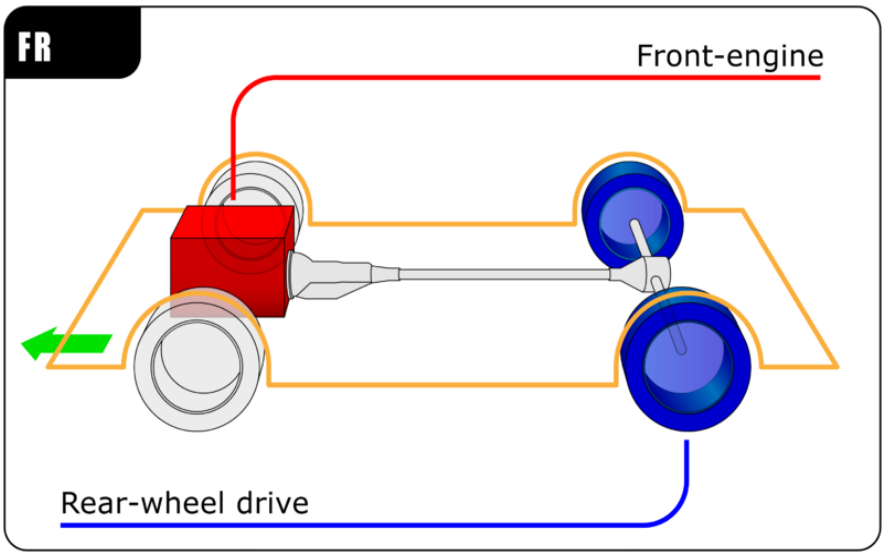

Figure 2-16: Front-engine, Rear-wheel drive (FR) Layout

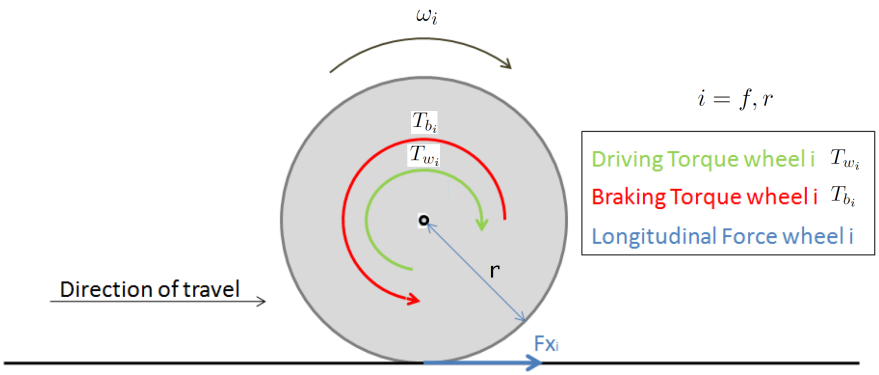

Figure 2-17: Torques exerted on the wheel

2-7 Steering Dynamics

The steering angle is defined as the angle between the front of the vehicle and the steered wheel direction as shown in Figure 2-18.

The dynamic behavior of the steering actuator is approximated by a first-order lag element as given

$$\dot{\delta}_f = -\frac{\delta_f}{\tau_\delta} + \frac{\delta_{f_{des}} K_\delta}{\tau_\delta} \tag{2-48}$$

where τ_δ denotes the dynamic time constant, $\delta_{f_{des}}$ the desired steering angle and δ_f the actual wheel steering angle, K_δ the ratio of steering wheel to wheel, δ_{SW} steering wheel angle [8]. The steering angle function can be used in the form of a transfer function in Simulink model. For doing so the Laplace transform is taken of the steering equation as

$$\delta_f(s) = \frac{\delta_{f_{des}} K_\delta}{1 + \tau_\delta s} = \frac{\delta_{SW}}{1 + \tau_\delta s} \tag{2-49}$$

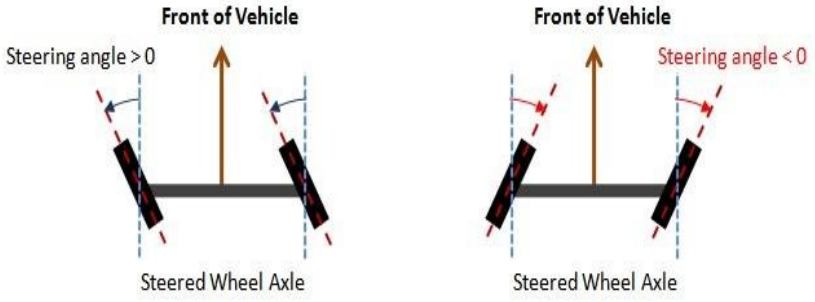

Figure 2-18: Definition of steering angle

2-8 Sensor Model

A model of a radar sensor in the host vehicle with ACC is used to provide simulated measurements of the distance and relative velocity between vehicles. The sensor is modeled as a relative distance measurement device with zero output for distances below 0.25 meter and above 200 meters. The radar has a field of vision of ±28 degree [36]. The presence of a 100-ms delay is also assumed. Radar sensor dynamics are modeled as the first-order system given by

$$d_{measured}(s) = \frac{d}{1 + \tau_r s} \tag{2-50}$$

$$v_{rel,measured}(s) = \frac{v_{rel}}{1 + \tau_r s} \tag{2-51}$$

where the $d_{measured}$ is the distance sensed between the host and target vehicles by the radar, d is the actual distance between vehicles, $v_{rel,measured}$ is the relative velocity measured between the host and target vehicles by the radar, v_{rel} is the relative velocity and τ_r is a time constant of radar model [7].

2-9 Simulation Results

This section presents some simple simulation results that were generated using the models that have been outlined. In order to achieve performance similar to a modern passenger vehicle, the selection of suitable values for the model parameters is crucial. Thereby, some vehicle parameters are adapted from Toyota Prius brochure, and the other parameters are collected from either technical articles or derived from physical and mathematical equations. Above-mentioned vehicle parameters are provided in Appendix A-2.

Some simple measures of performance are gleaned from the simulation data, in order to verify that the chosen vehicle parameters give a realistic performance. In particular, acceleration, braking and steering performance of the simulated vehicle are verified in the following.

2-9-1 Acceleration Performance

The acceleration performance of a passenger vehicle is normally taken as the time, in seconds, required to reach 100 km/h from a standing start. In the scope of this test, 60 seconds full

throttle input is applied to vehicle. Figure 2-19 shows the vehicle velocity in a simulation test, with dry tarmac as the road surface. It can be seen that the 0-100 km/h time is 6.3 seconds, which is reasonable for a passenger vehicle. Note that the top speed reached was 256 km/h, again which is a realistic figure for a vehicle with a such engine. Observe that discontinuities in engine speed occur due to gear-shifting process and the automatic gearbox exhibits satisfactory performance in compliance with gear shift schedule.

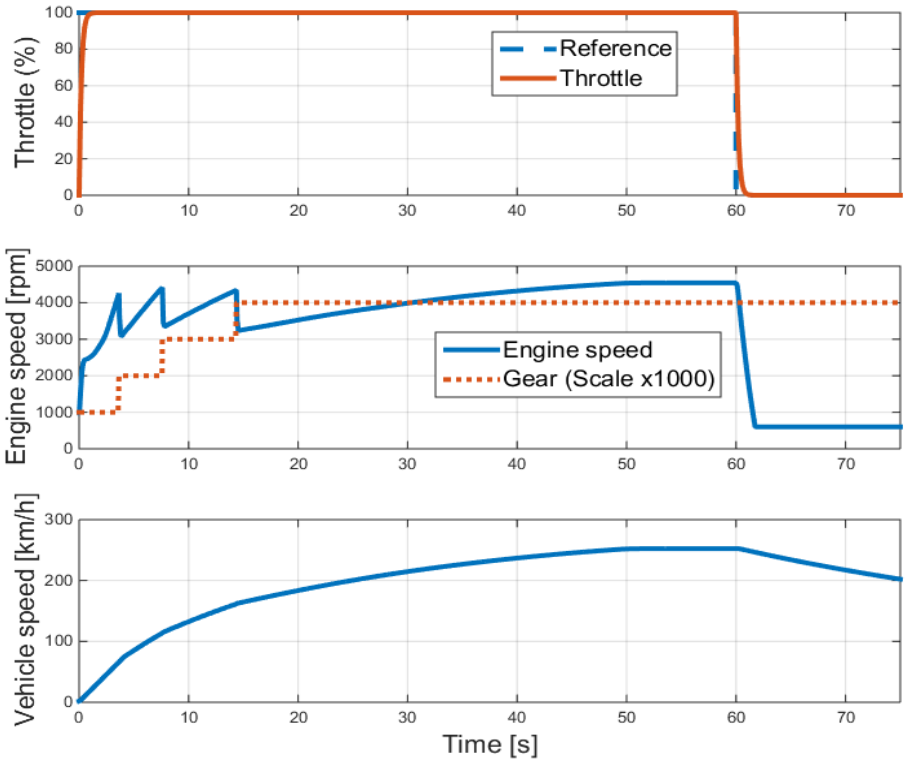

Figure 2-19: Acceleration performance

In addition to observing the vehicle velocity, a plot of each wheel velocities (front and rear) is displayed in Figure 2-20. It can be observed in this figure that the rear wheel is rotating faster than the front one: this indicates that there is slip present, creating the driving tractive force. The front wheel rotates at a value slightly less than the equivalent rotating circumference of the vehicle, due to the presence of wheel friction. Furthermore, it is visible that when no throttle input is applied, wheel velocities converge and attenuate slowly.

2-9-2 Braking Performance

Another common measure of vehicle performance is the braking distance at various speeds. Figure 2-21 shows the braking performance of the vehicle, when braked from 100 km/h to standstill. It can be seen that the braking distance is 47.2 meter which is reasonable for a passenger vehicle.

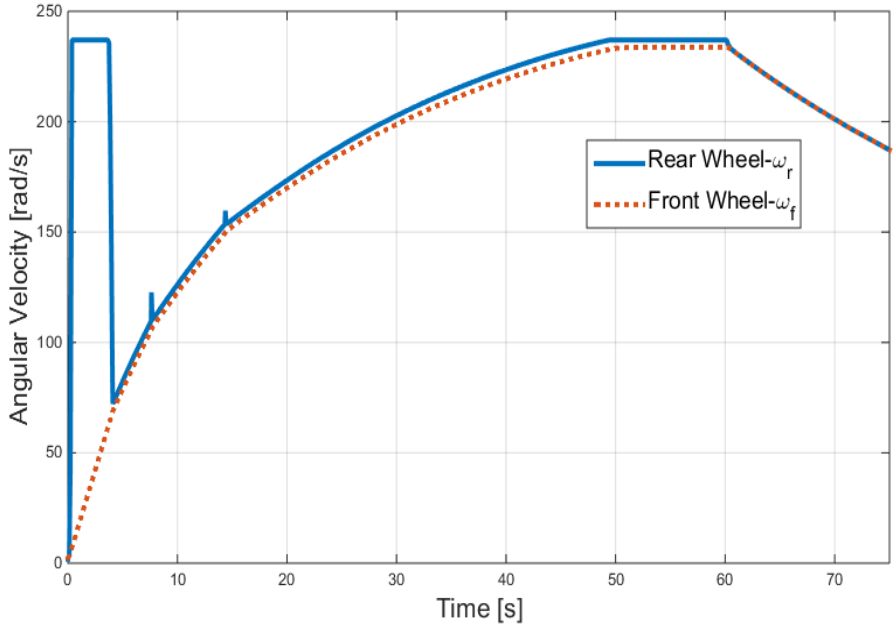

Figure 2-20: Wheel velocities

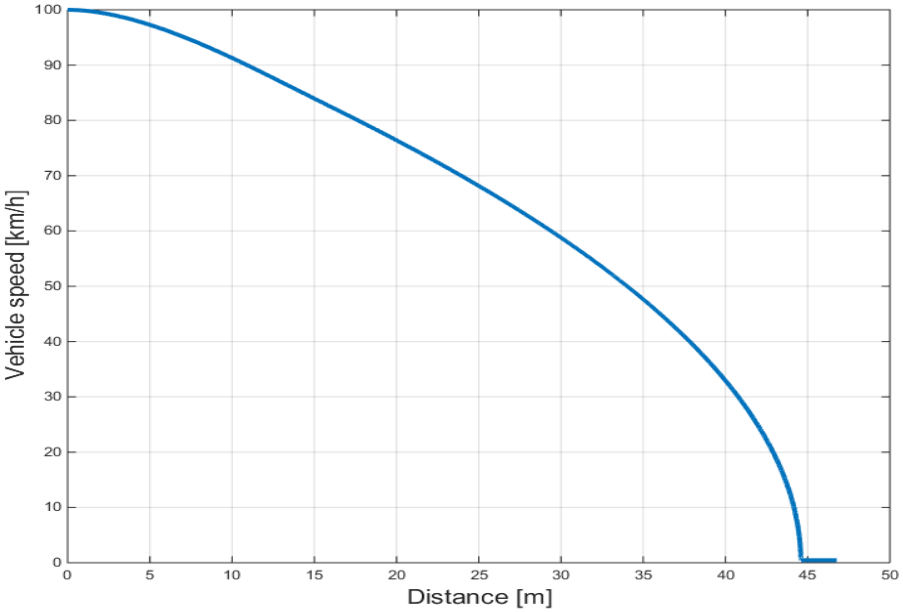

Figure 2-21: Braking performance

2-9-3 Steering Performance

A two-wheeled vehicle dynamics model can entail realistic behavior at moderate maneuvers. To substantiate the realism of the lateral vehicle dynamics model, a steering test is required. The experimental results of double-lane change test of Peugeot 308 at speed of 50 km/h was the basis of mentioned steering test [19]. Since major vehicle parameters (mass, wheelbase etc.) are similar, it allows to compare recorded empirical data with designed vehicle model results.

Figure 2-22 displays recorded lateral acceleration, steering wheel angle and running vehicle speed data respectively from the double-lane change test with Peugeot 308 [19]. It is observable from figure that roughly 50 degree steering wheel angle leads approximately 0.38 g lateral acceleration on a modern car (precise time interval marked in green box between 4-6 seconds).

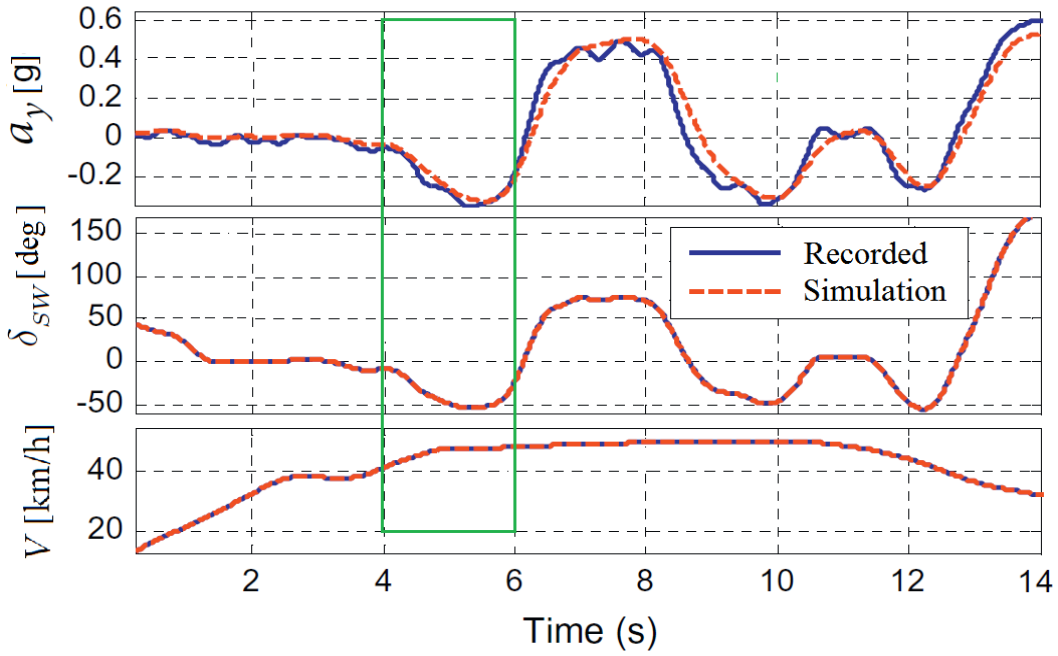

Figure 2-22: The recorded data correspond to a double-lane change test with the Peugeot 308

By originating from the knowledge about the time interval of double-lane change test between 4-6 seconds; the steering test, where ± 50 degree sinusoidal steering wheel angle is exerted on designed vehicle model running at 50 km/h, has been applied to vehicle as shown in Figure 2-23. As a result, peak of 0.35 g in lateral acceleration is observed in simulated vehicle model response.

It can be seen that the recorded empirical data on a modern car and simulated vehicle model response are within the same range. This proves that designed vehicle model exhibits realistic behaviors in lateral plane as well.

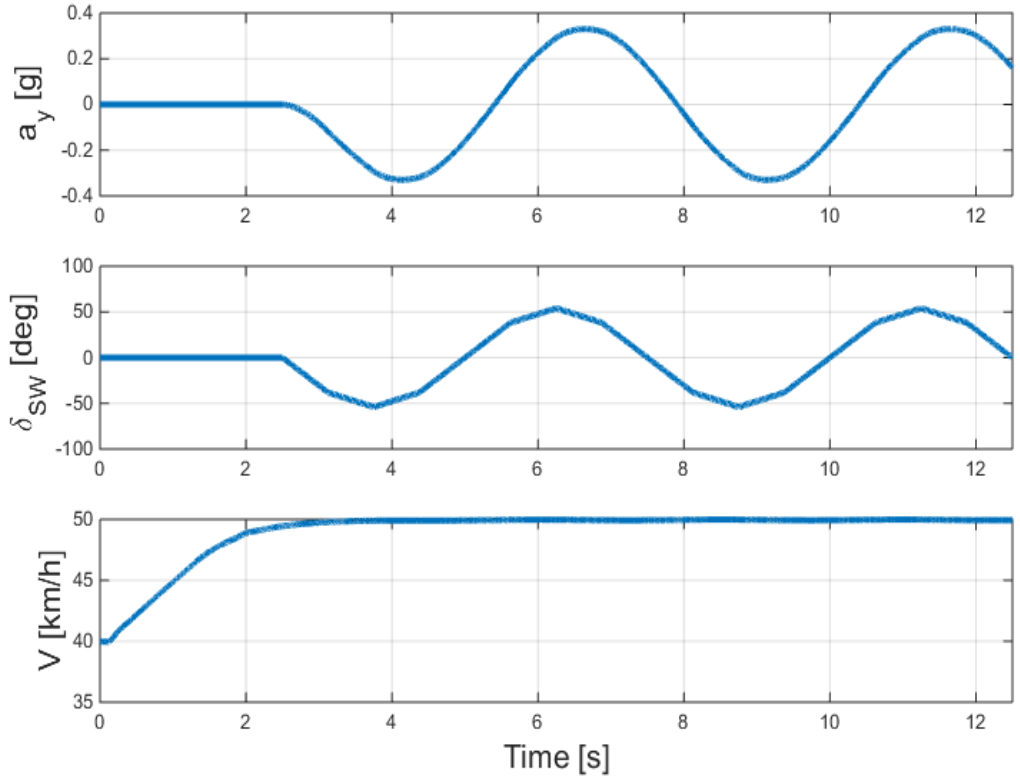

Figure 2-23: Steering performance

Chapter 3

Longitudinal Controller Design

An important aspect of an automated highway system design is the synthesis of an automatic vehicle following system. The term "longitudinal controller" is typically used in referring to any control system that maintains the longitudinal motion of the vehicle, for example, its longitudinal velocity, acceleration or adequate spacing between vehicles in the traffic stream and avoid rear-end collisions in emergency situations. One of the main challenges of automotive vehicle longitudinal control is integrating throttle and brake control.

The familiar examples of longitudinal control are the standard Cruise Control (CC) and Adaptive Cruise Control (ACC) systems. Considering the corresponding driving behavior, ACC systems are generally designed to have specific key characteristics, such as safety, comfort, fuel economy and traffic-flow efficiency. Besides these key characteristics, driver acceptance of the system requires ACC behavior to mimic human driving behavior to some extent.

Safety and comfort objectives can be chosen as the key characteristics of the desired behavior of an ACC. When coming to safety, however, it has to be underlined that the ACC is not a safety system such as an emergency braking system or a collision avoidance system. ACC is primarily a comfort system that incorporates safety in the sense that appropriate driving actions within surrounding traffic are guaranteed. However, for instance, safety of passenger and vehicle has priority in emergency situations and comfort objective is out of issue in oder to avoid possible collisions. To enable quantification of the key characteristics, desirable properties of these characteristics, so-called quantification measures, have to be defined.

The safety of the driving behavior is typically related to the inter-vehicle distance and the relative velocity of the vehicles. Typically, the safety of a traffic situation increases for an increasing inter-vehicle distance and a decreasing relative velocity. Furthermore, higher deceleration levels are beneficial, as a wider range of traffic situations can be handled in a safe manner. Hence, regarding safety, the inter-vehicle distance and the relative velocity will be used as quantifications measures.

Note that pedestrian, cyclist or animal interactions are not considered and target selection is disinterested. It is assumed that target vehicle is always well known with robust radar sensor data. This chapter is organized as follows: practical constraints and longitudinal controller.

3-1 Practical Constraints

The comfort of a driving action is often related to the number, size and frequency of vibrations or oscillations in the longitudinal acceleration of the vehicle due to, for example, external disturbances, engine torque peaks, drive-line characteristics, etc. Besides that, specifically focusing on ACC systems, peak values of longitudinal acceleration are often related to comfort.

For safety, the inter-vehicle distance should always be positive, thus avoiding collisions. For comfort, the values of the longitudinal acceleration of the host vehicle (a_{h_x}) should be constrained.

Additionally, experimental studies on human driving show that in manual driving for 125 people, 98% of the longitudinal accelerations(a_x) were between -2.17 and 1.77 ms^{-2}. Most drivers and passengers feel significantly uncomfortable when the vehicle deceleration is greater than 3 or 4 ms^{-2} (in absolute value). Drivers use large deceleration (greater than 4 ms^{-2} in absolute value) only when they really need to apply severe braking to prevent the vehicle-to-vehicle distance from dropping to an unsafe level. Following inequalities summarize the threshold values as

- Normal Driving : $-2.17\, ms^{-2} \leq a_x \leq 1.77\, ms^{-2}$
- Severe Braking : $-4\, ms^{-2} \leq a_x$

In vehicle-following situations, longitudinal acceleration analysis of manual-driving data over 125 drivers is displayed in Figure 3-1 [21].

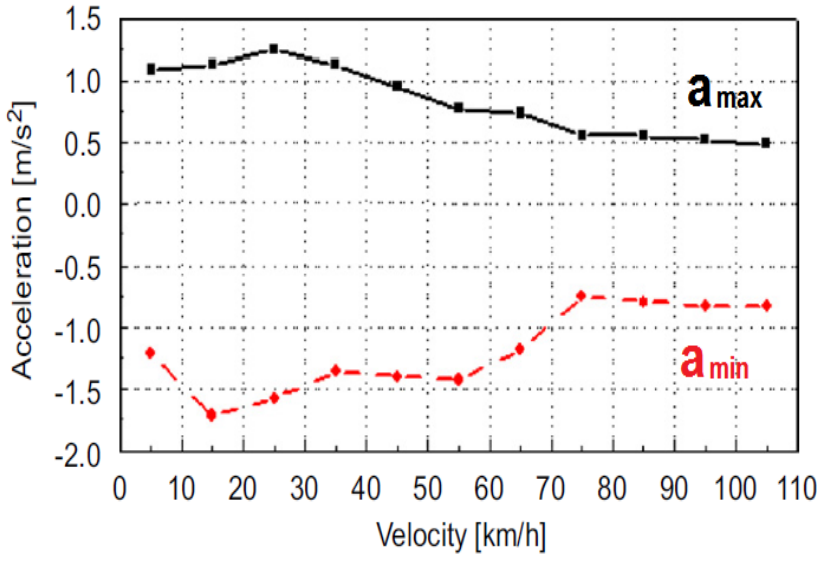

Figure 3-1: Acceleration analysis of manual-driving data over 125 drivers

Apart from the fact that human driving behavior is driver-specific and time-varying, it is also situation-dependent. Generally, situation-dependent behavior is incorporated in the ACC in an ad-hoc manner, by switching between different modes according to different situations.

The key characteristics and the desired situation dependency of the designs give rise to many tuning variables. This makes the design and tuning time consuming and prone to errors. The design of an ACC which is parameterized by few key characteristics is proposed, with at most one tuning variable for safety and comfort objectives. Hence, after the parameterization, the specific setting of the ACC can easily be changed, possibly even by the driver [20].

The design of a parameterized ACC with only a few design parameters, i.e. tuning knobs allows to change the behavior of the ACC. The limited number of intuitive tuning variables enable quick and easy adaptation of the ACC to different desirable driving behavior. Importantly, these variables can also be used by non-experts, like the driver, to change the behavior of the ACC system. Enabling the driver to set these variables, really makes the ACC driver dependent. To obtain an ACC with only a few, intuitive design parameters P_s and P_c are defined, indicating to what extent the driving behavior of an ACC-controlled vehicle is either safe or comfortable, with $P_s \in [0,1]$ and $P_c \in [0,1]$, where larger values for P_s and P_c indicate an increase in safety and comfort respectively. Incorporating P_s and P_c in the controller design yields a parameterized ACC, i.e. ACC(P_s, P_c), with P_s and P_c as tuning variables directly related to the behavior of the ACC. Hence, depending on the driver, the design parameters P_s and P_c can be chosen to accommodate the driver's desirable setting.

Moreover considering comfort and safety as key characteristics, it can be assumed that the key characteristics are complementary: the design of the relations shows that for increasing safety, comfort of the driving decreases, and vice versa. Consequently, these two key characteristics result in a single parameter P:

$$P = P_c, \quad P_s + P_c = 1, \quad P \in [0,1] \tag{3-1}$$

Changing the behavior of the ACC(P) system comes down to adjusting P. Allowing the driver to change $P \in [0,1]$ enables the driver to influence the behavior of the controller individually, focusing on either comfortable or safe driving [20].

The constraints on the acceleration are more involved. For comfort reasons, high accelerations at high velocities should be prohibited. At the same time, however, quickly driving off from standstill should be possible. Hence, the constraint on the maximum longitudinal acceleration $a_{x,max}$ is chosen to depend on the host velocity as a function given by

$$a_{x,max} = (a_{x,0} - P_c)(1 - \frac{v_{h_x}}{v_{h_{x,max}}}) \tag{3-2}$$

where $a_{x,0}$ can be appropriately chosen constant from experimental studies on human driving, such that $a_{x,max}$ decreases for increasing v_{h_x}. This implies approximately full acceleration possibilities at low velocity, whereas this decreases linearly to zero at maximum velocity [20]. For negative acceleration (deceleration) constraint, $a_{x,min} = -a_{x,max}$ is used.

3-2 Longitudinal Controller

Longitudinal controller operates in 2 main modes depending on the situation of the traffic ahead; Velocity Control (VC) and Spacing Control (SC) modes. It operates in the Velocity Control (VC) mode when the road in front of the ACC equipped vehicle is clear, i.e. there is no vehicle within clearance distance. In this situation vehicle travels at the desired cruising speed which is set up by the driver. Once it has approached to other vehicles (traveling at lower-speed) it switches to Spacing Control (SC) mode. In this mode, longitudinal controller attempts to keep the vehicle within the desired distance headway as depicted in Figure 3-2, by controlling the speed of the vehicle. The distance headway can be customized by the driver. The transition between the modes is performed automatically by considering the traffic condition ahead and the desired cruising speed [13].

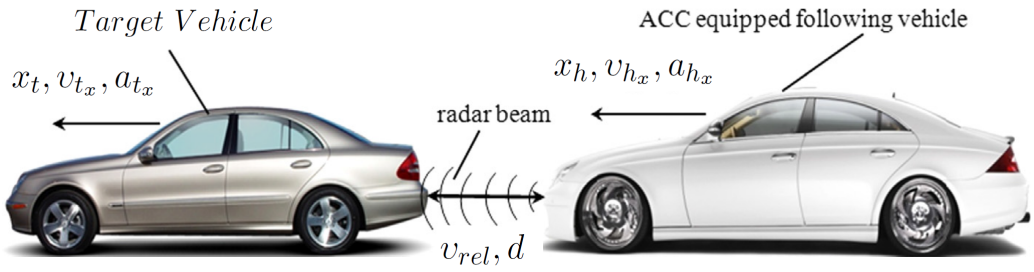

Figure 3-2: An ACC equipped vehicle following another vehicle in front

The longitudinal controller consists two levels of control: the upper-level and the low-level controller as demonstrated in Figure 3-3. The longitudinal acceleration is used to track the desired acceleration through feedback control.

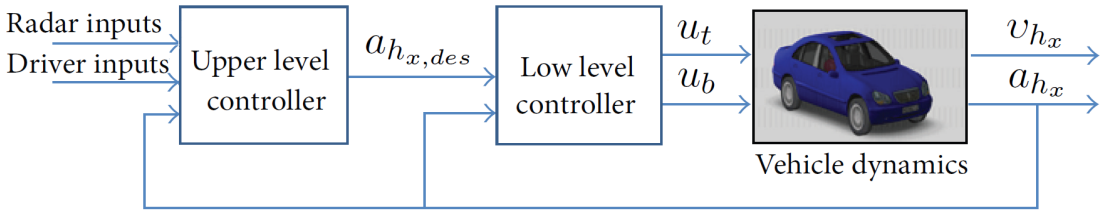

Figure 3-3: The block diagram of longitudinal controller

3-2-1 Upper-Level Controller

The main functionality of the upper-level controller is to compute the desired acceleration for the ACC-equipped vehicle that achieves the desired spacing or velocity by using the driver inputs: the radar measurements, and the current distance and velocity of the ACC-equipped vehicle relative to a target vehicle. The computed acceleration command is transmitted to the low-level controller to compute and implement the corresponding actuation commands as needed as depicted in Figure 3-3.

The upper-level controller determines the host vehicle's acceleration through a combination of relative speed and distance to maintain a desired headway between two vehicles. Maximum acceleration levels are limited for human comfort. The required acceleration is calculated, and the drive-line model and an inverse engine map are used to convert the required acceleration to the throttle command for the host vehicle.

The upper-level controller operates in two main control modes and the hierarchical structure has been drawn in Figure 3-4. In the following sections, these main control modes are presented.

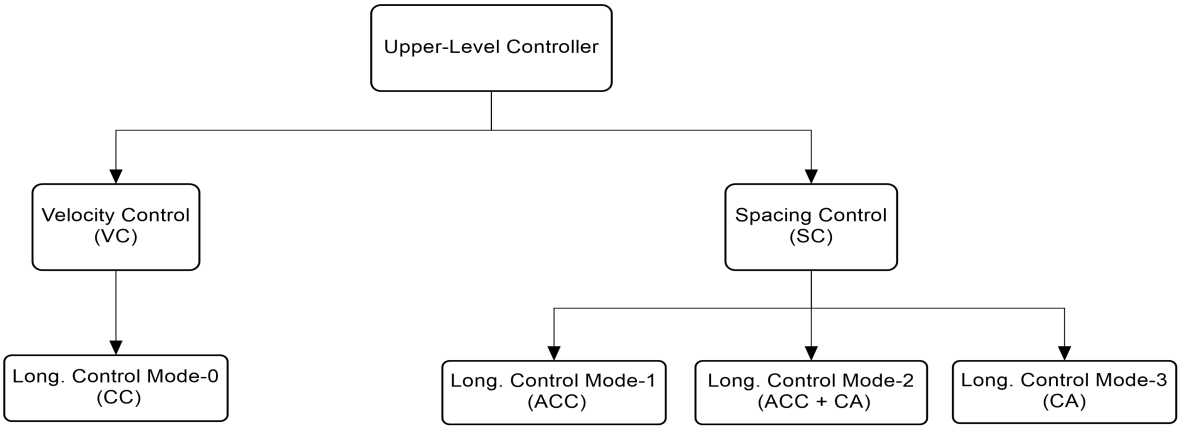

Figure 3-4: The hierarchy of upper-level controller

I. Velocity Control

In this mode or namely Longitudinal Control Mode-0, the radar does not detect any vehicle in the path of the ACC-equipped vehicle. The longitudinal controller essentially acts like the conventional Cruise Controller (CC). Therefore, the ACC equipped vehicle's velocity is maintained at desired velocity set by the driver.

In order to synthesizing a controller, initially plant modeling is done based on a block diagram model that implements known differential-algebraic equations governing vehicle dynamics. Nonlinear two-wheeled vehicle model is linearized around operating point which is a value of vehicle velocity. For this case, linearizing the nonlinear vehicle model involves approximating the behavior of that model that runs around 100 km/h. Bode plot for linearized model is demonstrated in Figure 3-5. Note that bode diagram is a graph of the frequency response of linearized model from point $a_{h_{x,des}}$ to v_{h_x}. The above-mentioned points are visualized in the block diagram of longitudinal controller in Figure 3-3.

A controller can then be synthesized based on these characteristics. A Proportional-Derivative (PD) controller is proposed based on these characteristics in order to adjust the throttle input such that the vehicle acceleration tracks the desired acceleration profile, which is designed so that the vehicle velocity converges to the user-set velocity. The control law for computing the desired acceleration command is defined as

$$v_{h,error}(t) = v_{h_x}(t) - v_{h,set}(t) \tag{3-3}$$

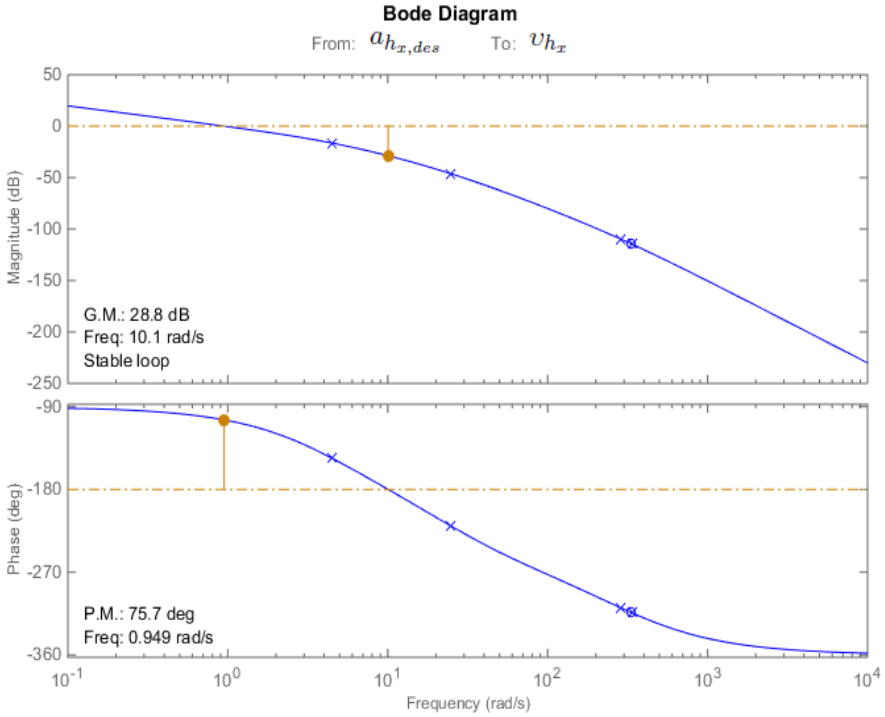

Figure 3-5: The Bode plot for the linearized model

$$a_{h_{x,CM0}}(t) = K_P v_{h,error}(t) + K_D \frac{d}{dt} v_{h,error}(t) \tag{3-4}$$

where K_P is the proportional control gain, K_D is the derivative control gain, $v_{h,set}$ is the user-set velocity of the host vehicle, and v_{h_x} is the velocity of the host or ACC-equipped vehicle. The control gains K_P and K_D are tuned carefully that the vehicle velocity converges quickly to the user-set velocity without steady-state error.

In order to improve ride quality and comfort, the desired acceleration is restricted between velocity-dependent $a_{x,max}(.)$ and $a_{x,min}(.)$ constraints:

$$a_{h_{x,des}}(t) = \begin{cases} a_{x,max}(v_{h_x}) & \text{if} \quad a_{h_{x,CM0}} > a_{x,max}(v_{h_x}) \\ a_{h_{x,CM0}} & \text{if} \quad a_{x,min}(v_{h_x}) \leq a_{h_{x,CM0}} \leq a_{x,max}(v_{h_x}) \\ a_{x,min}(v_{h_x}) & \text{if} \quad a_{h_{x,CM0}} < a_{x,min}(v_{h_x}) \end{cases} \tag{3-5}$$

II. Spacing Control

The Spacing Control (SC) mode is enabled when the radar detects a target vehicle in the ACC equipped vehicle's path, and the longitudinal control system controls the vehicle to maintain a desired distance based on the velocity of the host vehicle and a user-specified time gap.

A. Spacing Policy

Typically, the primary control objective of an ACC system is to follow a target vehicle at a desired distance d_{des}. Often, a so-called desired constant headway time t_{hw} is used to define

this desired distance, yielding

$$d_{des} = d_0 + v_{h_x} t_{hw} \tag{3-6}$$

with d_0 a constant representing the desired distance at standstill, and the desired headway time t_{hw} a measure for the time it takes to reach the current position of the target vehicle if the host vehicle continues to drive with its current velocity, i.e. for constant v_{h_x}. The design parameters of the cruise control principle, d_0 and t_{hw}, can be tuned to suit the driver.

The quantification measures related to safety are the distance and the relative velocity. The desired distance is translated into a desired headway time t_{hw}, which is typically varied between 1.0 and about 2.0 second. Human driving behavior shows a somewhat wider range, in between 0.5 and about 2.5 second. The larger the headway time signifies more time for the controller that it has to react to a certain traffic situation. Besides that, if the controller cannot handle a specific situation appropriately, the driver has more time to intervene. Hence, the larger the headway time, the safer the driving will be. A corresponding relationship between t_{hw} and P_s is

$$t_{hw} = 0.5 + 2P_s \tag{3-7}$$

yielding $t_{hw} \in [0.5, 2.5]$ which is a sufficiently large range [20].

B. Indexes for Driving Conditions

ACC and other advanced features, such as Collision Warning (CW) and Collision Avoidance (CA) systems always work with a co-existing human driver, they can be useful to the driver and their control logic and operational characteristics need to be similar to the decision-making and driving characteristics of the human driver.

To integrate ACC and CA systems, a longitudinal controller that consists of index-based control modes and scheduling of acceleration with respect to control modes is proposed [21]. The proposed control strategy enables a host vehicle to operate in three control modes: ACC, ACC+CA and CA. The developed control modes are determined by two indexes: a warning index and an inverse TTC. Since it is important to select the parameters which are related to the transitions between the three control modes, parameters of the proposed controller are tuned by using a confusion matrix and manual-driving data under no-crashing.

As shown in Figure 3-6, the design of an ACC system with Collision Avoidance consists of upper-level and low-level controllers. The upper-level controller uses the longitudinal velocity (v_{h_x}) obtained via speedometer; relative distance ($d_{measured}$) and relative velocity ($v_{rel,measured}$) provided through radar sensor's outputs. Actual definition of above-mentioned terms are given as below

$$v_{rel} = v_{t_x} - v_{h_x} \tag{3-8}$$

$$d = x_t - x_h \tag{3-9}$$

where v_{rel} is relative velocity, v_{t_x} is the velocity of the target vehicle, d is the actual gap distance between vehicles, x_t and x_h are displacement of target and host vehicle respectively.

These measurements are used to calculate indexes and the desired acceleration. Based on the calculated indexes, the upper-level controller determines driving situations that are classified

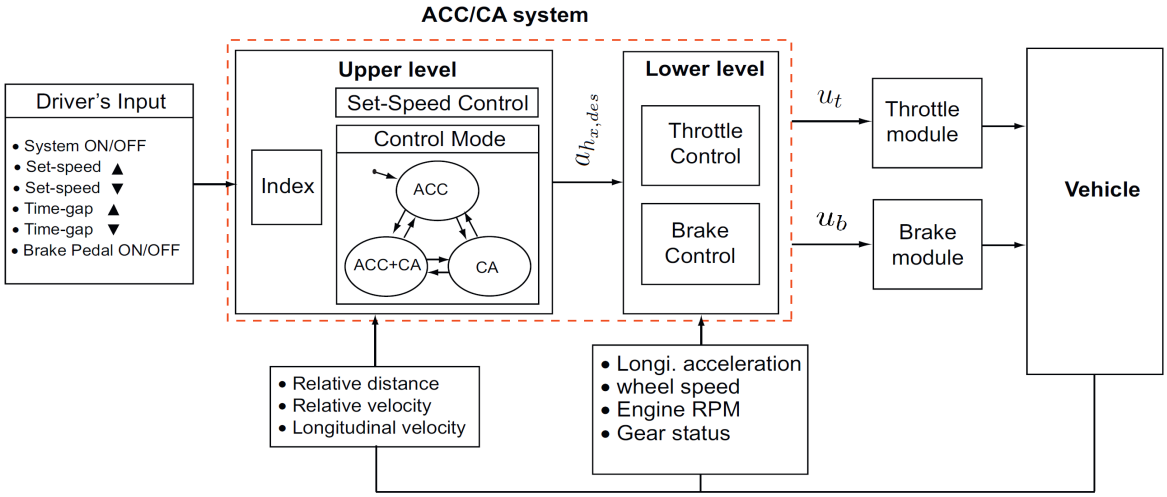

Figure 3-6: Scheme of an ACC system with a CA system

as: "safe", "warning" and "dangerous". In line with the driving situation, it determines the control input, which is the desired acceleration.

A non-dimensional warning index and an inverse TTC are used to determine driving situations. Time to Collision (TTC) has been used in the analysis of driving behavior of a driver of the host vehicle. Most of the existing CA/CW systems use a similar algorithm based on the braking-critical distance and the warning-critical distance. The non-dimensional warning index κ, which represents the danger of physical collision in the current driving situation, is defined as follows [21]:

$$\kappa = \frac{d_{measured} - d_{brc}}{d_{wc} - d_{brc}} \tag{3-10}$$

where $d_{measured}$ is the measured vehicle gap by radar, and d_{br} and d_w are the braking-critical and warning-critical distances respectively. If $d_{measured}$ exceeds d_{br} and d_w, then the warning index is a positive value that is greater than unity and indicates that the current driving situation is in a safe region. If $d_{measured}$ is below d_{br}, then the warning index is a negative value and indicates that the current driving situation can be dangerous. The warning-critical and braking-critical distances are defined as follows:

$$d_{brc} = v_{rel,measured}\tau_s + \frac{v_{h_x}^2 - (v_{h_x} - v_{rel,measured})^2}{2\mu g} \tag{3-11}$$

$$d_{wc} = v_{rel,measured}\tau_s + \frac{v_{h_x}^2 - (v_{h_x} - v_{rel,measured})^2}{2\mu g} + v_{rel,measured}\tau_h \tag{3-12}$$

where $v_{rel,measured}$ is the measured relative velocity between the host vehicle and the target vehicle by radar, τ_s is the system delay, which is given by the brake-system hardware, v_{h_x} is the velocity of the host vehicle, τ_h is the delay in human response between recognition and manipulation, g is gravitational acceleration, and μ is the tire-road friction coefficient. These terms can be derived from the kinematics of the two vehicles that brake to a full stop [21]. If the vehicles start at this distance and brake with their maximum decelerations, they will

come to a stop with their bumpers touching each other. To make the critical distance more conservative, two delay terms are added; these account for system and driver delays.

The steady-following is defined as a following situation at a small relative velocity. The inverse of the Time to Collision (TTC^{-1}) is used to define the driver's steady-following situation in this study. The TTC, which is a well-known parameter in CW/CA systems [21], is defined as

$$TTC = \frac{d_{measured}}{v_{rel,measured}} \tag{3-13}$$

In the case where the target vehicle's velocity is constant, the host vehicle's speed converges to the target vehicle's speed and the host vehicle follows the target vehicle at a nearly constant distance. Therefore, the steady-following of a human driver can be defined as a situation with a small value of the inverse of the TTC. If the inverse TTC is positive, it indicates that the host vehicle is moving too close to the target vehicle. The inverse TTC is related to the visual cues that might guide driver headway maintenance. The concept of looming, as described in human-factor studies, is employed in the analysis of human perception and longitudinal control behavior in driving situations.

Generally speaking, a driver executes three behaviors while driving a vehicle: perception, decision and manipulation. In this scope, the driver's perception of the target vehicle's motion, in relation to the host vehicle, is represented as two indexes, the warning index and the inverse TTC. The result of decision and manipulation of the driver for the given driving situation is considered to be the resultant acceleration of the host vehicle. In this context, relationships between the warning index and the deceleration of the host vehicle have been investigated using manual-driving data. Further, relationships between the inverse TTC and the deceleration of the host vehicle have been investigated. Therefore, the warning index and the inverse TTC can be used to determine a driving situation [21].

C. Driving Situations and Control Modes

When the vehicle deceleration is smaller than 2 ms^{-2} (in absolute value), the driving situation is considered to be a "safe situation". When the absolute magnitude of the vehicle deceleration is greater than 4 ms^{-2}, the driving situation is considered to be a "severe braking or dangerous situation" [21]. The driving situations are divided into: comfort-mode (Longitudinal Control Mode-1), large-deceleration mode (Longitudinal Control Mode-2) and severe-braking situation (Longitudinal Control Mode-3) as follows:

- Longitudinal Control Mode-1 (comfort mode) : $a_{h_x} > -2\, ms^{-2}$
- Longitudinal Control Mode-2 (large deceleration mode) : $-2\, ms^{-2} \geq a_{h_x} > -4\, ms^{-2}$
- Longitudinal Control Mode-3 (severe braking mode) : $-4\, ms^{-2} \geq a_{h_x}$

As shown in Figure 3-7, the driving situations can be analyzed in a two-dimensional graph of the warning index versus the inverse TTC. When the warning index is high and the inverse TTC is low, the driving situation is in a safe region. However, if the warning index decreases or the inverse TTC gradually increases, the danger of a rear-end collision increases and the vehicle needs to quickly decelerate to avoid the warning region. When the warning index is

low and the inverse TTC is high, the driving situation is critical and therefore, the emergency brake should be applied. The relationship between indexes and control modes are defined as follows:

- $\kappa \geq \kappa_1$ **AND** $TTC^{-1} \leq iT_1 \Rightarrow$ Longitudinal Control Mode-1, ACC
- $\kappa < \kappa_1$ **OR** $iT_1 < TTC^{-1} \Rightarrow$ Longitudinal Control Mode-2, ACC + CA
- $\kappa \leq \kappa_2$ **AND** $iT_2 < TTC^{-1} \Rightarrow$ Longitudinal Control Mode-3, CA

where κ_1 and κ_2 are the warning-index thresholds and iT_1 and iT_2 are the inverse TTC thresholds. It is important to select appropriate threshold values for the warning index and the inverse TTC that are acceptable to drivers and that improve safety. For example, frequent warning and braking are likely to annoy the driver and are therefore unnecessary. On the other hand, less sensitive warning and braking may cause the driver to feel unsafe. Therefore, the parameters in expression for transition of the control mode should be based on manual-driving data in no-crash driving situations.

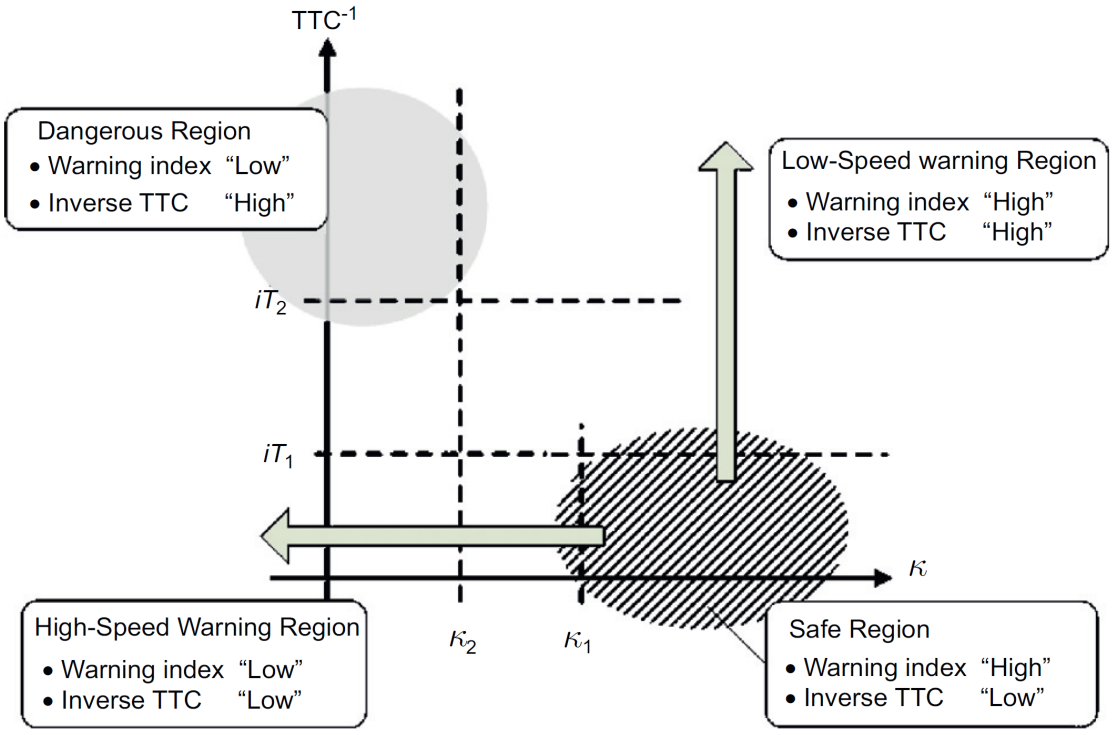

Figure 3-7: The warning index and the inverse TTC for various driving situations

Generally, human factors are crucial for vehicles with ACC systems and are of primary importance in the development of CW/CA systems. In this context, it is important to tune the parameters in integrated ACC/CA systems. To be acceptable by a human driver, the parameters for transition of the control mode (namely, the threshold values) should be determined based on manual-driving data in no-crash driving situations, including comfort-driving and severe-braking situations.

In the case of ACC/CA controllers, the driving situation is determined through two indexes, the warning index and the inverse TTC. Therefore, it is necessary to investigate a relationship between these two indexes and the deceleration level to find the threshold values for the three control modes.

Table 3-1: Threshold values for the warning index and the inverse TTCs

Acceleration(ms^{-2})	Warning index (κ)	TTC^{-1}
-2	1.19	0.21
-4	0.81	0.49
-6	0.65	0.68
-8	0.10	1.30

As summarized in Table 3-1, the threshold values of the warning index are determined as $\kappa_1 = 1.19$, $\kappa_2 = 0.81$; and the threshold values of the inverse TTC are determined as $iT_1 = 0.21$, $iT_2 = 0.49$ [21].

D. Computation of the Desired Acceleration for Control Modes

Basically, linear optimal control theory has been used to design the desired acceleration in normal vehicle-following situations. Using integrators to model the vehicles, a state-space model for the host and target vehicles can be written as follows

$$\dot{\chi}_x = A_x\chi_x + B_x u_x + \Gamma_x w_x = \begin{bmatrix} 0 & -1 \\ 0 & 0 \end{bmatrix} \chi_x + \begin{bmatrix} 0 \\ -1 \end{bmatrix} u_x + \begin{bmatrix} \tau \\ 1 \end{bmatrix} w_x \tag{3-14}$$

where τ is the linear coefficient, i.e. the t_{gap}, the input u_x is the host vehicle's acceleration, the disturbance w_x is the target vehicle's acceleration and states are

$$\chi_x^T = \begin{bmatrix} \chi_{x,1} & \chi_{x,2} \end{bmatrix} = \begin{bmatrix} d_{error} & \upsilon_{rel,measured} \end{bmatrix} \tag{3-15}$$

$$d_{error} = d_{des} - d_{measured} \tag{3-16}$$

where d_{error} is distance error [21]. The control of the ACC/CA vehicle can be seen as a linear-quadratic optimization problem, namely, the design of the state-feedback control principle for minimizing the following-distance error and the speed error, and the control input:

$$J_x = \int_0^\infty (\chi_x^T Q_x \chi_x + u_x^T R_x u_x) dt \tag{3-17}$$

The weighting matrices Q_x and R_x are defined as follows

$$Q_x = \begin{bmatrix} Q_{d_{error}} & 0 \\ 0 & Q_{\upsilon_{rel}} \end{bmatrix} \quad R_x = \begin{bmatrix} R_{a_{h_x}} \end{bmatrix} \tag{3-18}$$

The gains for the state-feedback principle $u_x = -K_x\chi_x$, are chosen to minimize the cost function. The desired acceleration of the host vehicle can be determined by solving Equation (3-17). According to Lyapunov's second method and Riccati equation:

$$A_x^T P_x + P_x A_x - P_x B_x R_x^{-1} B_x^T P_x + Q_x = 0 \tag{3-19}$$

The coefficient matrix K_x can be obtained by

$$K_x = R_x^{-1} B_x^T P_x \tag{3-20}$$

where P_x is the positive-definite steady-state solution of the Riccati equation. Therefore, the desired acceleration is represented by

$$a_{h_{x,CM1}}(t) = -K_x(t)\chi_x(t) = -k_{x,1}(v_{h_x}(t))d_{error}(t) - k_{x,2}(v_{h_x}(t))v_{rel}(t) \tag{3-21}$$

where $k_{x,1}(.)$ and $k_{x,2}(.)$ are the control gains as a function of the host vehicle's speed $v_{h_x}(t)$, and have been obtained by tuning the weighting matrices Q_x and R_x. Since the weighting matrices Q_x and R_x, impact on the performance of this following-system, the weighting factors $Q_{d_{error}}$, $Q_{v_{rel}}$ and $R_{a_{h_x}}$ have been chosen to achieve naturalistic behavior of the host vehicle that would seem natural to a human driver in normal-driving situations.

Furthermore, the weight $Q_{d_{error}}$, which is the weight on the error d_{error} between the desired and the actual distance, has to be considered. The larger $Q_{d_{error}}$, the smaller the time to reach a steady-state situation, i.e. $d_{error}(k) = 0$, which is desirable regarding safety. A corresponding relation between $Q_{d_{error}}$ and P_s is $Q_{d_{error}} = q_{d_{error}} P_s$ with $q_{d_{error}} \geq 0$ a positive constant. Although the focus is on safety, it has to be remarked that for increasing $Q_{d_{error}}$, the acceleration and deceleration peaks will increase as well, which indicates less comfortable driving behavior.

Also the relative velocity $v_{rel,measured}$ should be minimized as fast as possible. This is influenced by the weight $Q_{v_{rel}}$. Hence, whether increasing or decreasing $Q_{v_{rel}}$ increases or decreases the safety of the driving behavior, depends on the situation. Consequently, a constant value $Q_{v_{rel}} = q_{v_{rel}}$ is adopted, ensuring on average desirable behavior.

The weight $R_{a_{h_x}}$ is naturally related to resulting acceleration peak values and, hence, to the amount of comfort. The higher $R_{a_{h_x}}$, the lower the corresponding acceleration peak values are and, consequently, the more comfortable the driving behavior is. This yields $R_{a_{h_x}} = r_{a_{h_x}} P_c$ with $q_{a_{h_x}} \geq 0$ positive constant [20].

In addition, alternative weighting factors have been used for low-, medium-, and high-speed ranges. For "Longitudinal Control Mode-1", the desired acceleration is represented by

$$u_x(t) = a_{h_{x,des}}(t) = \begin{cases} a_{x,max}(v_{h_x}) & \text{if} \quad a_{h_{x,CM1}} > a_{x,max}(v_{h_x}) \\ a_{h_{x,CM1}} & \text{if} \quad a_{x,min}(v_{h_x}) \leq a_{h_{x,CM1}} \leq a_{x,max}(v_{h_x}) \\ a_{x,min}(v_{h_x}) & \text{if} \quad a_{h_{x,CM1}} < a_{x,min}(v_{h_x}) \end{cases} \tag{3-22}$$

As shown in Equation (3-22), the desired acceleration is restricted by the maximum and minimum acceleration, $a_{x,max}(.)$ and $a_{x,min}(.)$ to improve ride comfort. The velocity-dependent $a_{x,max}(.)$ and $a_{x,min}(.)$ are based on the statistical analysis of the manual-driving data of 125 drivers. Manual-driving data for normal vehicle-following situations show that drivers use relatively large acceleration in low-speed, vehicle-following situations [21].

The desired acceleration is computed by using the velocity-dependent optimal gain and restricted by the acceleration limit. The control gains for low-speed driving situations are determined by Equation (3-20) to obtain good vehicle-following performance. Since in the case of high-speed driving situations, ride comfort is a more important factor in target vehicle

following, the control gains are designed to obtain smooth vehicle behavior. All velocity-dependent control gains $k_{x,1}(.)$ and $k_{x,2}(.)$ are designed towards naturalistic behavior of the host vehicle similar to the behavior of manually driven vehicles in normal-driving situations.

In the case of "Longitudinal Control Mode-2" the desired acceleration is computed in the same manner as for "Longitudinal Control Mode-1" and the deceleration limit is extended to -4 ms^{-2}; refer Equation (3-23). This implies that the desired acceleration of this mode can be larger than that of "Longitudinal Control Mode-1" for improving safety:

$$a_{h_{x,CM2}}(t) = -K_x(t)\chi_x(t) = -k_{x,1}(v_{h_x}(t))d_{error}(t) - k_{x,2}(v_{h_x}(t))v_{rel}(t) \tag{3-23}$$

$$u_x(t) = a_{h_{x,des}}(t) = \begin{cases} a_{h_{x,CM2}}(t) & \text{if} \quad a_{h_{x,CM2}}(t) > -4\, ms^{-2} \\ -4\, ms^{-2} & \text{else} \end{cases} \tag{3-24}$$

In the case of "Longitudinal Control Mode-3", the desired acceleration is computed by using non-linear functions that map the indexes to the desired accelerations. The functions, $f_1(.)$ and $f_2(.)$, are obtained by using the confusion-matrix method on manual-driving data in no-crash driving situations, including comfort-driving and severe-braking situations. As shown in Figure 3-8, the function $f_1(.)$ is a table that represents the relationship between the warning index and the deceleration of the vehicle while $f_2(.)$ is a table that represents the relationship between the inverse TTC and the deceleration of the vehicle. From the investigation of manual-driving data, it is found that the warning index is closely related to the driver's decisions and to the vehicle-acceleration behavior in medium-and high-speed driving situations and to the inverse TTC in low-speed driving situations. These facts have been incorporated into the design of the desired vehicle acceleration $a_{h_{x,des}}$ in severe-braking situations. The desired acceleration is computed as

$$a_{h_{x,CM3}}(t) = W_1(v_{h_x}(t))f_1(\kappa) + W_2(v_{h_x}(t))f_2(TTC^{-1}) \tag{3-25}$$

$$u_x(t) = a_{h_{x,des}}(t) = \begin{cases} a_{h_{x,CM3}}(t) & \text{if} \quad a_{h_{x,CM3}}(t) > -\mu g \quad ms^{-2} \\ -\mu g \quad ms^{-2} & \text{else} \end{cases} \tag{3-26}$$

where W_1 and W_2 are the weighting factors, which are defined as a function of the vehicle speed. The computation of the desired acceleration in severe-braking situations is illustrated in Figure 3-8. The weight function is used to develop a non-linear function for the warning index and the inverse TTC.

Equation (3-10), (3-11) and (3-12) imply that the warning index can be sensitive in high-speed driving. As a human driver tends to maintain a large distance in high-speed driving, the inverse TTC in high-speed driving can be smaller than that in low-speed driving. Therefore, the inverse TTC can be sensitive in low-speed driving [21]. In this context, the weight function is established as shown in Figure 3-8.

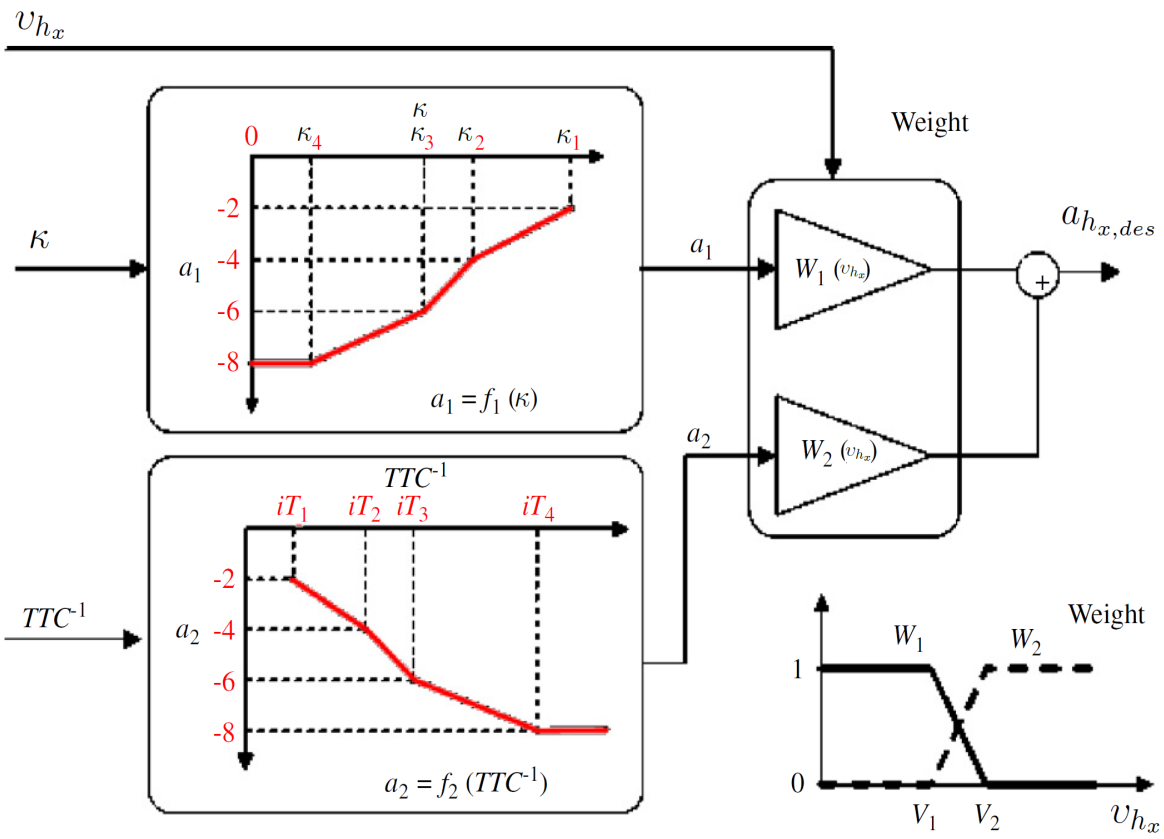

Figure 3-8: Design of the desired acceleration in severe-braking situations

III. Velocity/Spacing Control Mode Switching Logic

A switching logic has devised for the longitudinal control system which is utilized to implement automated switching between the two main operation modes: Velocity Control (VC) and Spacing Control (SC) modes. The switching rules for transition between these modes are illustrated in Table 3-2 [13].

Table 3-2: Logical rule for switching between VC and SC modes

	$v_{h_x} < v_{h,set}$	$v_{h_x} \geq v_{h,set}$ and $v_{rel} < 0$	$v_{h_x} \geq v_{h,set}$ and $v_{rel} \geq 0$
$d_{measured} \leq d_{des}$	SC	SC	VC
$d_{measured} > d_{des}$	VC	VC	VC

3-2-2 Low-Level Controller

The main objective of the low-level controller is twofold. First, using the desired acceleration command from the upper-level controller, the low-level controller determines whether to apply braking control or throttle control. Secondly, the required control command is applied to the vehicle so that the acceleration of the vehicle tracks a desired acceleration. The applied

control command is either throttle or braking input. In short, the control principles of the throttle or brake are based on reverse dynamics.

I. Throttle/Brake Control Switching Logic

A proper logical algorithm needs to be devised in order to provide smooth switching between the brake and throttle controllers. Coordinated operation between the brake and throttle is crucial due to the following reasons:

Frequent switching between the brake and the throttle or chattering has negative impact on the longitudinal dynamic of the vehicle as it causes the variation of vehicle's acceleration which provides an uncomfortable environment for passengers. Also, this behavior causes rapid damage in vehicle's components. The frequent and rapid switching between throttle and brake causes loss of the energy, and therefore increases the fuel consumption. Inappropriate switching can be a source of instability and disturbance in the system which makes the control design task more complicated [13].

The switching logic component shown in Figure 3-9 determines, based on the desired acceleration from the upper-level controller, whether a brake torque or engine torque is required to achieve the desired acceleration. Typically, it is common to assume that a simple logic for choosing between brake and engine control can be based on the sign of the desired acceleration; that is, if the acceleration is greater than or equal to zero, then engine control should be applied, otherwise the brake control should be applied [12].

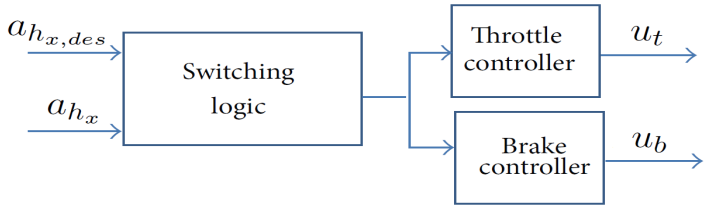

Figure 3-9: Low-level controller

Switching logic with the boundary layer h_b is necessary to avoid frequent switching between throttle and brake controls [17]. Depending on the desired acceleration that the ACC vehicle must follow, the ACC controller applies throttle or brake control. Figure 3-10 shows a switching line with boundary layer. The switching line indicates the vehicle acceleration (the minimum acceleration $a_{h,min}$) when the throttle is closed ($u_t = 0$) for a host vehicle velocity. The minimum acceleration line has been used as a switching line in the throttle/brake controls. The ACC controller applies throttle control when $a_{h_{x,des}} \geq a_{h,min} + h_b$ or brake control when $a_{h_{x,des}} \leq a_{h,min} - h_b$ for a given vehicle speed.

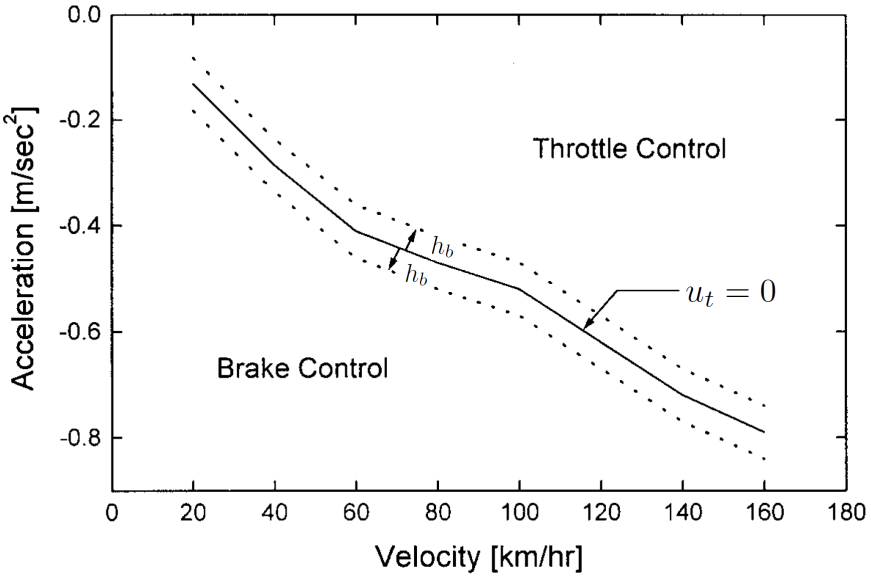

Figure 3-10: Throttle/brake switching logic with the boundary layer

II. Throttle Control

At low level of acceleration, wheel slip is quite small. A throttle control law has been derived under a no-slip condition of the driving wheels [17]. A block diagram of the throttle control law is shown in Figure 3-11.

It uses the desired and actual longitudinal acceleration $a_{h_x}, a_{h_{x,des}}$, driving resistance forces F_D, F_R, F_g, engine speed N_e and gear status i_g, i_f. When engine control torque is required, the throttle controller converts the computed desired acceleration into a throttle input $u_{t,des}$ that is required to achieve the acceleration.

The controller first converts desired acceleration into a desired engine net torque. Since the inertia of the wheel and axle is relatively small compared with the vehicle mass, the desired engine net torque $T_{e,des}$ can be computed with $T_b = 0$ as follows [17]

$$T_{e,des} = \frac{r(ma_{h_{x,des}} + F_D + F_R \pm F_g) + T_b}{i_g i_f} \tag{3-27}$$

where r is the effective tire radius and T_b the total brake torque. The computed desired torque is converted into a throttle input command by using an inverse engine map based on the current engine speed. In inverse engine map technique, it is performed by interpolating the data from an engine map lookup table for the vehicle. Due to the inaccuracies from the obtained engine map, an additional Proportional-Integral (PI) controller is integrated to throttle controller to ensure that the desired acceleration is achieved [12].

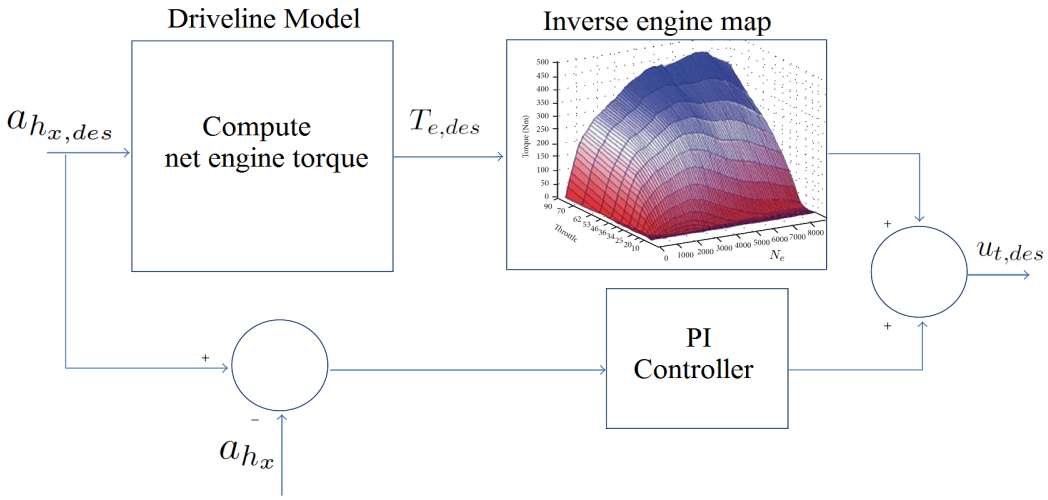

Figure 3-11: Throttle controller

III. Brake Control

The brake torque is applied when the engine braking is not sufficient to follow the desired acceleration. When braking control torque is required, the brake controller converts the desired acceleration to an appropriate brake command. A block diagram of the brake control algorithm is shown in Figure 3-12. When the desired acceleration for a given vehicle velocity is smaller than the switching line, i.e. the brake control region, the desired brake torque, $T_{b,des}$ is computed as follows [17]

$$T_{b,des} = -r(ma_{h_{x,des}} + F_D + F_R \pm F_g) + T_w \tag{3-28}$$

The computed desired brake torque is then converted to an equivalent brake line pressure. Since the total brake torque which is computed from the motion of the vehicle is proportional to the brake pressure, the desired brake pressure, $P_{b,des}$, can be obtained as

$$P_{b,des} = \frac{1}{K_b} T_{b,des} \tag{3-29}$$

where K_b is the lumped gain for the entire brake system. K_b lumps all the uncertainties in the brake model from the brake pressure to the brake torque. At last step, the value of position of the brake pedal $u_{b,des}$ is applied as the control input to the vehicle.

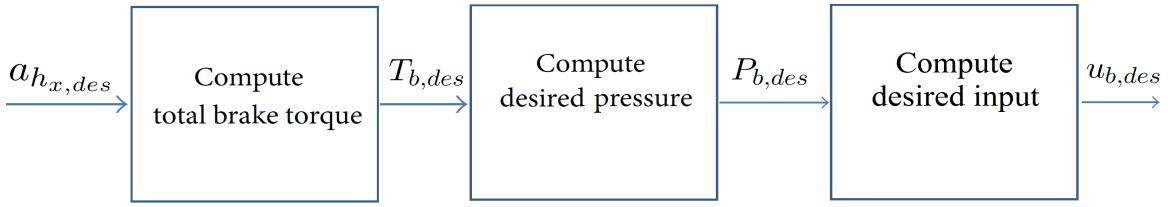

Figure 3-12: Brake controller

Chapter 4

Lateral Controller Design

Lateral vehicle control involves the steering of the vehicle. There are two ways to design steering controllers: either imitating human drivers or controller design using dynamic models of vehicle. The first approach does not need detailed knowledge of vehicle dynamics, much in the way the driver of a vehicle does not. The control system approach requires detailed knowledge of the dynamics of the vehicle and has to use different algorithms to perform the different maneuvers.

Lateral control primarily maintains the host vehicle in the center of the lane while maintaining good passenger comfort by restricting lateral acceleration of the host vehicle. Since some highway fatalities are caused from single vehicles leaving the road, automated steering could greatly reduce highway deaths by preventing lane departure and steering overcorrection.

The main objective of lane keeping is to perform automatic steering of the vehicle in order to keep it in the middle of the road in spite of changes in road conditions, curvatures and other disturbances. The control system for lane keeping is usually designed to detect any difference between host vehicle and the reference line on the road with on-board sensors.

Lane keeping is modeled as a path tracking problem for the purpose of designing the steering controller. For a nominal road curvature , the controller is designed to track the lateral position and yaw angle trajectories using measurements of the vehicle's lateral position and yaw angle relative to the present lane center. The lateral position and yaw angle trajectories are determined from desired lateral acceleration and yaw rate for the given road curvature.

Lane keeping is simply combination of lateral control and desired speed determination. In lane keeping, path planning is the most important part of this motion. It is assumed that pre-stored GPS data is accurate for path trajectory. Note that lane changing or overtaking maneuver of host vehicle is not considered. This chapter is organized as follows: practical constraints, road information, linearized model, steering controller and desired speed determination.

4-1 Practical Constraints

For human comfort, the values of the lateral acceleration of the host vehicle (a_{h_y}) should be constrained as well. The experimental study on human driving which primarily concerns lateral acceleration (a_y) in highways reveals comfort limits in lateral plane [3]. According to this experimental study, the threshold values of comfort, medium comfort and discomfort levels are summarized respectively as

- Comfort Level : $|a_y| \leq 1.8\, ms^{-2}$
- Medium Comfort Level: $|a_y| \leq 3.6\, ms^{-2}$
- Discomfort Level : $|a_y| \leq 5\, ms^{-2}$

Figure 4-1 shows the distribution of the lateral accelerations for three highways with six lanes. With three lanes in the same driving direction, it is easy for a driver to overtake a slower passenger car by changing lanes and reaching expected speed. The characteristic percentiles of the lateral acceleration were obtained in each speed section: the minimum value (a_{ymin}), maximum value (a_{ymax}), 50th percentile (a_{y50}), 85th percentile (a_{y85}), and average value (a_{yave}). As shown in Figure 4-1, the minimum value of lateral acceleration was almost constant, and the other lateral acceleration decreased with an increase in the speed. A unitary regression model was set up for each percentile line. The a_{y85}, a_{y50}, and a_{yave} values were slightly concave in form and negatively related to the speed [3]. In addition, the lateral acceleration a_{y85} percentile is the most appropriate for a limit value. The relation between a_{y85} and the speed can be expressed as follows

$$|a_{h_y}| = a_{y85} = a_{y,0}(1 - P_c)(1 - \frac{\upsilon_{h_x}}{\upsilon_{h_{x,max}}}) \tag{4-1}$$

where $a_{y,0}$ can be appropriately chosen constant.

Furthermore, the steering system has physical constraints on maximum and minimum steering $-30deg \leq \delta_f \leq 30deg$ [9]. For comfort and safety reasons, high steering at high speeds should be prohibited. In order to allow high steering capability at low speeds and limited steering capability at high speeds, the relation between steering angle δ_f and the speed is chosen to depend on the host velocity as a logarithmic function given by

$$|\delta_f| = \frac{\delta_{f,0}}{\ln(\upsilon_{h_x})} \tag{4-2}$$

As a result of technological developments, vehicles become faster and more comfortable. Constructing of fast, safe, comfortable and economical transportation systems is an important expectation among the people. To meet the expectations, during the design of transportation structures such as highway, railway, high velocity railway etc.; the correct selection and implementation of standards related to road geometry is of great importance. Horizontal and vertical curves used in transportation systems are the critical sections on the alignment.

In order to increase road safety and comfort, highways have been constructed with limited curvatures. Note that minimum curve radius of highways has been determined based on

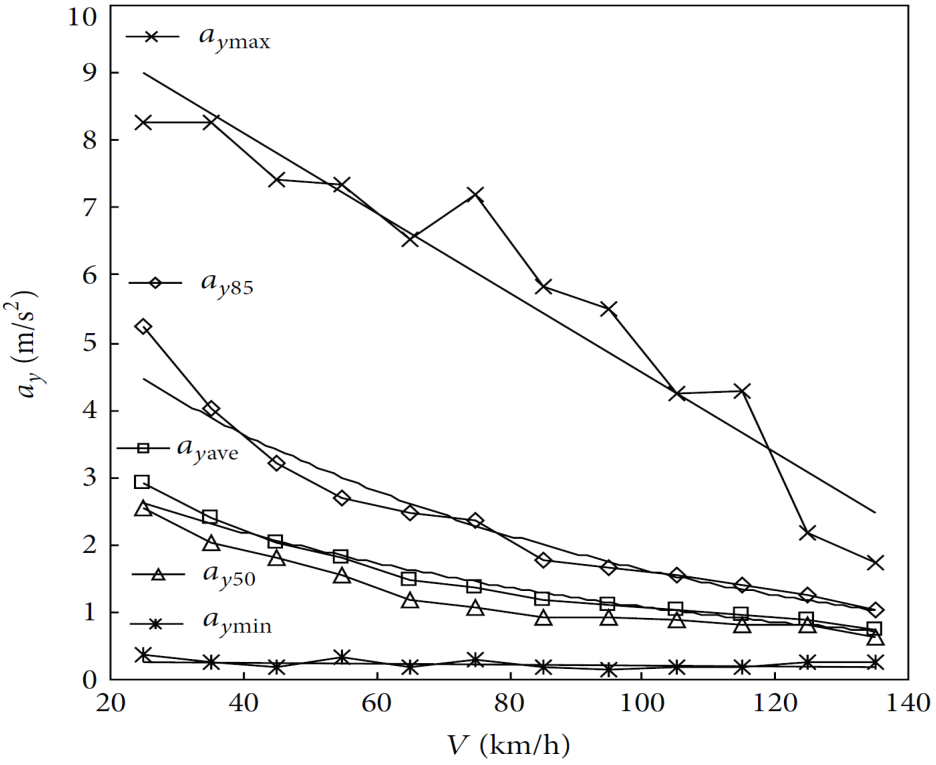

Figure 4-1: Scatter diagram of lateral acceleration over speed

the limit values of lateral acceleration and jerk. On the horizontal curve, lateral acceleration formed by centripetal force adversely affects the road safety and reduces vehicle travel comfort.

The German RAL Guide has specified the critical absolute value of lateral acceleration as 1.47 ms^{-2} for highways. Based on this regulation, Table 4-1 gives the minimum curve radius from 20 to 130 km/h for highways [38].

Table 4-1: Minimum horizontal curve radius for highways

Velocity [km/h]	ρ_{min} [m]
20	15
30	35
40	55
50	85
60	125
70	170
80	220
90	280
100	345
110	415
120	495
130	580

A road speed limit is the limit of speed allowed by law for motorised road vehicles, either maximum limit or minimum limit. Speed limits are commonly set by the legislative bodies of national or local governments. Generally in most of countries, highway speed limits are in the range of 80-130 km/h for passenger cars [39].

4-2 Road Information

Roads in the real world can be divided into two types, structured roads and unstructured roads. Structured roads usually refer to some roads that have better structure, such as highway. Unstructured roads refer to roads that have no significant artificial markings. A path planning algorithm for autonomous driving in unstructured road can generate arbitrary trajectories irrespective of road structure. However, in a structured road, the algorithm rolls out a trajectory that is parallel to the road shape [33].

Road curves which are regular bends in the horizontal plane are known as horizontal curves, so that they may be circular or parabolic. The path is a geometric curve defined in the X and Y coordinates as shown in Figure 4-2. Suppose that the path is smooth. In two dimensions, let a plane curve be given by Cartesian parametric equations $x = X(t)$ and $y = Y(t)$. Then the curvature Υ is defined by

$$\Upsilon \equiv \frac{d\phi}{ds} = \frac{\frac{d\phi}{dt}}{\frac{ds}{dt}} = \frac{\frac{d\phi}{dt}}{\sqrt{(\frac{dx}{dt})^2 + (\frac{dy}{dt})^2}} = \frac{\frac{d\phi}{dt}}{\sqrt{(x')^2 + (y')^2}} \tag{4-3}$$

where ϕ is the tangential angle and s is the arc length. As can readily be seen from the definition, curvature therefore has units of inverse distance. The $d\phi/dt$ derivative in the above equation can be found using the identity as given

$$\tan(\phi) = \frac{dy}{dx} = \frac{\frac{dy}{dt}}{\frac{dx}{dt}} = \frac{y'}{x'} \tag{4-4}$$

so

$$\frac{d}{dt}(\tan(\phi)) = \sec^2(\phi)\frac{d\phi}{dt} = \frac{x'y'' - x''y'}{(x')^2} \tag{4-5}$$

and

$$\frac{d\phi}{dt} = \frac{d}{dt}(\tan(\phi))\frac{1}{\sec^2(\phi)} = \frac{x'y'' - x''y'}{(x')^2 + (y')^2} \tag{4-6}$$

Combining Equations (4-3) and (4-6) then gives [26] as

$$\Upsilon = \frac{x'y'' - x''y'}{((x')^2 + (y')^2)^{\frac{3}{2}}} \tag{4-7}$$

Thus the radius of curvature is defined as the reciprocal of the curvature:

$$\rho = \frac{1}{\Upsilon} \tag{4-8}$$

Another way to understand the curvature is physical. Suppose that a particle moves along the curve with unit speed. Taking the time s as the parameter for curve C_{path}, this provides a natural parametrization for the curve. The unit tangent vector $\hat{T}$ (which is also the velocity vector, since the particle is moving with unit speed) also depends on time. The curvature is then the magnitude of the rate of change of $\hat{T}$. Symbolically it is

$$\Upsilon = \|\frac{d\hat{T}}{ds}\| \tag{4-9}$$

where ds denotes the incremental change. It can be expressed as

$$ds = \sqrt{dx^2 + dy^2} \tag{4-10}$$

where dx and dy are the incremental changes in X and Y directions, respectively.

Geometrically, the curvature Υ measures how fast the unit tangent vector to the curve rotates. If a curve keeps close to the same direction, the unit tangent vector changes very little and the curvature is small; where the curve undergoes a tight turn, the curvature is large. The $\hat{T}$ vector on a plane curve is displayed in Figure 4-2.

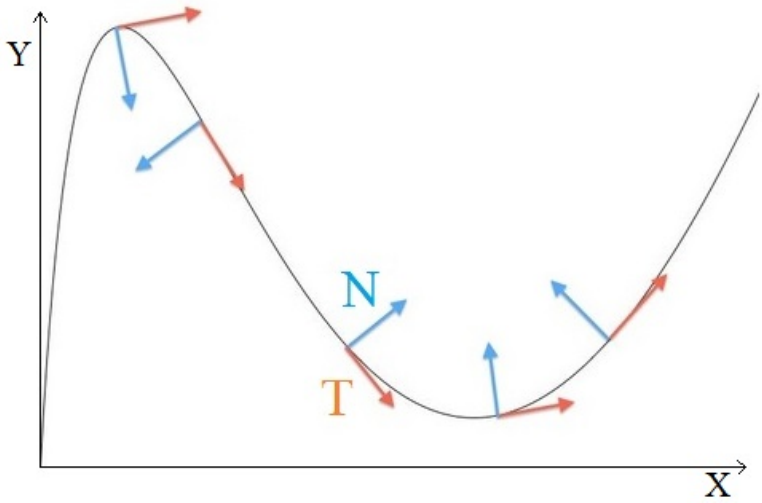

Figure 4-2: Normal and tangent vectors along a 2-D curve

The desired heading or yaw angle ε_d dictated by the desired path is the angle between unit tangent vector $\hat{T}$ and unit vector in the direction of the x-axis in Cartesian coordinate system. It can be obtained as follows

$$\varepsilon_d = \arccos(\frac{\hat{T}\,\hat{x}}{\|\hat{T}\|\|\hat{x}\|}) \tag{4-11}$$

The driver-vehicle system indicates relation between the vehicular current state and the future road information as shown as in Figure 4-3. The lateral position error y_r is defined as the lateral distance between the vehicle Center of Gravity (CoG) and the centerline of the desired path C_{path}. Yaw angle error $(\varepsilon - \varepsilon_d)$ is defined using the yaw angle of the vehicle ε and the desired yaw angle as dictated by the desired path ε_d [6].

The rate of change of the lateral position error $\dot{y}_r$ and yaw angle error $(\varepsilon - \varepsilon_d)$ are defined as

$$\dot{y}_r = \upsilon_{h_y} + \upsilon_{h_x}(\varepsilon - \varepsilon_d) \tag{4-12}$$

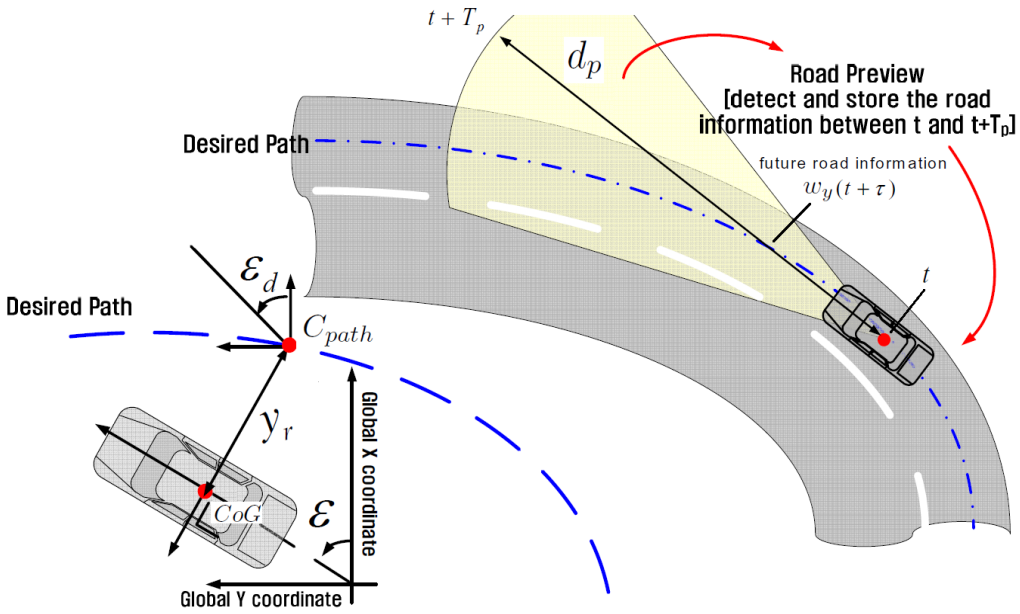

Figure 4-3: Driver-vehicle system

$$\dot{\varepsilon}_d = \frac{v_{h_x}}{\rho} \tag{4-13}$$

where ρ denotes the curvature radius of the desired path [6].

4-3 Linearized Model

The linearized model is used assuming that the vehicle is traveling at a constant desired velocity on a curved road and the lateral tire force is linearly related to the side slip angle by the cornering stiffness as given in Equation (2-31). Also, separate cornering stiffness coefficient C_{y_f} and C_{y_r} are defined for the front and rear tires based on the static distribution of weight between the front and rear axles. The tire side-slip angles are given in Equation (2-24) and (2-25) as

$$\begin{aligned} F_{y_f} &= C_{y_f}\alpha_f \\ F_{y_r} &= C_{y_r}\alpha_r \end{aligned} \tag{4-14}$$

Note that a straight road can be described as a curved road with infinite radius of curvature [15]. This linearization gives a four state model where the states are the vehicle's lateral position error y_r and the yaw angle error $(\varepsilon - \varepsilon_d)$ of the vehicle and rate of change of these two states. The steering control input $u_y = \delta_f$ (assuming that a rear wheel cannot be steered $\delta_r = 0$) is chosen as front wheel steering angle command to stimulate a steering actuator.

Using a small angle approximation, the tire slip angles are given as [6]

$$\alpha_f = \delta_f - (\frac{v_{h_y} + l_f\dot{\varepsilon}}{v_{h_x}}) \tag{4-15}$$

$$\alpha_r = -(\frac{v_{h_y} - l_r\dot{\varepsilon}}{v_{h_x}}) \tag{4-16}$$

From the linear tire model in Equation (4-14), (4-15) and (4-16), the lateral tire forces can be expressed by substituting Equations (4-12) and (4-13) into it as given

$$F_{y_f} = C_{y_f}\left\{\delta_f - (\frac{\upsilon_{h_y} + l_f\dot{\varepsilon}}{\upsilon_{h_x}})\right\} = C_{y_f}\left\{\delta_f - (\frac{\dot{y}_r + l_f(\dot{\varepsilon} - \dot{\varepsilon}_d)}{\upsilon_{h_x}}) + (\varepsilon - \varepsilon_d) - \frac{l_f}{\upsilon_{h_x}}\dot{\varepsilon}_d\right\} \quad (4\text{-}17)$$

$$F_{y_r} = C_{y_r}\left\{-(\frac{\upsilon_{h_y} - l_r\dot{\varepsilon}}{\upsilon_{h_x}})\right\} = C_{y_r}\left\{-(\frac{\dot{y}_r - l_r(\dot{\varepsilon} - \dot{\varepsilon}_d)}{\upsilon_{h_x}}) + (\varepsilon - \varepsilon_d) + \frac{l_r}{\upsilon_{h_x}}\dot{\varepsilon}_d\right\} \quad (4\text{-}18)$$

A 2-DOF bicycle model is used to design the steering controller. Equation (2-11), (2-12), (2-14) and (2-15) show the lateral dynamic equations for a 2- DOF bicycle model. Assuming longitudinal and lateral motions of vehicle are decoupled and small angle approximation for steering angle since it is less than 5 degree for highway driving situations, following lateral dynamic equations are obtained as

$$m(\dot{\upsilon}_{h_y} + \upsilon_{h_x}\dot{\varepsilon}) = F_{y_f} + F_{y_r} \quad (4\text{-}19)$$

$$I_z\ddot{\varepsilon} = l_f F_{y_f} - l_r F_{y_r} \quad (4\text{-}20)$$

The linear model has a state-space representation can be obtained by substituting Equation (4-17) and (4-18) into Equation (4-19) and (4-20) as

$$\dot{\chi}_y = A_y\chi_y + B_y u_y + \Gamma_y w_y \quad (4\text{-}21)$$

$$\chi_y^T = \begin{bmatrix} y_r & \dot{y}_r & (\varepsilon - \varepsilon_d) & (\dot{\varepsilon} - \dot{\varepsilon}_d)\end{bmatrix} \quad (4\text{-}22)$$

with matrices

$$A_y = \begin{bmatrix} 0 & 1 & 0 & 0 \\ 0 & \frac{A_{y,1}}{\upsilon_{h_x}} & -A_{y,1} & \frac{A_{y,2}}{\upsilon_{h_x}} \\ 0 & 0 & 0 & 0 \\ 0 & \frac{A_{y,3}}{\upsilon_{h_x}} & -A_{y,3} & \frac{A_{y,4}}{\upsilon_{h_x}} \end{bmatrix} \quad B_y = \begin{bmatrix} 0 \\ B_{y,1} \\ 0 \\ B_{y,2} \end{bmatrix} \quad \Gamma_y = \begin{bmatrix} 0 & 0 \\ 1 & 0 \\ 0 & 0 \\ 0 & 1 \end{bmatrix} \quad w_y = \begin{bmatrix} w_{y,1} \\ w_{y,2} \end{bmatrix} \quad (4\text{-}23)$$

$$A_{y,1} = \frac{-2(C_{y_f} + C_{y_r})}{m} \quad A_{y,2} = \frac{2(-l_f C_{y_f} + l_r C_{y_r})}{m} \quad (4\text{-}24)$$

$$A_{y,3} = \frac{2(-l_f C_{y_f} + l_r C_{y_r})}{I_z} \quad A_{y,4} = \frac{-2(l_f^2 C_{y_f} + l_r^2 C_{y_r})}{I_z} \quad (4\text{-}25)$$

$$B_{y,1} = \frac{2C_{y_f}}{m} \quad B_{y,2} = \frac{2l_f C_{y_f}}{I_z} \quad (4\text{-}26)$$

$$w_{y,1} = \frac{-\upsilon_{h_x}^2}{\rho} + \frac{A_{y,2}}{\upsilon_{h_x}}\dot{\varepsilon}_d \quad w_{y,2} = \frac{A_{y,4}}{\upsilon_{h_x}}\dot{\varepsilon}_d - \ddot{\varepsilon}_d \quad (4\text{-}27)$$

The disturbance term w_y where ρ is the radius of curvature, $\frac{1}{\rho}$ the disturbance input (denoted as the road curvature), is defined from road information $(\dot{\varepsilon}_d, \ddot{\varepsilon}_d)$. The outputs are the lateral position error and the yaw angle error [6].

4-4 Steering Controller

It is significant to consider human factors for the design of the intelligent safety vehicle beyond the general vehicle's performance. In order to imitate the human driving pattern, research considering the human factors is essential. The drivers detect the road information, and then make a decision based upon it through their physical recognition process. The preview distance is assumed as one of the primary human factor. Several tests for the study of the human factors are conducted. These tests yield that the preview distance is the function of the vehicle velocity as well as the road curvature:

$$d_p = f(v_h, \rho) \tag{4-28}$$

The average preview distance is obtained from the test results [28]. Its distribution with respect to both velocity v_h and road curvature ρ is presented in Figure 4-4. The preview distance is increased linearly to the velocity and logarithmically to the road curvature.

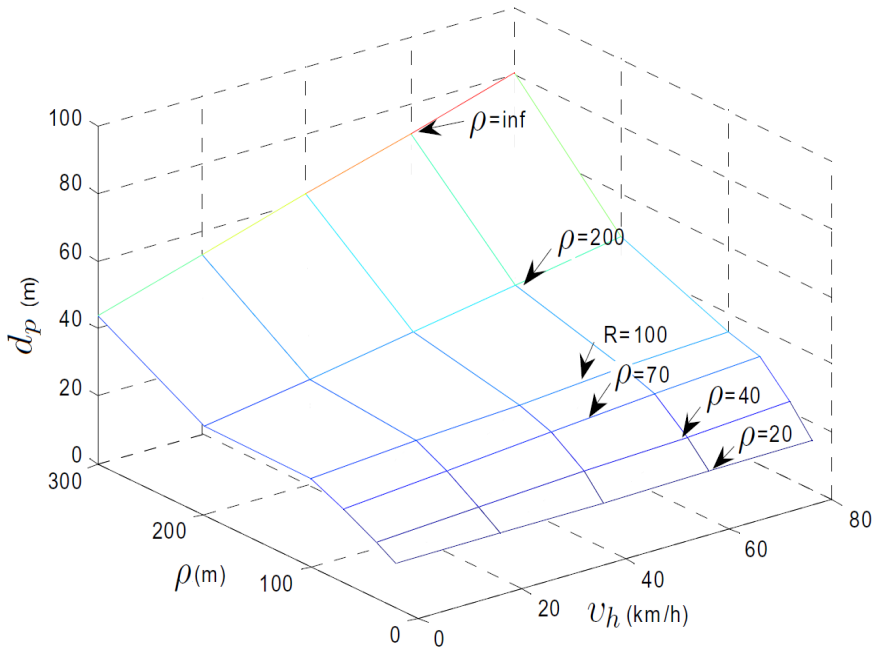

Figure 4-4: 3-D preview distance distribution

An optimal finite preview control method is used to develop a steering controller. The applied control algorithm strategy manipulates not only the current error deviated from the target but also the prediction using a future information [28]. Therefore, it is able to depict the human driving pattern to employ both the vehicle current states and the future road information.

It has been intended to eliminate lateral and yaw angle error through a combination of feedback and feed-forward control. The feedback control input of the steering controller for path-tracking is computed using lateral position error and yaw angle error. The feed-forward control input is computed using the road information within the preview distance. The feed-forward preview control input can improve not only the tracking performance of the steering controller, but also the ride quality. To develop the steering controller using finite preview

control theory, preview distance is transformed into preview time T_p in the following manner as [6]

$$T_p = \frac{d_p}{\upsilon_{h_x}} \tag{4-29}$$

where preview time T_p, preview distance d_p and vehicle longitudinal velocity υ_{h_x}. The steering input and vehicle trajectory are strongly correlated. When the preview distance is longer, the steering input is earlier initiated; reversely when the preview distance is shorter, the steering input is larger. It is natural that the vehicle trajectory is deviated from the target road as the steering input is larger.

The steering control input $u_y = \delta_f(t)$ is computed to minimize the performance index given as

$$J_y(\chi_y, \lambda, t) = \int_0^\infty (\frac{1}{2}\chi_y^T Q_y \chi_y + \frac{1}{2}u_y^T R_y u_y + \lambda^T (A_y \chi_y + B_y u_y + \Gamma_y w_y - \dot{\chi}_y))dt \tag{4-30}$$

The weighting matrices are positive semi-definite $Q_y \geq 0$ and positive definite $R_y > 0$. The solution that minimizes the performance index is given by the well-known Euler Lagrange equation:

$$\frac{\partial J_y}{\partial \chi_y} - \frac{d}{dt}(\frac{\partial J_y}{\partial \dot{\chi}_y}) = 0 \Longrightarrow \dot{\lambda} = -Q_y \chi_y - A_y^T \lambda \tag{4-31}$$

$$\frac{\partial J_y}{\partial u_y} - \frac{d}{dt}(\frac{\partial J_y}{\partial \dot{u}_y}) = 0 \Longrightarrow u_y = -R_y^{-1} B_y^T \lambda \tag{4-32}$$

$$\frac{\partial J_y}{\partial \lambda} - \frac{d}{dt}(\frac{\partial J_y}{\partial \dot{\lambda}}) = 0 \Longrightarrow \dot{\chi}_y = A_y \chi_y - B_y R_y^{-1} B_y^T \lambda + \Gamma_y w_y \tag{4-33}$$

In order to obtain solutions for $\chi_y(t)$, $\lambda(t)$ and $u_y(t)$; Lagrange multiplier $\lambda(t)$ is assumed to take the form shown

$$\lambda(t) = P_y(t)\chi_y(t) + H(t) \tag{4-34}$$

where $H(t)$ is a Feed-Forward control. The differential form of Equation (4-34) is shown below

$$\dot{\lambda} = \dot{P}_y \chi_y + P_y(A_y \chi_y - B_y R_y^{-1} B_y^T \lambda + \Gamma_y w_y) + \dot{H} = -Q_y \chi_y - A_y^T (P_y \chi_y + H) \tag{4-35}$$

By grouping terms, the following two equality conditions are obtained as

$$\dot{P}_y + A_y^T P_y + P_y A_y - P_y B_y R_y^{-1} B_y^T P_y + Q_y = 0 \tag{4-36}$$

$$\dot{H} = -A_c^T H - P_y \Gamma_y w_y \quad \text{where} \quad A_c = A_y - B_y R_y^{-1} B_y^T P_y \tag{4-37}$$

Equation (4-36) is the standard LQ Riccati equation. As $t \to \infty$, the solution $P_y(t)$ of Equation (4-36) tends to approach its steady state value and is independent of the final condition $P_y(\infty)$. Then, Equation (4-36) becomes the well-known Control Algebraic Riccati Equation as given

$$A_y^T P_{y,ss} + P_{y,ss} A_y - P_{y,ss} B_y R_y^{-1} B_y^T P_{y,ss} + Q_y = 0 \tag{4-38}$$

If the road information beyond the preview time T_p is set equal to zero $w_y(t) = 0 \quad \forall t \in [t + T_p, \infty]$, then Equation (4-37) becomes

$$H(t, T_p) = \int_t^{t+T_p} (e^{-A_c^T (t-\tau_h)} P_{y,ss} \Gamma_y w_y(t)) d\tau_h \tag{4-39}$$

As a result, the steering control input is computed as [33]

$$u_y = \delta_{f,des}(t) = \delta_{f,FB} + \delta_{f,FF} = -K_y \chi_y + M(t) \tag{4-40}$$

to minimize the cost function where K_y is optimal state feedback gain, $M(t)$ is the finite preview control term. The optimal state feedback gain K_y is given as

$$K_y = -R_y^{-1} B_y^T P_{y,ss} \tag{4-41}$$

In Equation (4-41), $P_{y,ss} \geq 0$ is the positive-definite steady-state solution of the Riccati equation. The finite preview control term is expressed as

$$M(t) = -R_y^{-1} B_y^T \int_0^{T_p} (F_l(\xi) w_y(t+\xi)) d\xi \quad \text{where} \quad F_l(t) = e^{-A_c^T t} P_{y,ss} \Gamma_y \tag{4-42}$$

From Equation (4-40), it is clear that the steering control input is computed by using the road information between t and $t + T_p$. Figure 4-5 shows the block diagram for the steering controller [6]. The desired steering angle which is computed by the steering controller is constrained by using Equation (4-2) and then applied to the vehicle model.

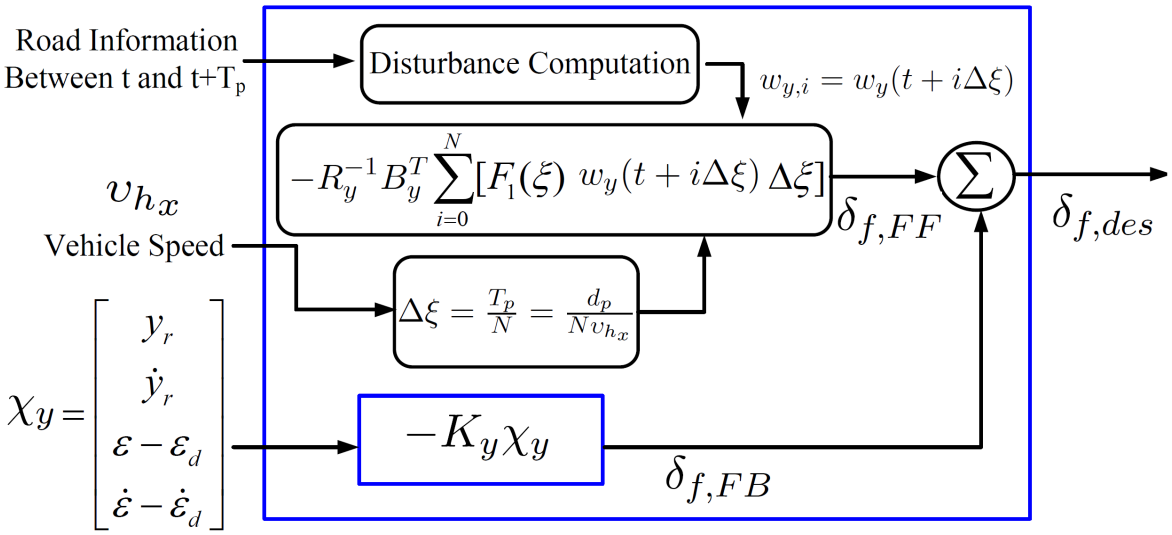

Figure 4-5: Block diagram of steering controller

4-5 Desired Speed Determination

The determination of desired speed is essential so that the lateral acceleration of the host vehicle does not exceed an arbitrary critical value in order to improve the safety of lateral vehicle behavior. If a lateral acceleration is increased, vehicle model goes nonlinear and controlling the vehicle becomes more difficult. Therefore, absolute value of lateral acceleration should be limited and velocity-dependent constraints are opted by considering human comfort as given

$$|a_{h_{y,des}}(v_{h_x})| = a_{h_{y,0}}(1 - P_c)(1 - \frac{v_{h_x}}{v_{h_{x,max}}}) \tag{4-43}$$

where $a_{h_{y,des}}$ is the desired lateral acceleration of the host vehicle. Furthermore, a vehicle can be well-represented by the linear vehicle model with lateral accelerations less than medium comfort level of 3.6 ms^{-2} [33]. In order to satisfy this constraint on lateral acceleration, the velocity of the host vehicle in the terms of comfort $v_{h,comfort}$ in curve is calculated as

$$v_{h,comfort} = \sqrt{\rho |a_{h_{y,des}}(v_{h_x})|} \tag{4-44}$$

where ρ denotes the curvature radius of the desired path. More striking point, velocity of the host vehicle is required not to exceed maximum allowable velocity $v_{h,limit}$ defined in Equation (2-3) in curve in order to create safe lateral vehicle behavior by means of keeping the vehicle on the road without being driven away from the curve:

$$v_{h_x} \leq v_{h,limit} \tag{4-45}$$

Chapter 5

Integrated Controller Design

Modern motor vehicles are increasingly using active chassis control systems to replace traditional mechanical systems in order to improve vehicle handling, stability, and comfort. These chassis control systems can be classified into the three categories, according to their motion control of vehicle dynamics in the three directions, i.e. vertical, lateral, and longitudinal directions.

These control systems are generally designed by different suppliers with different technologies and components to accomplish certain control objectives or functionalities. Especially when equipped into vehicles, the control systems often operate independently and thus result in a parallel vehicle control architecture. Two major problems arise in such a parallel vehicle control architecture. First, system complexity in physical meaning comes out to be a prominent challenge to overcome since the amount of both hardware and software increases dramatically. Second, interactions and performance conflicts among the control systems occur inevitably because the vehicle motions in vertical, lateral, and longitudinal directions are coupled in nature.

To overcome the problems, an approach called Integrated Vehicle Dynamics Control (IVDC) was proposed around the 1990s. Integrated vehicle dynamics control system is an advanced system that coordinates all the chassis control systems and components to improve the overall vehicle performance including safety and comfort.

Note that the practical constraints previously determined for longitudinal and lateral controllers are valid for integrated controller as well in order to fulfill safety and comfort objectives. This chapter presents integrated vehicle dynamics control and its multi-layer structure.

5-1 Integrated Vehicle Dynamics Control

To improve handling performance and active safety of vehicles, a considerable number of active control systems for vehicle lateral dynamics and longitudinal collision-safety have been developed and utilized commercially over the last two decades. For example, Adaptive Cruise

Control (ACC), Stop-and-Go (SG), Lane Keeping Assist (LKA), Collision Warning and Collision Avoidance (CW/CA), Vehicle Stability Control (VSC), etc. have been extensively researched and there has been many development since the 1990s. These systems are believed to reduce the risk of accidents, improve safety, and enhance comfort and performance for drivers [30].

These advanced driver assistance and active safety systems open new possibilities in accident prevention. With the introduction of these systems, there is the possibility of creating synergies, but also a risk of introducing conflicts. For example, since the ACC/Collision Avoidance (CA) and VSC systems share the brake, an independent integration of the ACC/CA and VSC system may result in unexpected behavior of the controlled vehicle and even worse dynamic behavior compared to an uncontrolled vehicle case. Moreover, coordinated control of the actuators is necessary to obtain both lateral stability and safe clearance of autonomous driving vehicle, and also to avoid rear-end collisions in severe driving situations [30].

For more complicated integrated systems, some researchers currently tend to adopt a multi-layer control structure to cope with the coordination and distribution of subsystems [31]. Considering the comprehensive advantages in the use of sensor information, hardware, and control strategies, a more suitable structure scheme, the so-called "Multi-layer Control Structure", is currently adopted, as shown in Figure 5-1.

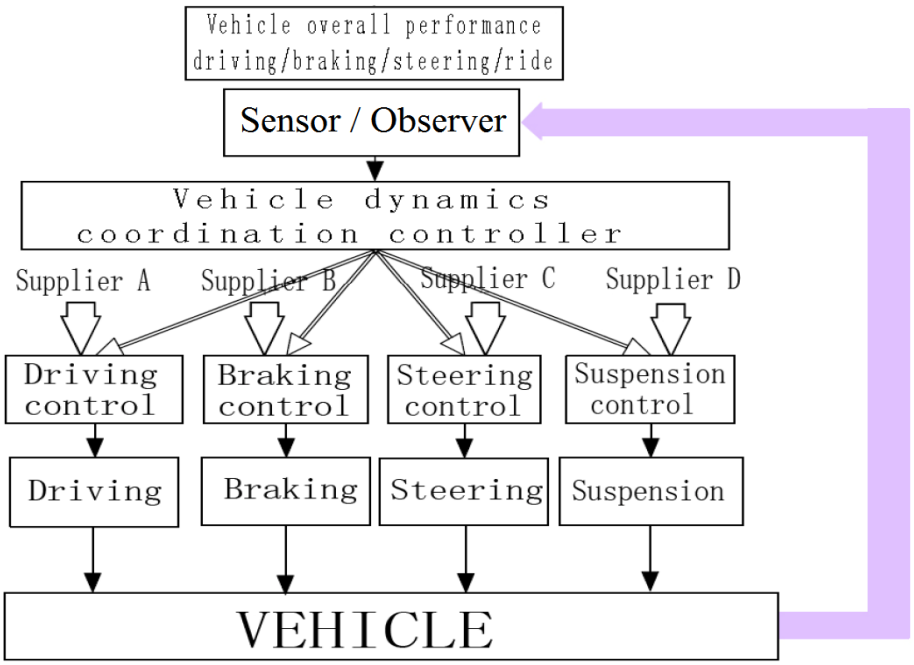

Figure 5-1: Multi-layer control structure

In order to solve the problems corresponding complexity, interactions with physical meaning and performance conflicts of subsystems, a Multi-layer Integrated Vehicle Dynamics Control (IVDC) is applied to the vehicle equipped with ACC, CA and VSC systems. Figure 5-2 shows the overall control system scheme.

In this scope, the purpose of the integrated controller is to navigate the vehicle quickly to a predesignated way point, while avoiding collisions with other vehicles in the environment.

Note that pedestrian, cyclist or animal interaction is not considered. Assuming that target vehicle is always well known, target selection is disinterested. Furthermore, lane changing or overtaking maneuver of the host vehicle is not allowed. The proposed controller consists of 4 main layers which aim to create synergies and safe interaction between throttle, brake and steering actuators: Supervisor, Decision, Control Algorithm and Coordinator.

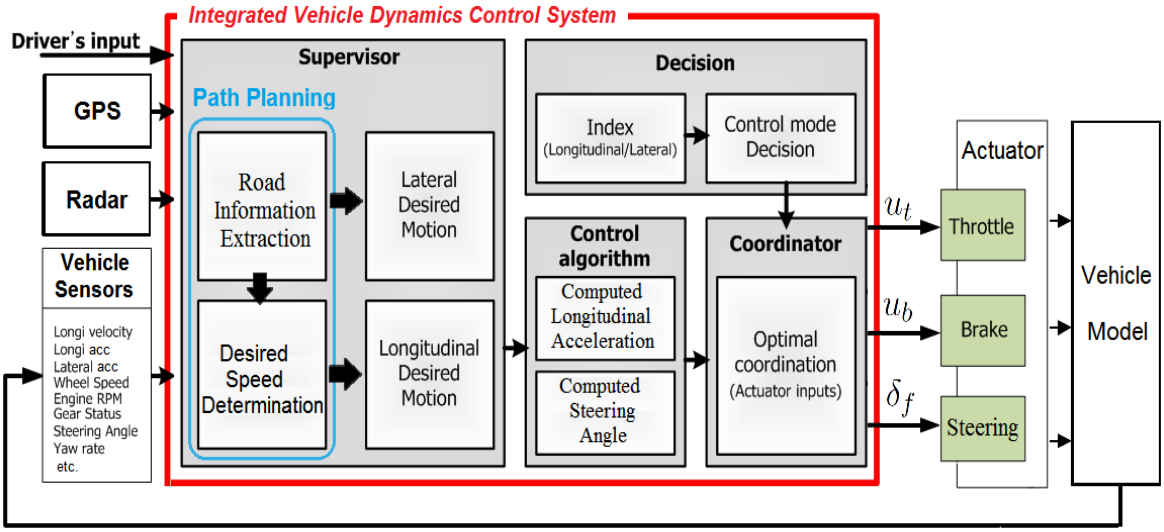

Figure 5-2: Scheme of multi-layer integrated vehicle dynamics control system

The function of supervisor layer is twofold: to perform path planning and to determine desired vehicle motions. The decision determines control modes which are "Normal Driving", "Integrated Safety I", and "Integrated Safety II" based on a longitudinal and lateral index to illustrate the danger of collision and lateral sliding in the current driving situation. The control algorithm calculates steering angle and longitudinal acceleration to track the desired path and to achieve desired longitudinal acceleration, respectively. From the control algorithm and the decision, the coordinator distributes the actuator inputs optimally based on the current status of the host vehicle.

5-1-1 Supervisor

In order to follow the reference road, the path planning module uses pre-stored GPS data. Relevant road geometric information such as global coordinates (X, Y) of desired path, radius of curvature, desired yaw angle as defined in Section 4-2 are extracted from GPS data. Next, desired velocity of the host vehicle $v_{h,des}$ is determined based on road information and driver's input:

$$v_{h,set} \leq v_{h,limit} \tag{5-1}$$

$$v_{h,des} = \begin{cases} v_{h,set} & \text{if} \quad v_{h,set} < v_{h,comfort} \\ v_{h,comfort} & \text{if} \quad v_{h,comfort} \leq v_{h,set} \end{cases} \tag{5-2}$$

where $v_{h,limit}$ is the maximum allowable velocity of the host vehicle in curve, $v_{h,set}$ is the user-set velocity of the host vehicle and $v_{h,comfort}$ is the determined velocity of the host vehicle concerns lateral acceleration constraint.

Another task of the supervisor is to determine desired vehicle motions such as a desired steering angle to provide a higher tracking performance in the road and improve vehicle lateral stability, and a desired longitudinal acceleration to avoid rear-end collisions.

In literature, it has been proposed to achieve the automatic driving and collision safety by the longitudinal force while the lateral stability has been ensured by the yaw moment control. In yaw rate control, the brake pressures of each wheel are determined by using an optimal differential braking algorithm to improve the maneuverability of the vehicle [30]. Note that this differential braking algorithm is applicable for four-wheeled vehicles.

In addition, it has been proposed to use the vehicle body side slip angle β to compute desired steering angle [32]. Note that vehicle slip angle is not directly measurable by sensors and it can be derived theoretically from the lateral dynamics of vehicle.

Since yaw moment control is not applicable for chosen two-wheeled vehicle model and vehicle slip angle is not directly measurable, following methods are opted to determine desired longitudinal acceleration and steering angle.

The desired longitudinal acceleration is determined based on traffic condition ahead and the user-set cruising velocity of the host vehicle. The desired longitudinal acceleration considering a ride quality, a driving characteristic of the driver and collision avoidance is determined by using a linear optimal control theory as in Section 3-2-1. It calculates the desired longitudinal acceleration to improve driver's comfort during normal, safe-driving situations and to completely avoid rear-end collision in vehicle following situations. In case of unstable lateral motion of the host vehicle, this MSc thesis offers to determine desired longitudinal acceleration based on physical limitation in braking with cornering situations as defined in Section 2-3.

The desired steering angle is assigned to track the desired path obtained from GPS data and to improve vehicle lateral stability especially where the desired path presents curvatures. For this goal, the desired steering angle can be theoretically determined by using finite preview optimal control theory as in Section 4-4.

5-1-2 Decision

In the conventional system, the lateral stability control has a control priority than the longitudinal safety control, i.e., if there are both rear end collision danger and unstable lateral motion of the vehicle in the current driving situation, only the lateral stability control system without the longitudinal safety control system should be operated by the conventional system. Therefore, control modes based on a longitudinal and lateral index to illustrate the danger of collision and lateral sliding in the current driving situation are proposed [30].

A task of the decision is to determine the control mode based on the index-plane using longitudinal and lateral indexes. The index-plane consists of a "Normal Driving Mode", an "Integrated Safety Mode I", and an "Integrated Safety Mode II". Integrated safety modes are dedicated to sense the danger of collision and unstable lateral motion of vehicle, and then to perform emergency maneuvers to keep the driving situation under control.

In order to determine the control mode, it is necessary to monitor the reference indexes related with a lateral stability and the collision danger between the host vehicle and the target vehicle.

Figure 5-3 shows the proposed index-plane. If the longitudinal index (lateral index) exceeds unit, the danger of collision (unstable lateral motion) is high.

The object of proposed control system is to satisfy both longitudinal safety and lateral stability. However, since both of them always cannot be satisfied, one of the two control systems should be given off by the control mode. As shown in the Figure 5-3, in the case of the "Integrated Safety Mode I", the longitudinal safety control has control priority to avoid rear end collision . In contrast, in the case of the "Integrated Safety Mode II", the lateral stability control has control priority to improve vehicle lateral motion.

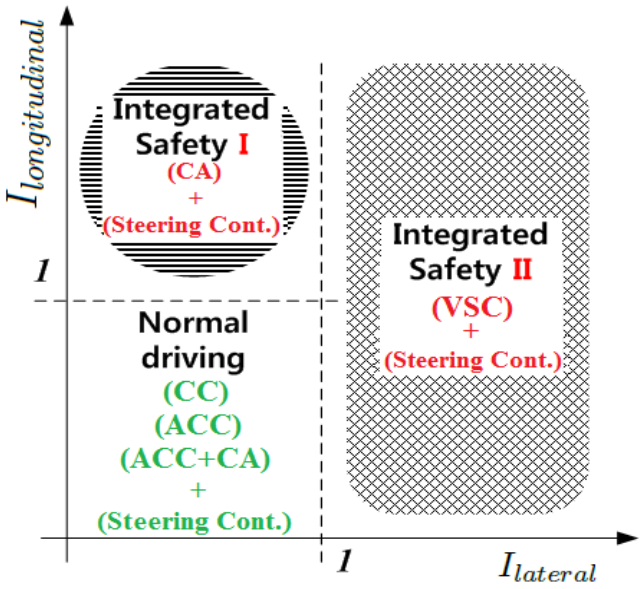

Figure 5-3: Control modes in the index-plane

The longitudinal index to monitor the vehicle-to-vehicle collision can be determined by using a warning index and an inverse TTC which are developed previously as in Section 3-2-1. As shown in Figure 5-4, the inputs are the warning index and the inverse TTC, and the output is the longitudinal index $I_{longitudinal}$.

In literature, the vehicle body side slip angle β has been used to evaluate the lateral motion of vehicle [32]. In addition, it has been proposed to determine the lateral index by using the desired yaw moment [30]. Note that no particular threshold values for desired yaw moment and the error in slip angle have been suggested. Furthermore, up to the present there exists no experimental study on human driving particularly concerns the desired yaw moment and the error in slip angle.

Since driver acceptance of proposed control system is crucial, this MSc thesis offers to determine lateral index based on experimental study on human driving. Thereby, firstly regression model of maximum value lateral acceleration (a_{ymax}), which is displayed in Figure 4-1 for experimental study on human driving, is expressed as

$$a_{ymax}(v_{h_x}) = \mu g(1 - \frac{v_{h_x}}{v_{h_{x,max}}}) \tag{5-3}$$

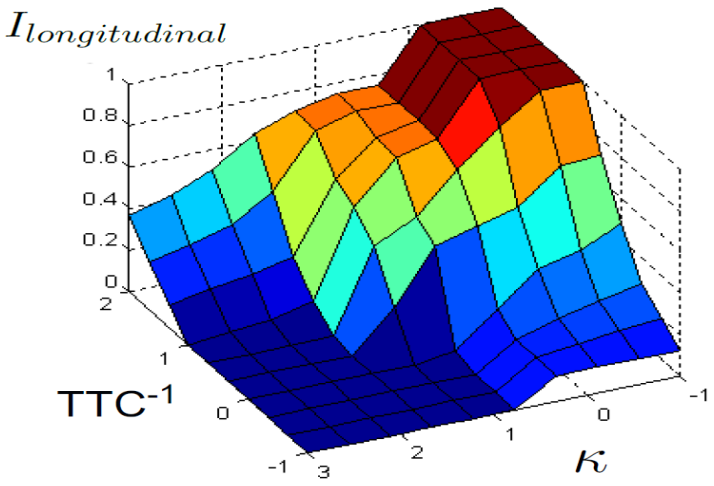

Figure 5-4: Longitudinal index of a collision-danger

The values above a_{ymax} definitely cause discomfort for human driving and also complicate controlling of vehicle. In the light of this knowledge, the lateral index can be defined as

$$I_{lateral} = \frac{|a_{h_y}|}{a_{ymax}(v_{h_x})} \tag{5-4}$$

where a_{h_y} is the lateral acceleration of the host vehicle. If either $I_{longitudinal}$ or $I_{lateral}$ exceeds a unit level, the vehicle must conduct an emergency maneuvers to satisfy both longitudinal safety and lateral stability.

5-1-3 Control Algorithm

Control algorithm respectively calculates a steering angle to track the desired path and improve vehicle lateral stability, a longitudinal acceleration to reach desired speed or to avoid rear-end collisions.

The steering angle is computed as in Equation (4-40) defined in Section 4-4 for all integrated control modes which are "Normal Driving Mode", "Integrated Safety Mode I", and "Integrated Safety Mode II".

"Normal Driving Mode" as shown in Figure 5-3 covers Longitudinal Control Mode-0 (CC), Longitudinal Control Mode-1 (ACC) and Longitudinal Control Mode-2 (ACC + CA) defined in Section 3-2-1. In addition to that "Integrated Safety Mode I" corresponds to Longitudinal Control Mode-3 (CA).

Thus, in the case of "Normal Driving Mode", longitudinal acceleration $a_{h_{x,des}}$ is obtained from Equations (3-5), (3-22) and (3-24) respectively depend on either velocity control or spacing control mode.

In the case of the "Integrated Safety Mode I", calculation of longitudinal acceleration is expressed as in Equation (3-26). Additionally in this mode, the constraint on longitudinal acceleration is tighten by using Equation (2-33) while taking into consideration physical limitation in braking with cornering as depicted in Figure 2-11 whether the road presents curvatures.

The VSC system has control priority in the case of the "Integrated Safety Mode II" in order to improve vehicle lateral motion and keep the vehicle in the desired path. This task is realized by optimal combination of braking and steering inputs. The calculation of desired longitudinal acceleration is originated from physical limitation in braking with cornering situation, so-called Kamm circle of friction forces as defined in Section 2-3.

The longitudinal and lateral tire forces (F_{x_i}, F_{y_i}) are limited physically by the adhesion limit between tire and road as expressed in Equation (2-33). Since tire forces are the primary forces affect on vehicle model, above-mentioned physical limitation can be induced from tires to whole vehicle. Thus, this induction can be expressed for vehicle with following inequality as given by

$$(\sum F_x)^2 + (\sum F_y)^2 \leq (\mu \sum F_z)^2 \tag{5-5}$$

where μ is the friction coefficient, $\sum F_x, \sum F_y, \sum F_z$ are the summation of forces along the vehicles X, Y, Z axes respectively. Then, the desired longitudinal acceleration $a_{h_{x,des}}$ can be derived as

$$a_{h_{x,des}} = -\frac{\sqrt{(\mu m g)^2 - (\sum F_y)^2}}{m} \tag{5-6}$$

where m is the total mass of the vehicle, g is the gravitational acceleration.

The automatic driving in desired path, collision safety and lateral stability are achieved by optimal combination of longitudinal acceleration and steering angle control.

5-1-4 Coordinator

Based on the desired longitudinal acceleration and steering angle, the coordinator manipulates throttle, brake and steering actuators. There are three coordination methods associated with the control modes. As shown in the coordination scheme in Figure 5-5, first the coordinator converts the computed longitudinal acceleration into a throttle/ brake actuator input (u_t or u_b) that is required to achieve the acceleration; then transmits the steering (δ_f) to track the desired path and it preserves the vehicle stability based on the coordination methods.

In the case of the "Normal Driving Mode", since the current driving situation is neither rear-end collision nor unstable vehicle lateral motion, throttle/brake input is determined by "Coordination I". However in the case of the "Integrated Safety Mode I and II", since the current driving situation is rear-end collision or unstable vehicle lateral motion, brake is determined by "Coordination II or III". Note that the computed steering angle obtained from Equation (4-40) is transmitted to steering actuator without processing through coordinator. From this point of view, coordinator layer can be seen as low-level controller as described in Section 3-2-1.

In the case of the "Normal Driving Mode", the throttle/brake input is generated by the "Coordination I" method. The computed longitudinal acceleration, obtained from Equations (3-5), (3-22) and (3-24) respectively depend on either velocity control or spacing control mode, is converted into a throttle/brake actuator input.

If the longitudinal index exceeds unit and the lateral index below unit, brake input to avoid the rear-end collision is generated by the "Coordination II". Due to the danger of rear-end collision, the longitudinal control should have control priority. The computed longitudinal acceleration, obtained from Equation (3-26) is converted into brake actuator input.

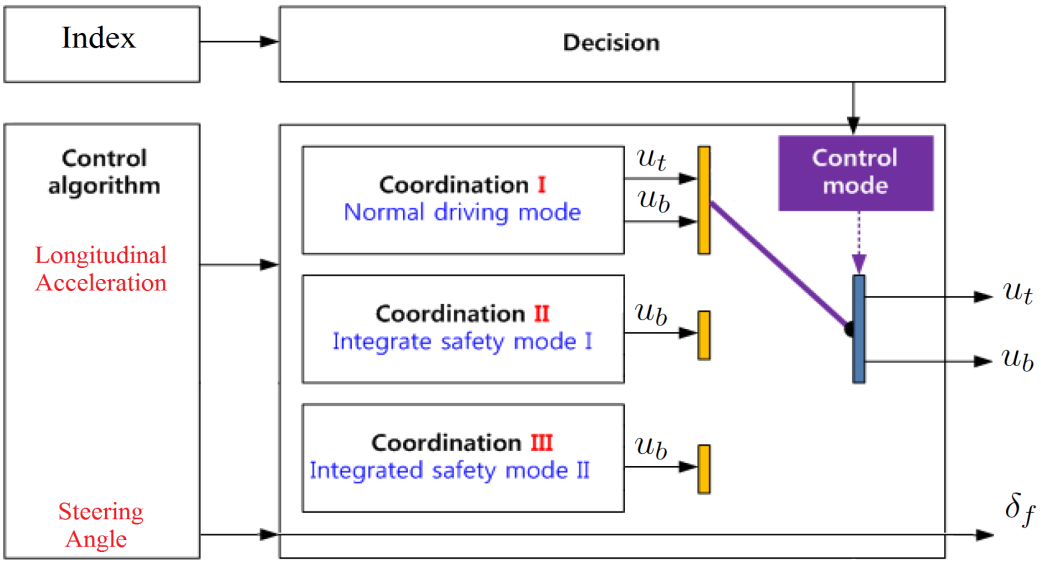

Figure 5-5: Coordination scheme

If the lateral index exceeds unit regardless of the longitudinal index, appropriate braking and steering inputs which can accomplish to continue to track the desired path and to improve vehicle lateral stability, are generated by the "Coordination III". However, if there is a danger of the rear-end collision, brake inputs considering the collision should be determined by the "Coordination II". The computed longitudinal acceleration, obtained from Equation (5-6) is converted into brake actuator input.

Chapter 6

Evaluation of Designed Controllers

For the (performance) evaluation of the designed controllers, firstly the performance specifications for this evaluation are described. Secondly, several test scenarios are determined to allow evaluation for the total envelope of working conditions of the designed controllers. Simulation results are discussed.

In this chapter, longitudinal and lateral performance specifications are determined and used to evaluate the performance of the integrated control system. This chapter is organized as follows: performance specifications and simulation results.

6-1 Performance Specifications

In order to able to evaluate performance of designed controllers on vehicle model, some numerical specifications should be determined for longitudinal and lateral performance. In the determination of performance specifications, the features such as safety, applicability to real driving situations, functionality of the newly designed controller for a complete envelope of working conditions and human comfort are qualified.

6-1-1 Longitudinal Performance Specifications

The primary objective of longitudinal control systems is either to track user-set velocity or to ensure following of a target vehicle in safe clearance. Therefore, separate performance specifications for velocity and spacing control modes are suggested.

In the case of velocity control mode, the primary requirement is that the steady-state error between the user-set velocity and the actual velocity of the host vehicle remain less than 1 km/h :

- $|v_{h,error}| = |v_{h,set} - v_{h_x}| \leq 1\, km/h$

In the case of spacing control mode, the distance error between target and host vehicle must have magnitude less than 0.5 meter and the relative velocity must be less than 1 m/s or 3.6 km/h at steady-state:

- $|d_{error}| \leq 0.5\, m$
- $|v_{rel,measured}| \leq 3.6\, km/h$

Furthermore, constraints on the longitudinal acceleration which are defined in Section 3-1 are considered in order to provide comfort to the passengers.

6-1-2 Lateral Performance Specifications

The objective of lateral control is to assure that the host vehicle travels safely on the road. Since highways can be described by a series of curves and road curvature can be known in advance from GPS data, this problem can be identified as a path tracking problem.

The primary requirements for path tracking are that the lateral position tracking error remain less than 0.2 meter at all times and that the steady-state error in the relative yaw angle have magnitude less than 1 degree.

- $|y_r| \leq 0.2\, m$
- $|(\varepsilon - \varepsilon_d)| \leq 1\, deg$

The specifications for human comfort during cornering must address the surges in lateral acceleration due to changes in road curvature. Lateral acceleration values above medium-comfort level are prevented in the light of analytic results of the manual driving data on human drivers as defined in Section 4-1.

6-2 Simulation Results

In this section, designed longitudinal, lateral and integrated controllers are tested through simulations conducted by using Matlab/Simulink and their driving performances are critically analyzed by using determined performance specifications.

For comfort and safety key characteristics which barely affect the behavior of proposed controller as defined in Section 3-1, if not specified otherwise, a setting $P = P_c = 0.5$ is used for all simulations.

The symbols used in legends are given in Table 6-1.

Table 6-1: Symbols in legends

Symbol	Explanation
$v_{h,set}$	User-set velocity of the host vehicle
v_{h_x}	Longitudinal velocity of the host vehicle
a_{h_x}, a_{h_y}	Longitudinal and lateral accelerations of the host vehicle
v_{t_x}	Longitudinal velocity of the target vehicle
d_{des}	Desired distance
$d_{measured}$	Measured distance between the host and target vehicles by the radar
d_{error}	Distance error between the desired distance and the sensed distance between vehicles
$v_{rel,measured}$	Measured relative velocity between the host and target vehicles by the radar
$v_{h,des}$	Desired velocity of the host vehicle
δ_f	Front wheel steering angle
y_r	Lateral position error
$(\varepsilon - \varepsilon_d)$	Yaw angle error

6-2-1 Longitudinal Control

In this section, several test scenarios are used in order to examine longitudinal controller performance in different driving situations. The simulations consist of two vehicles, a target vehicle and an ACC-equipped vehicle which is refer to the host vehicle. Switching efficiency between velocity and spacing control modes is observed. The simulation results are compared with determined longitudinal performance specifications in terms of safe clearance. The longitudinal control parameters are provided in Appendix A-3. The test scenarios are described as follows.

Test Scenario 1: CC

In this scenario, there is no target vehicle in front of the host vehicle within the range of the radar, and, hence, the host vehicle is under the velocity control mode or the conventional Cruise Control. This scenario has a duration of 10 seconds.

Figure 6-1 shows vehicle test results in the case of set velocity up. Comparisons of vehicle velocity and user-set velocity, desired and actual vehicle accelerations and longitudinal control mode are shown in Figure 6-1 respectively. The host vehicle's initial velocity is 80 km/h and the user-set velocity has been set to 100 km/h. Note that system is activated at 1 s.

As soon as system is activated, the throttle actuator is automatically controlled on the basis of the throttle control algorithm. The longitudinal accelerations of the host vehicle have been limited in accordance with constraints defined in Section 3-1. As illustrated in Figure 6-1, the velocity of the host vehicle is smoothly increased to the user-set velocity and the vehicle acceleration tracks the desired acceleration very closely.

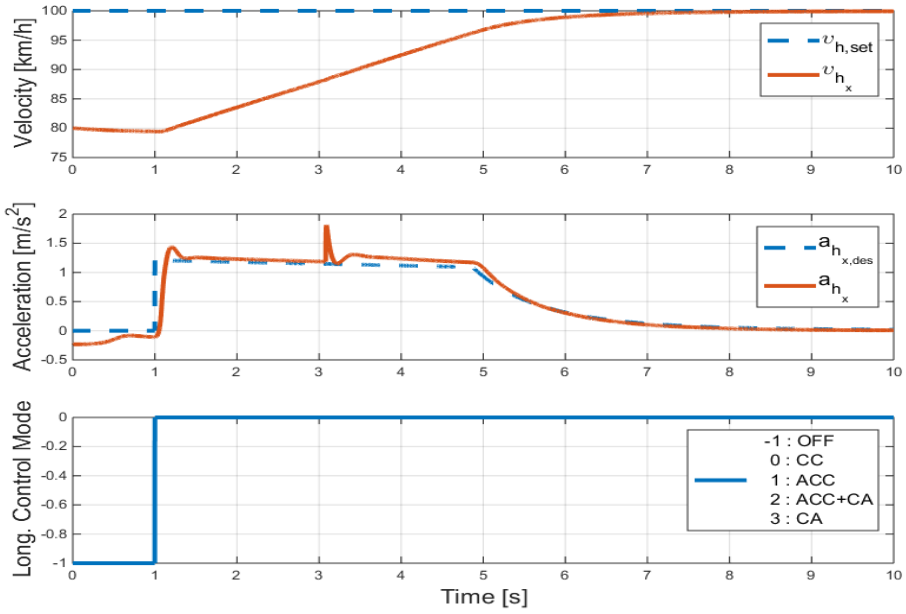

Figure 6-1: Simulation results for test scenario 1 (velocity, acceleration, control mode)

Test Scenario 2: ACC

Vehicle-following tests were conducted using two vehicles: a host vehicle and the target vehicle. This scenario has a duration of 25 seconds and it is composed of two phases as shown in Figure 6-2. After activation of system at 1 second the radar detects a target vehicle. The transition has been realized by system automatically to the Spacing Control (SC) mode to maintain the distance between the two vehicles based on a desired headway time. In the first phase, the host vehicle accelerates in order to achieve the desired spacing. In the second phase which is time segment of 10-25 seconds, the target vehicle decelerates so the host vehicle also starts to decrease its velocity in order to maintain the desired spacing between the vehicles.

The vehicle velocities, the desired and actual accelerations of the host vehicle are shown in Figure 6-2. It is observable that the acceleration of the host vehicle very closely tracks the desired acceleration profile and ranges between -1 and 1 ms^{-2} to improve the quality of the ride. The control mode shown in the same figure indicates that the current driving situation is safe.

Although the velocity of the target vehicle varies, the host vehicle follows the velocity of target vehicle adequately and, at the same time, maintains the spacing policy. The desired and actual distances are compared in Figure 6-3. The initial distance between the target and host vehicles is about 30 m. It can be seen that controller minimizes distance error and relative velocity, and their state-steady errors are in previously determined performance ranges.

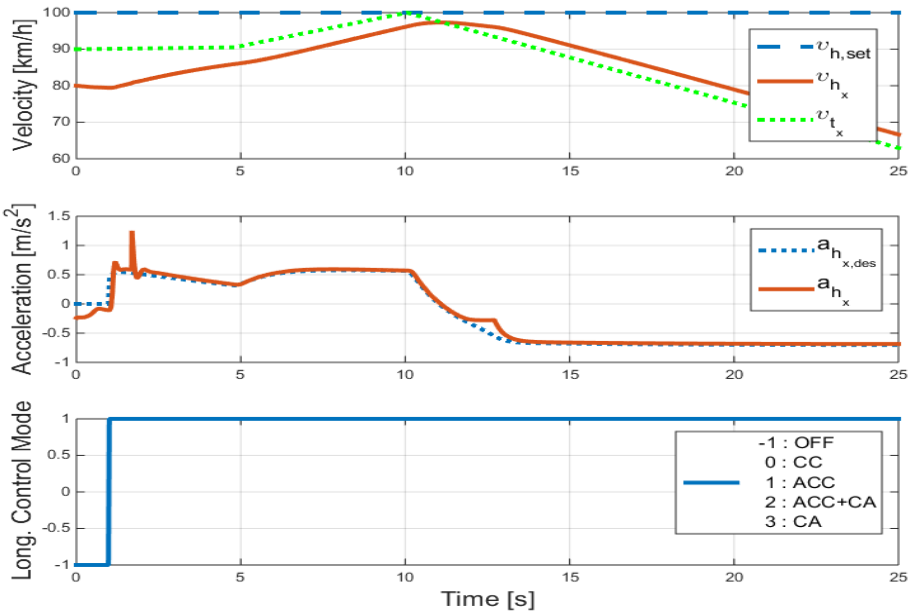

Figure 6-2: Simulation results for test scenario 2 (velocity, acceleration, control mode)

In order to investigate the influence of varying P_c on proposed controller, the same scenario is simulated for different settings $P_c = 0.25, 0.50, 0.75$ respectively. The results are illustrated in Figure 6-4 and 6-5.

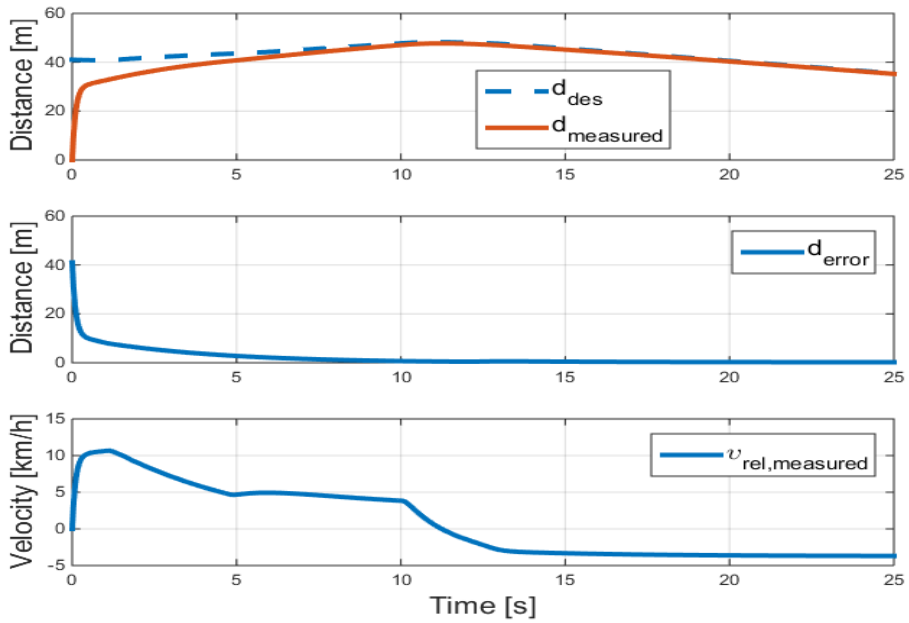

Figure 6-3: Simulation results for test scenario 2 (distance, distance error, relative velocity)

For increasing $P_c = 0.25, 0.50, 0.75$, the desired distance between host vehicle and target vehicle decrease gradually as shown in Figure 6-5. Smaller desired distance implies closer following situations which can be interpreted more risky regarding safety. In addition, this variance in desired distance severely affects controller mode since switching logic between velocity and spacing control modes primarily based on desired and actual distances.

Furthermore, the velocity-dependent dynamic constraints on longitudinal and lateral accelerations are tighten up for increasing P_c as illustrated in Figure 6-6. The results in Figure 6-4 clearly indicate more comfortable behavior for increasing P_c. The larger P_c, the smaller the resulting absolute acceleration peak values are. Furthermore, varying P_c affects controller behavior such as less or more aggressive respond.

It is observable from Figure 6-4 that there is undesirable chattering between control modes after 15 second for $P_c = 0.25$. This unnecessary switching between control modes occurs because of insufficiency of used switching logic as given in Section 3-2-1. According to this logical rule, mode switching is performed based on inequalities and it causes frequent switching. In physical systems, currently used switching logic should be replaced with more sophisticated ones in order to prevent frequent switching.

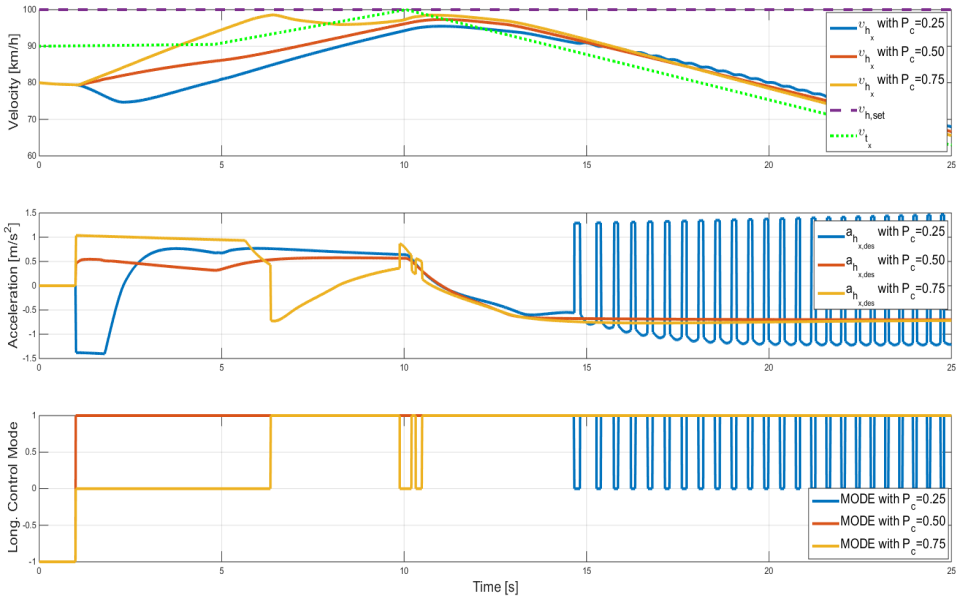

Figure 6-4: The influence of varying P_c (velocity, acceleration, control mode)

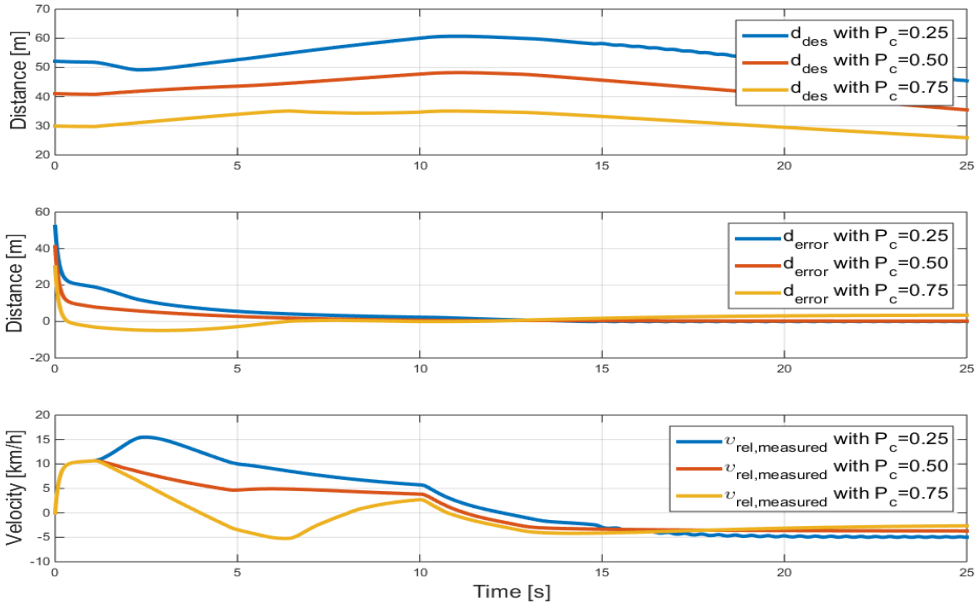

Figure 6-5: The influence of varying P_c (desired distance, distance error, relative velocity)

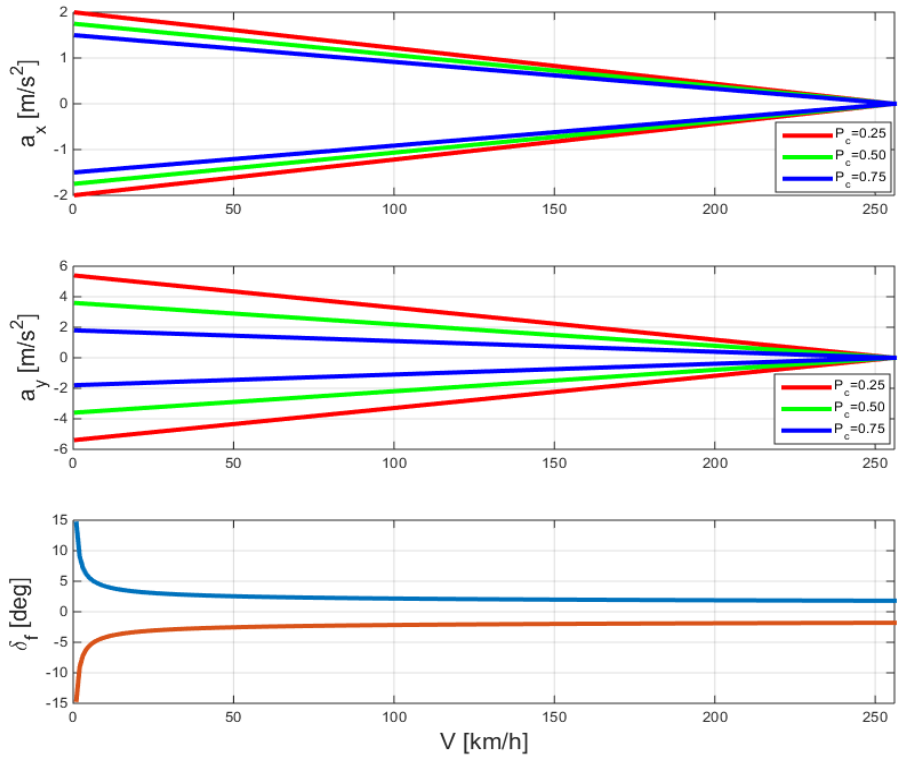

Figure 6-6: Velocity-dependent dynamic constraints on accelerations and steering angle

Test Scenario 3: CC/ACC+CA/ACC

The scenario has a time duration of 25 s and it consists several control mode switching. The scenario starts with the host vehicle in CC mode until the left neighboring vehicle changes to in-lane and simply it exhibits cut-in behavior. The initial relative distance of 5 m and the headway time of 1.5 seconds have been used in this test. The host vehicle's set velocity is 100 km/h and a vehicle with 90 km/h velocity appears in front of the host vehicle at 3 s.

Since the host vehicle has a chance of colliding with the cut-in vehicle and the lane change is not considered; the proposed system immediately determines the cut-in vehicle as the primary target as shown in Figure 6-7. The proposed control system recognizes this cut-in behavior as a dangerous situation based on the warning index and the inverse TTC. Then, the control system enables the ACC+CA mode at 3 second and the system on ACC+CA mode automatically controls the host vehicle.

Figure 6-7 shows the simulation results: a comparison of the host and the cut-in vehicle velocities, a comparison of the desired acceleration profile and actual acceleration and longitudinal control mode.

Since the velocity of the cut-in vehicle is approximately equal to velocity of the host vehicle, the controller activates the brake control such that the actual distance converges to the headway time distance and the host vehicle velocity converges to the target vehicle's velocity. Between time segment 10-15 seconds, target vehicle applies hard braking and reduces its velocity. The proposed controller senses again danger situations and applies necessary acceleration to vehicle. Between 15-25 seconds, target vehicle accelerates rapidly and its velocity passes user-set velocity of the host vehicle. Thus, the actual distance between the two vehicles start to increase and since acceleration of the host vehicle is limited for passenger comfort, control system enables first ACC mode and then CC mode gradually.

The throttle/brake controller forces the vehicle acceleration to converge to the desired acceleration. It is shown as in Figure 6-7 that the vehicle acceleration tracks the desired acceleration very closely. As illustrated in 6-8, the host vehicle follows target vehicle adequately and actual distance between vehicle smoothly converges to the desired distance.

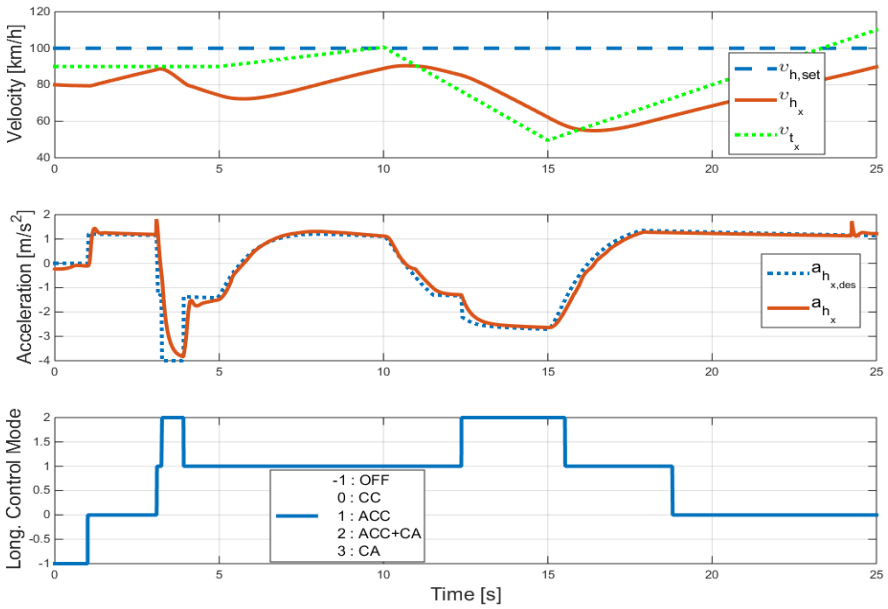

Figure 6-7: Simulation results for test scenario 3 (velocity, acceleration, control mode)

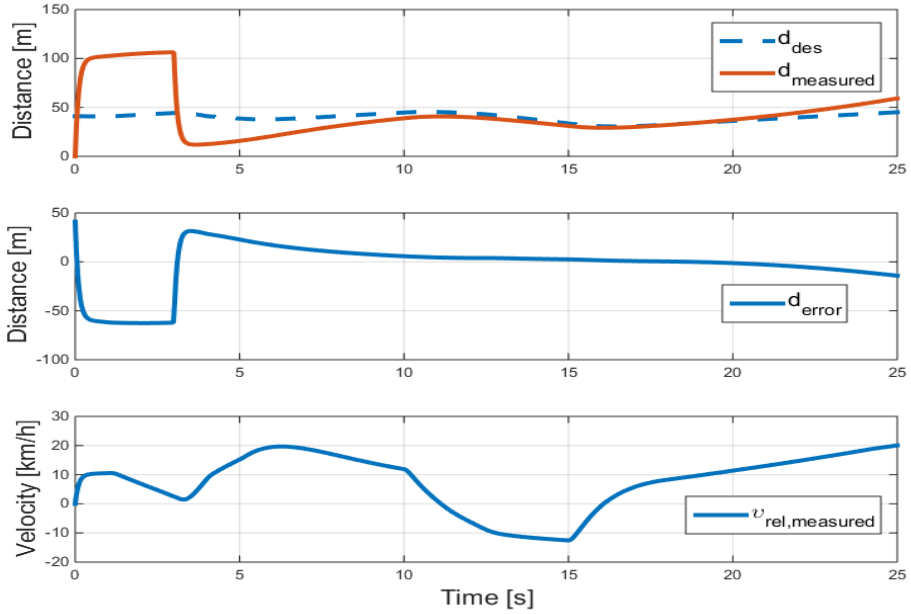

Figure 6-8: Simulation results for test scenario 3 (distance, distance error, relative velocity)

Test Scenario 4: ACC/ACC+CA/CA

This scenario is dedicated to test Collision Avoidance (CA) and Stop & Go (SG) functions. At 7 second, target vehicle applies severe braking and it waits between 10-12 seconds at full-stop. Then target vehicle starts to move again at low speed.

Initially ACC mode is enabled to increase the velocity of the target vehicle so that the distance error and relative velocity converge to zero. When target vehicle applies severe braking; warning index decreases, the inverse TTC abruptly increases, and the longitudinal control mode changes gradually from Mode-1 to Mode-3. In order to avoid collision with the rear-end of the target vehicle, severe brake is applied to host vehicle to reduce the velocity and increase the clearance. After severe braking, host vehicle waits also at standstill for a while and then it continues to follow target vehicle adequately. The distance between the two vehicles is adjusted according to the chosen headway time distance.

Comparisons of vehicle velocities, desired and actual vehicle accelerations, and longitudinal control mode are shown in Figure 6-9 respectively. Observe that at around 9 seconds the proposed system activates a large deceleration such -8 ms^{-2} to avoid collision with the rear-end of the target vehicle and then velocity of the host vehicle is zero between 13-15 seconds. Although velocity of the host vehicle is zero, longitudinal acceleration is around 10 ms^{-2} which seems irrational. Such unreasonable situation arises from the calculation of the longitudinal wheel-slip ratio as given in Equation (2-26). It can be seen that when vehicle velocity is equal to zero, the slip is mathematically infinity for braking situations. This results in largest tractive forces. Therefore, in order to fix the situation the longitudinal wheel-slip ratio should be taken as zero for simulation purposes when velocity of the host vehicle is zero.

The results from Figure 6-9 and 6-10 reveal that proposed system achieves to avoid a collision and satisfies Stop & Go function in driving situations.

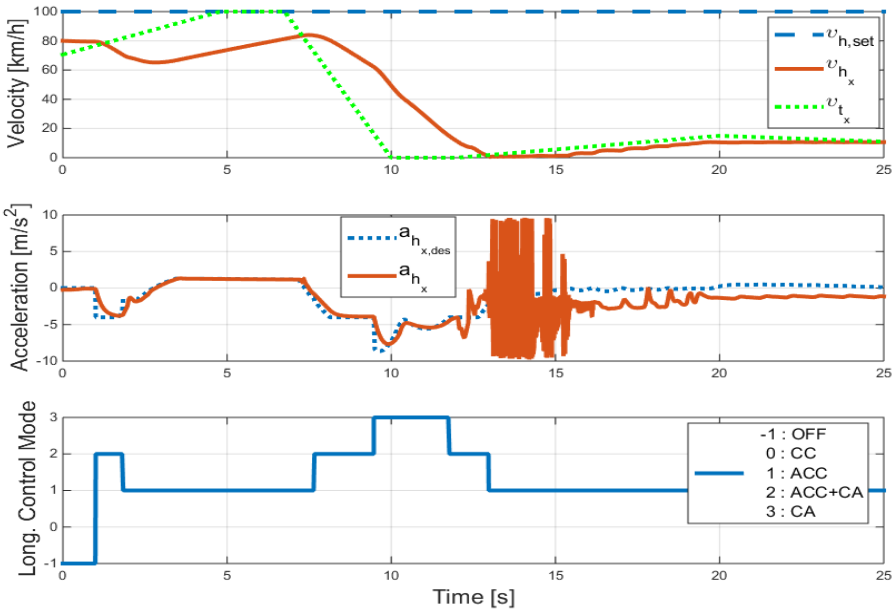

Figure 6-9: Simulation results for test scenario 4 (velocity, acceleration, control mode)

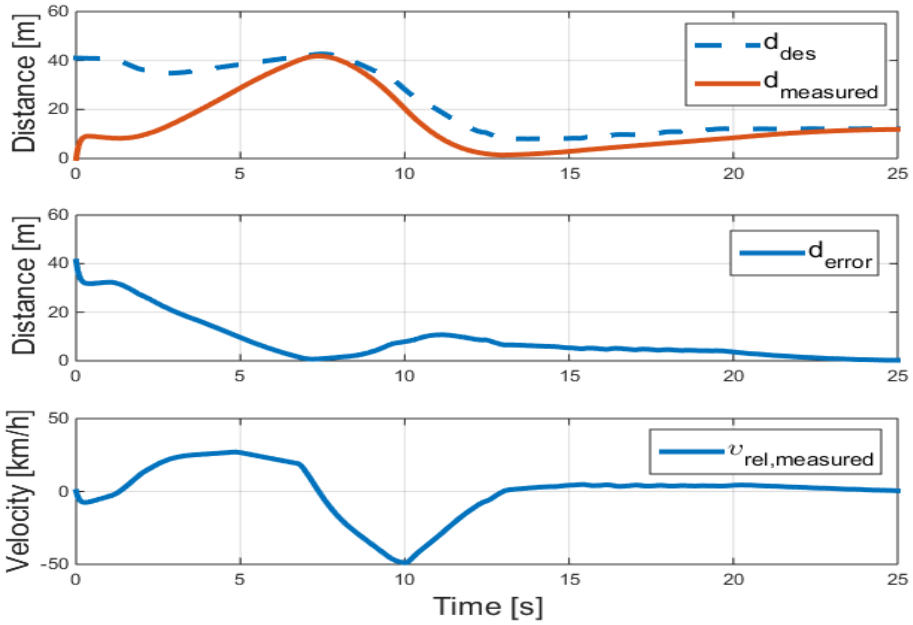

Figure 6-10: Simulation results for test scenario 4 (distance, distance error, relative velocity)

Test Scenario 5: ACC/CC

This test scenario is simulated in Figure 6-11. In this scenario, the target vehicle begins to increase its velocity. As a result, the velocity of the host vehicle also increases in order to maintain a desired distance in ACC mode. The host vehicle's initial velocity is 80 km/h and the user-set velocity has been set to 100 km/h.

Between the time segment 7-12 seconds, when the target vehicle pass over a velocity of 100 km/h, the host vehicle enables CC mode and maintains it is velocity at the user-set velocity of 100 km/h, since the driver-set velocity is the desired velocity of the host vehicle based on the CC algorithm. It can be seen from Figure 6-12 that the distance between the two vehicles increases due to the difference in velocity of the vehicles.

Then target vehicle slows down and the control system detects this change in velocity of target vehicle, switches to ACC mode, and lowers its velocity to match that of the target vehicle in order to follow. The target vehicle ceases to be a target when it changes lanes at 22 second as depicted in Figure 6-12. Consequently, the host vehicle stops detecting a target in its lane and adjusts its velocity back to the user-set cruise control velocity accordingly under CC mode.

To prevent the driver from feeling uncomfortable, proposed controller restricts the desired acceleration as shown in Figure 6-11. The acceleration of the host vehicle does not exceed 1.5 ms^{-2} for passenger comfort.

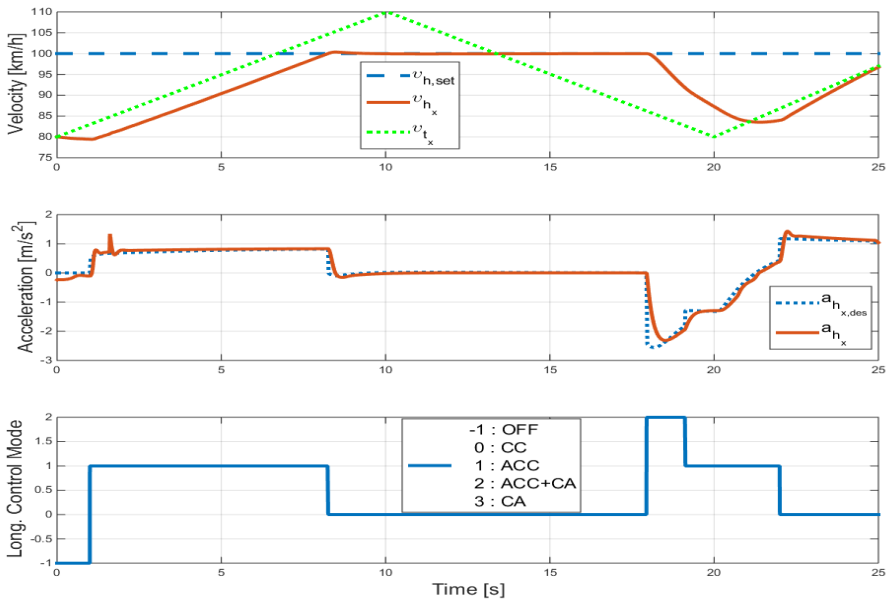

Figure 6-11: Simulation results for test scenario 5 (velocity, acceleration, control mode)

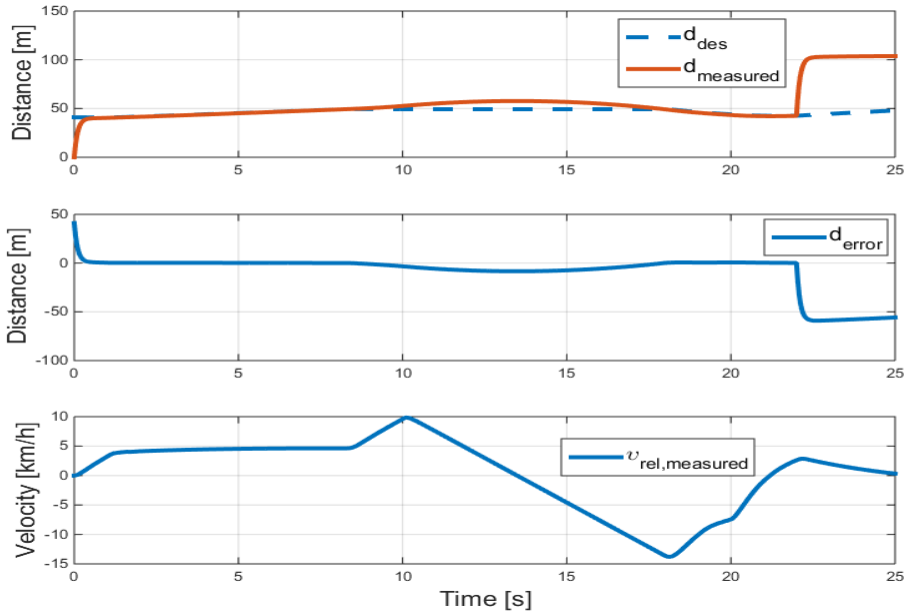

Figure 6-12: Simulation results for test scenario 5 (distance, distance error, relative velocity)

6-2-2 Lateral Control

In the light of highway speed limits, test circuits with the minimum curve radius 220 and 580 meter for 80 and 130 km/h respectively are used in order to examine lateral controller performance. In this section, path tracking algorithm has been verified by using the simulations. Note that the road information is extracted from GPS data with 1 meter resolution. The lateral control parameters are provided in Appendix A-4. Relevant test scenarios are presented in following.

Test Scenario 6: Steering Controller ($\rho = 220$ m)

The test scenario is simulated on test circuit which consists 30 meter straight line and curve with radius 220 meter shown in Figure 6-13.

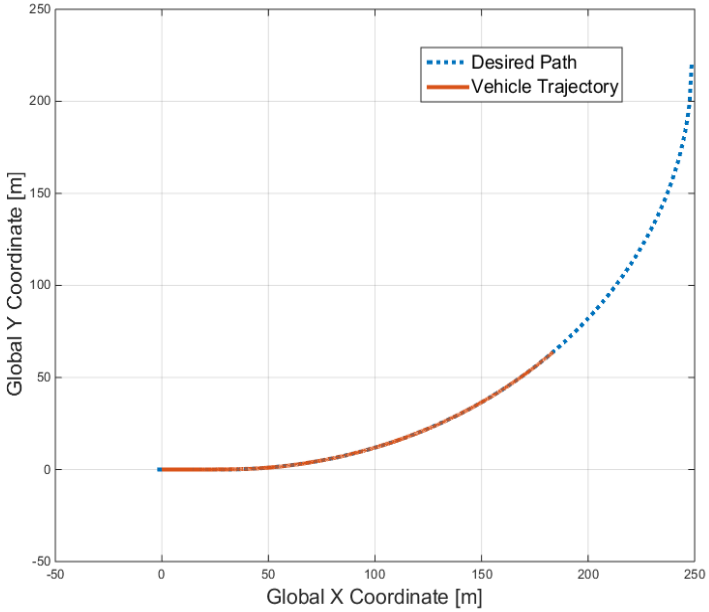

Figure 6-13: Test circuit with minimum curve radius 220 meter

In this scenario, there is no target vehicle in front of the host vehicle within the range of the radar. The host vehicle's initial velocity is 80 km/h and the user-set velocity has been set to 100 km/h as shown in Figure 6-14. Note that system is activated at 1 s. At joint point between straight line and curve, system determines desired velocity based on road information. From now on, the velocity of the host vehicle tracks the new determined desired velocity instead of user-set velocity, and the vehicle acceleration tracks the desired acceleration very closely within comfort limits in longitudinal direction. Observe that also the lateral acceleration of the host vehicle does not exceed medium-comfort limit defined in Section 4-1.

In the scope of path tracking performance of steering controller, simulations results are displayed in Figure 6-15. It can be seen that computed steering angle is within limits. The test results agree on satisfactory path tracking performance, with the magnitudes of lateral

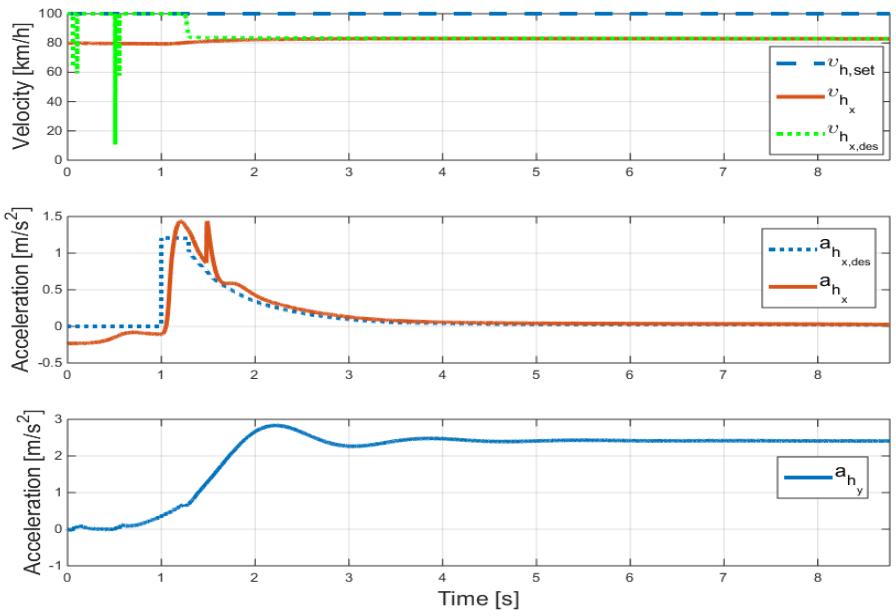

Figure 6-14: Simulation results for test scenario 6 (velocity, accelerations)

position and yaw angle error below 0.1 m and around 1 degree, respectively. The trajectory traveled by the host vehicle is drawn in 6-13. These errors are of the same order of magnitude as previously determined in lateral performance specifications.

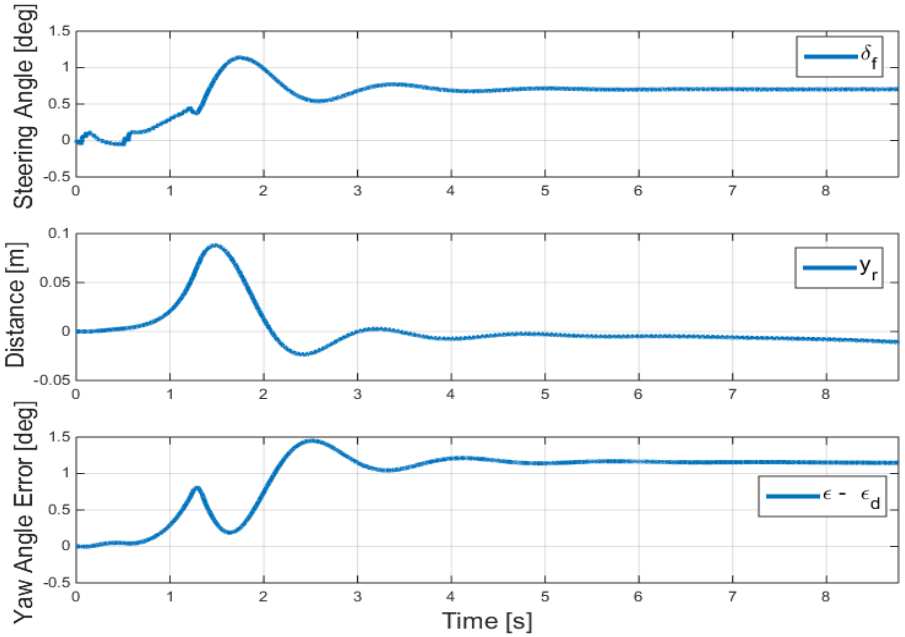

Figure 6-15: Simulation results for test scenario 6 (steering angle,lateral position,yaw angle error)

Test Scenario 7: Steering Controller ($\rho = 580$ m)

The test circuit links up 30 meter straight line and curve with radius 580 meter shown in Figure 6-16.

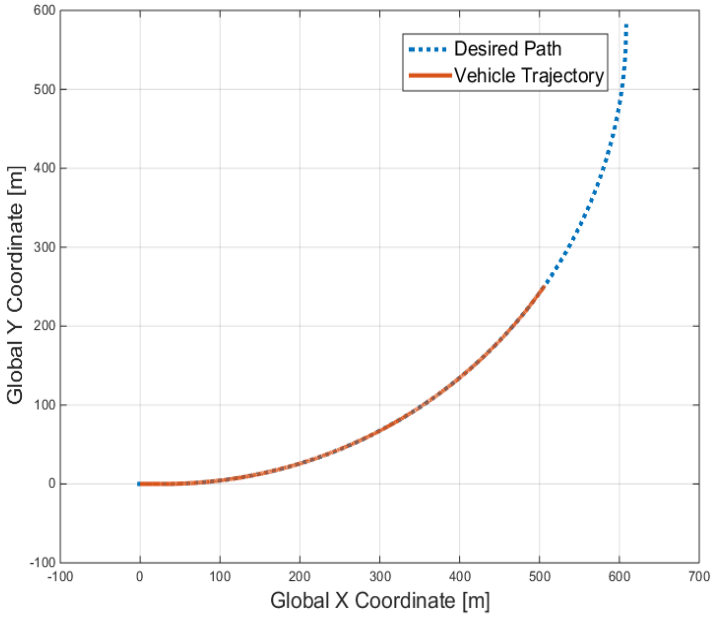

Figure 6-16: Test circuit with minimum curve radius 580 meter

In this scenario, again there is no target vehicle, host vehicle's initial velocity is 110 km/h and the user-set velocity has been set to 140 km/h as shown in Figure 6-17. The desired velocity in order to keep the vehicle on the road without being driven away from the curve is determined by proposed controller automatically based on road information.

It is observable that the velocity of the host vehicle tracks the new determined desired velocity instead of user-set velocity. Also longitudinal acceleration tracks the desired acceleration very closely within comfort limits. Furthermore, the simulation results also show that the lateral acceleration of the host vehicle does not exceed 2 ms^{-2} during vehicle travels along curvy path.

The vehicle tracks desired path very closely as shown in Figure 6-16. The magnitude of lateral position and yaw angle errors displayed in Figure 6-18 are not exceeding 0.08 m and 1 deg, respectively. Observe that computed steering angle is in limits and it has relatively lower magnitude in comparison with steering angle computed for previous circuit with radius 220 m. This confirms that at higher speeds small steering angle achieves cornering maneuvers safely and in comfort.

As a result, it is found that the lateral safety of the host vehicle is satisfied with the steering controller.

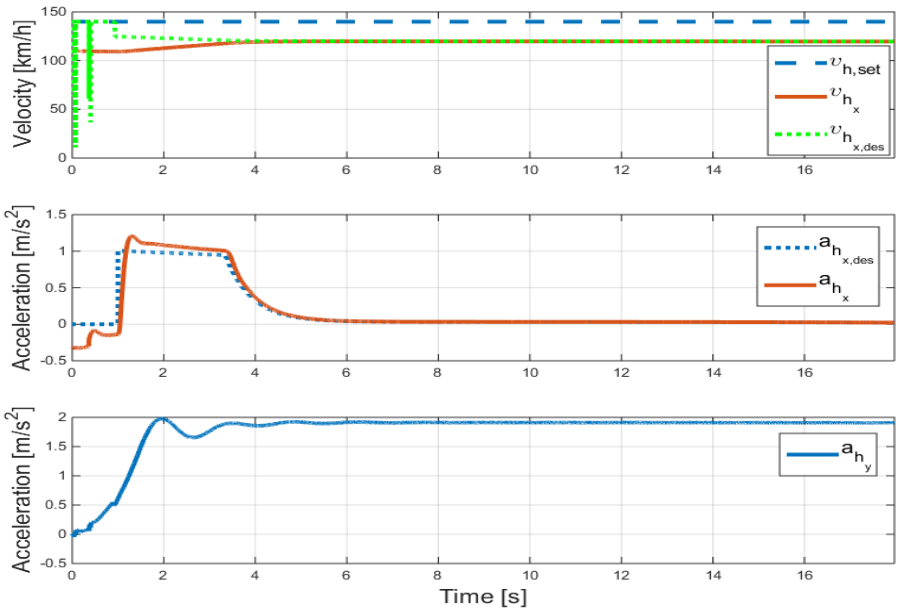

Figure 6-17: Simulation results for test scenario 7 (velocity, accelerations)

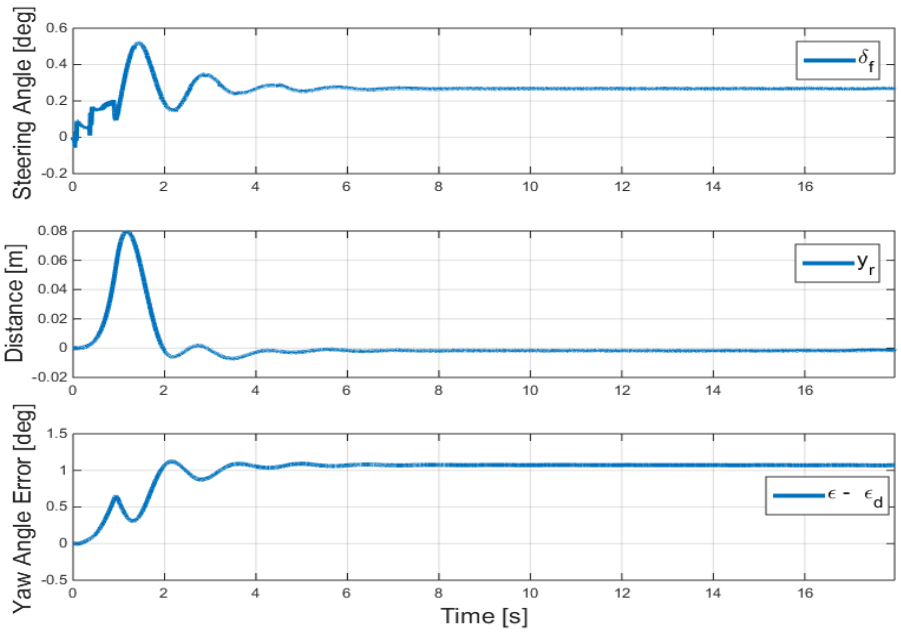

Figure 6-18: Simulation results for test scenario 7 (steering angle,lateral position,yaw angle error)

6-2-3 Integrated Control

The response of the vehicle with the Integrated Vehicle Dynamics Control (IVDC) has been evaluated via simulations. The integrated control parameters are provided in Appendix A-5. In the following, the cornering test scenarios were performed on circular test circuits to evaluate the performance of the integrated system for both lateral stability and safe clearance of autonomous driving vehicle.

Test Scenario 8: Normal Driving Mode

This test scenario is conducted by using a host vehicle and the target vehicle on the test circuit given in Figure 6-19.

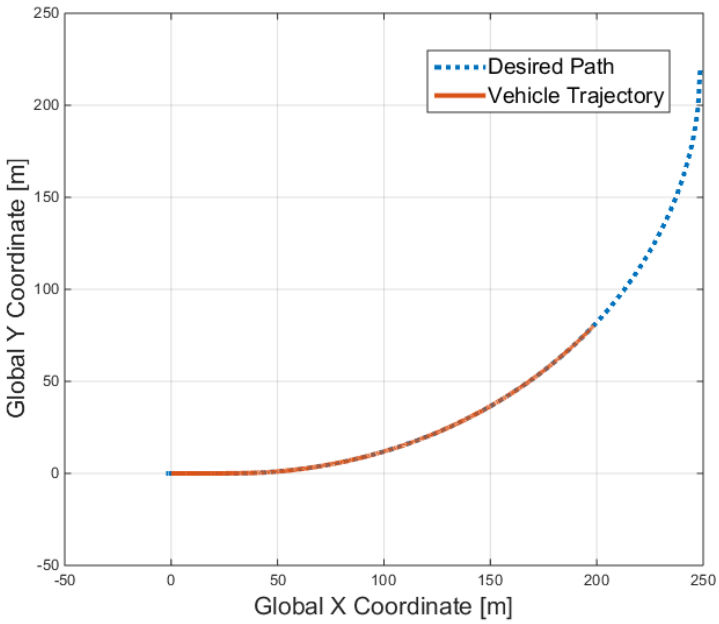

Figure 6-19: Test circuit and vehicle trajectory for test scenario 8

After activation of system at 1 second, the radar detects a target vehicle. The transition has been realized by system automatically to ACC mode to maintain the distance between the two vehicles based on a desired headway time. Then target vehicle begins to slow down at 4 second, and as a result, the host vehicle also starts to decrease its velocity as shown in Figure 6-20. Integrated and longitudinal control modes are displayed in Figure 6-21. The integrated control mode shown in the same figure indicates that the current driving situation is safe.

The vehicle velocities, the desired and actual accelerations of the host vehicle are compared in Figure 6-20. It is observable that the longitudinal acceleration of the host vehicle very closely tracks the desired acceleration profile in comfort limits defined in Section 3-1. Furthermore, the simulation results show that the lateral acceleration of the host vehicle does not exceed medium comfort level defined in Section 4-1.

The desired and actual distances are compared in Figure 6-21. The initial distance between the target and host vehicles is about 20 m. It can be seen that controller minimizes distance error and relative velocity, and their state-steady errors are in previously determined longitudinal performance ranges.

From the aspect of lateral performance, the host vehicle in spacing control mode tracks desired path very closely as shown in Figure 6-19. The lateral position error of the host vehicle while following target vehicle does not exceed 0.08 m and yaw angle error is below 1 degree as demonstrated in Figure 6-22. Note that computed steering angle is also within limits.

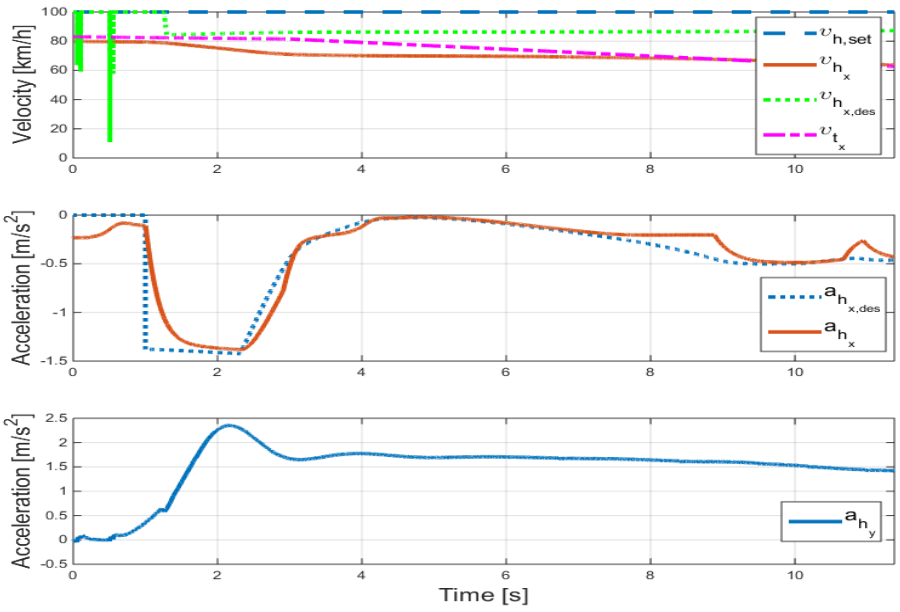

Figure 6-20: Simulation results for test scenario 8 (velocity, accelerations)

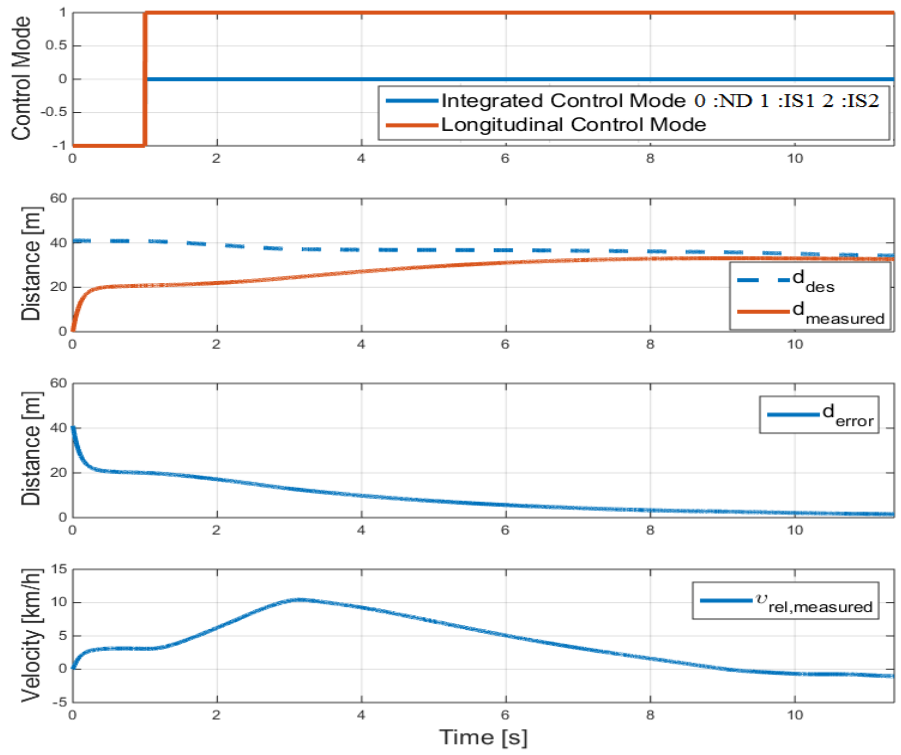

Figure 6-21: Simulation results for test scenario 8 (mode,distance,distance error,relative velocity)

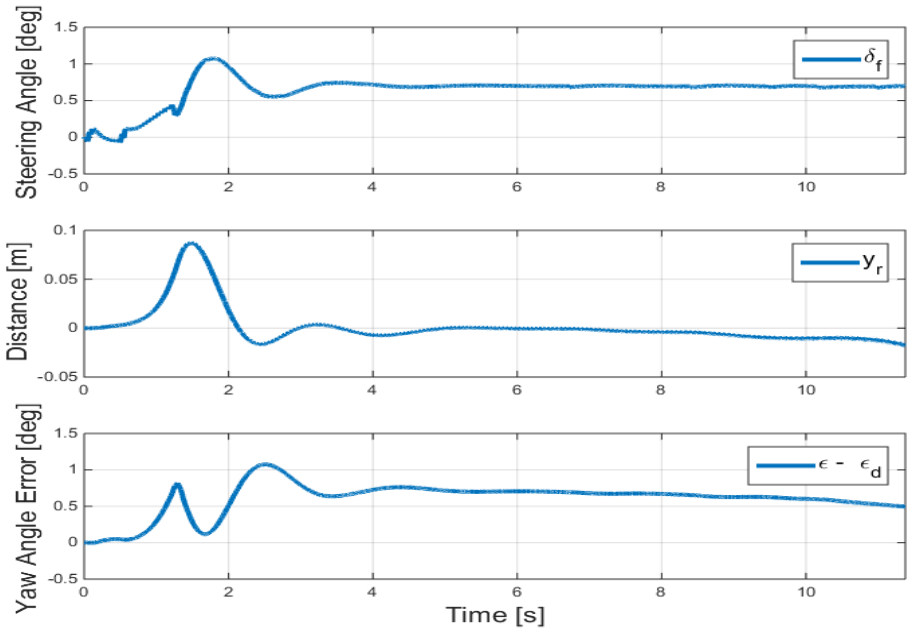

Figure 6-22: Simulation results for test scenario 8 (steering angle,lateral position,yaw angle error)

Test Scenario 9: Integrated Safety I

This test scenario is dedicated to examine longitudinal safety control performance in case of possible rear-end collision where the host and target vehicle act on the test circuit given in Figure 6-23.

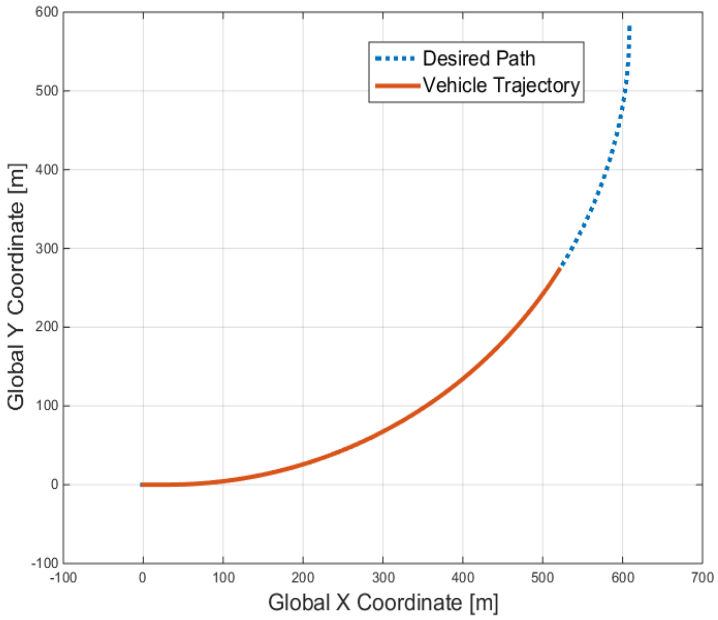

Figure 6-23: Test circuit and vehicle trajectory for test scenario 9

In this scenario, after activation of integrated control system at 1 second the radar detects a slower target vehicle in front with 100 meters gap. The host vehicle's initial velocity is 110 km/h and the user-set velocity has been set to 130 km/h as shown in Figure 6-24.

At 3 second, the target vehicle starts to decelerate during cornering. The integrated control system recognizes target vehicle as dangerous based on the warning index and the inverse TTC. For this situation, severe braking for in order to avoid collision with the target vehicle is applied to vehicle in CA mode. After 20 second, target vehicle starts to accelerate fast and acceleration of the host vehicle is limited for passenger comfort, system enables first CC mode.

Note that the danger of vehicle lateral unstable motion does not exist in this situation. Integrated and longitudinal control modes shown in Figure 6-25 indicate that longitudinal safety control to avoid rear end collision has control priority in current driving situation.

Comparisons of vehicle velocities, desired and actual longitudinal accelerations are shown in Figure 6-24 respectively. Observe that the proposed system activates a large deceleration about -8 ms^{-2} to avoid collision with the rear-end of the target vehicle.

After severe braking, the host vehicle follows the velocity of target vehicle adequately to maintain the spacing policy as shown in Figure 6-25. It can be seen that controller minimizes distance error and relative velocity.

Since the scenario needs longitudinal safety control for the collision avoidance without lateral stability control, the conventional systems determine a braking input considering only the collision avoidance. However, proposed integrated control system assures lateral stability by manipulating steering angle as shown in Figure 6-26. The test results agree on satisfactory path tracking performance, with the magnitudes of lateral position and yaw angle error below 0.08 m and 1 degree during whole simulation. These errors are below previously determined in lateral performance specifications. Since lateral acceleration of the host vehicle does not violate medium comfort level during whole simulation as shown in Figure 6-24, it proves that optimal combination of computed braking and steering inputs achieve lateral stability.

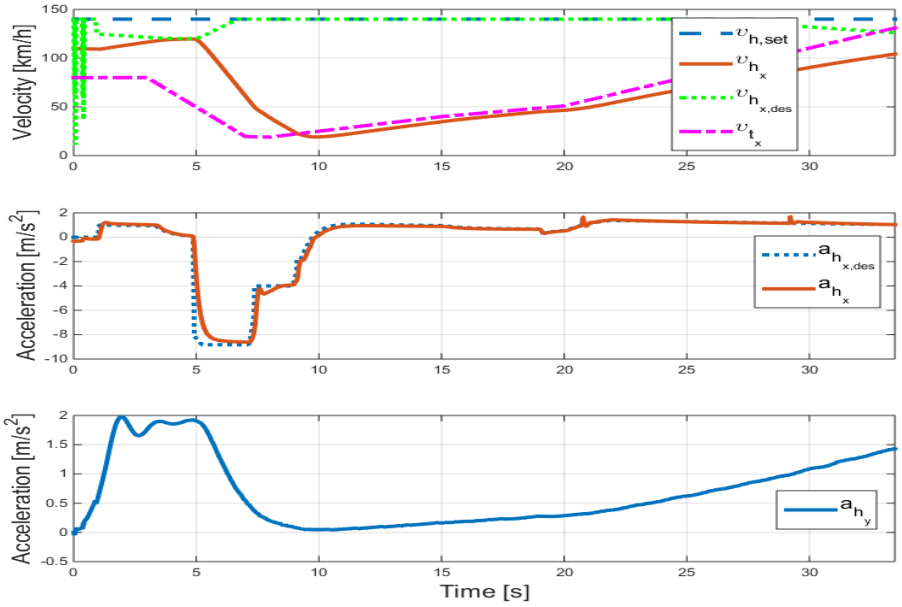

Figure 6-24: Simulation results for test scenario 9 (velocity, accelerations)

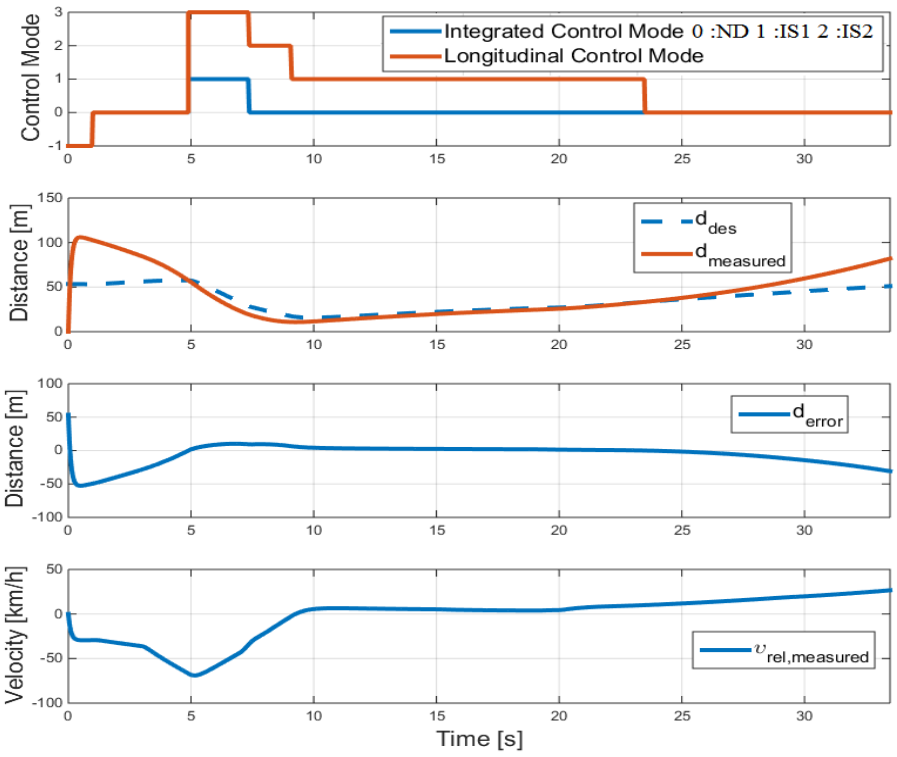

Figure 6-25: Simulation results for test scenario 9 (mode,distance,distance error,relative velocity)

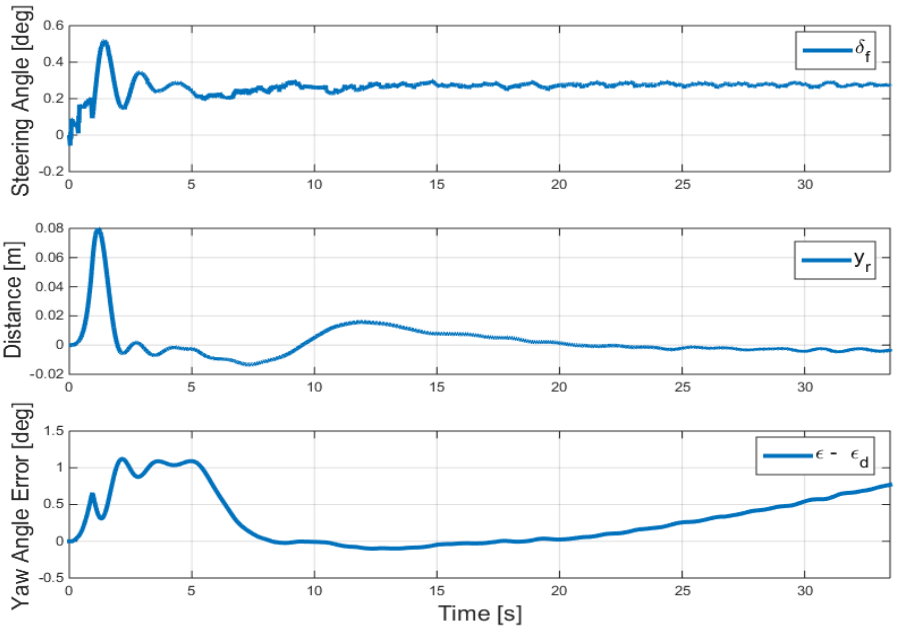

Figure 6-26: Simulation results for test scenario 9 (steering angle,lateral position,yaw angle error)

Test Scenario 10: Integrated Safety II

In the case of unstable lateral motion of the host vehicle, performance of lateral safety control has been investigated in this test scenario. The host and target vehicle run on the test circuit demonstrated in Figure 6-27.

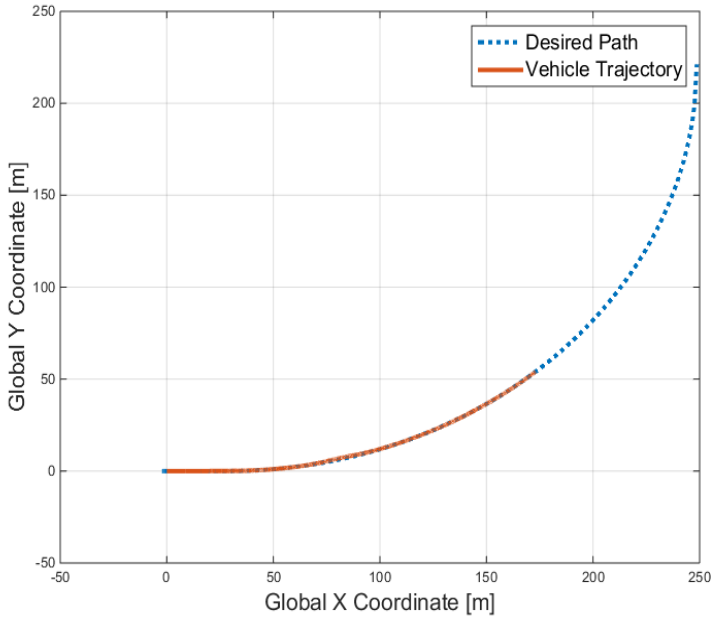

Figure 6-27: Test circuit and vehicle trajectory for test scenario 10

Several reasons such as external forces, road and weather conditions etc. may cause to unstable lateral motion in vehicles. Since assuming friction coefficient is constant, unstable lateral motion caused by road and weather conditions simply is not considered. This test scenario has been constructed on that external force has exerted on vehicle. Fictionally this situation can be expressed as that another passenger vehicle bumps into host vehicle sidewards.

Test scenario is initialized as that the host vehicle follows a target vehicle along curvy path in ACC mode. A lateral disturbance force (magnitude of 7125 N) is applied to host vehicle between 3-4 seconds. Note that such a lateral disturbance force can easily cause the host vehicle driven away from the road and complicate controlling of vehicle. Therefore, this vehicle behavior can be interpreted as unstable lateral motion. As a consequence of this disturbance, lateral index exceeds unit level and proposed integrated controller evaluates driving situation as unstable lateral motion for host vehicle. Integrated Safety II mode is triggered as displayed in Figure 6-29.

The computed braking and steering inputs, which can simultaneously accomplish to continue to track the desired path and to improve vehicle lateral stability, are applied to vehicle.

Then the host vehicle slows down in order to improve lateral stability. Since target vehicle speeds up, the host vehicle continues to travel along the rest of desired path in CC mode as shown in Figure 6-28. It is observable that magnitude of longitudinal acceleration pass over -8 ms^{-2} in order to regain lateral stability and to achieve keeping vehicle on desired path as much as possible. Except time interval in which vehicle is subject of disturbance, longitudinal and lateral accelerations do not exceed comfort limits during whole simulation.

In the scope of path tracking performance of steering controller, simulations results are displayed in Figure 6-30. It can be seen that computed steering angle reacts immediately to reject disturbance. The magnitudes of lateral position and yaw angle errors are displayed respectively.

The simulation results agree on satisfactory path tracking performance that maximum deviation from desired path under disturbance is below 0.8 m. Then host vehicle converges to desired path again. The proposed integrated controller handles unstable lateral vehicle motion adequately and quickly. The resulting trajectory of the host vehicle is drawn in 6-27.

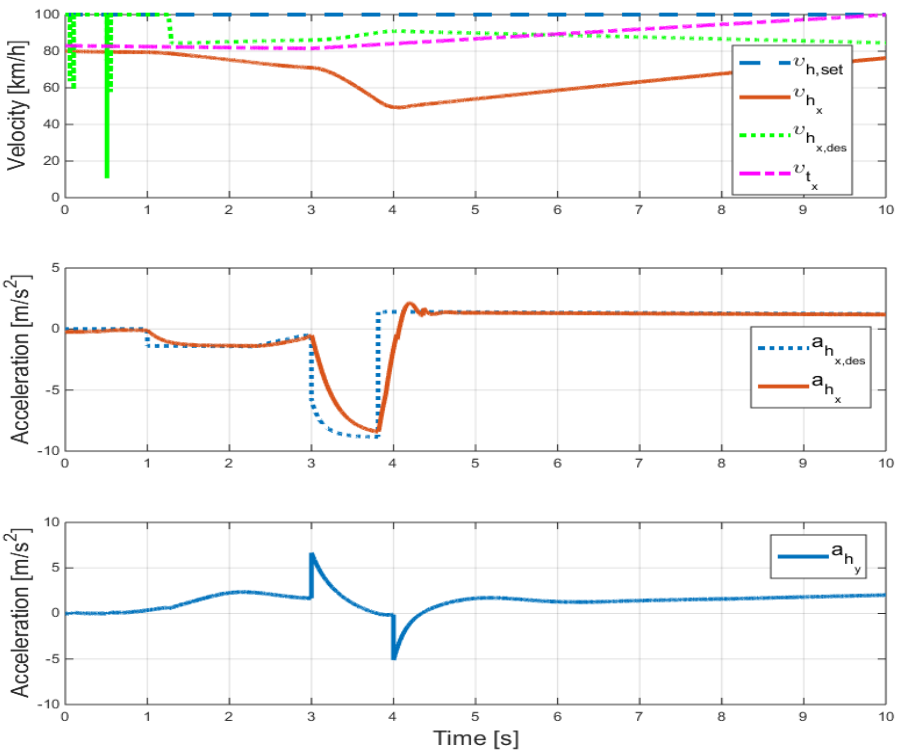

Figure 6-28: Simulation results for test scenario 10 (mode,distance,distance error,relative velocity)

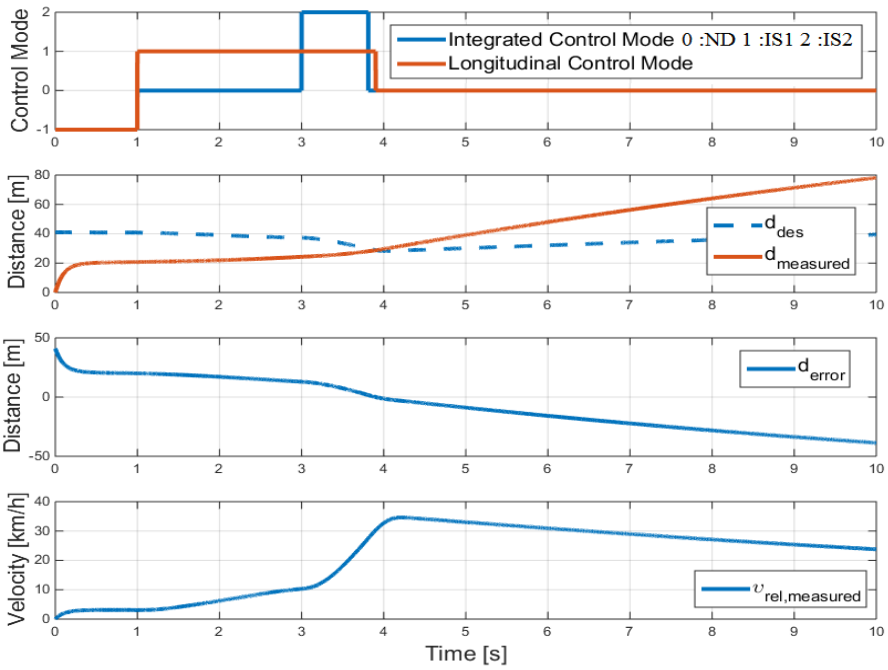

Figure 6-29: Simulation results for test scenario 10 (mode, distance, distance error, relative velocity)

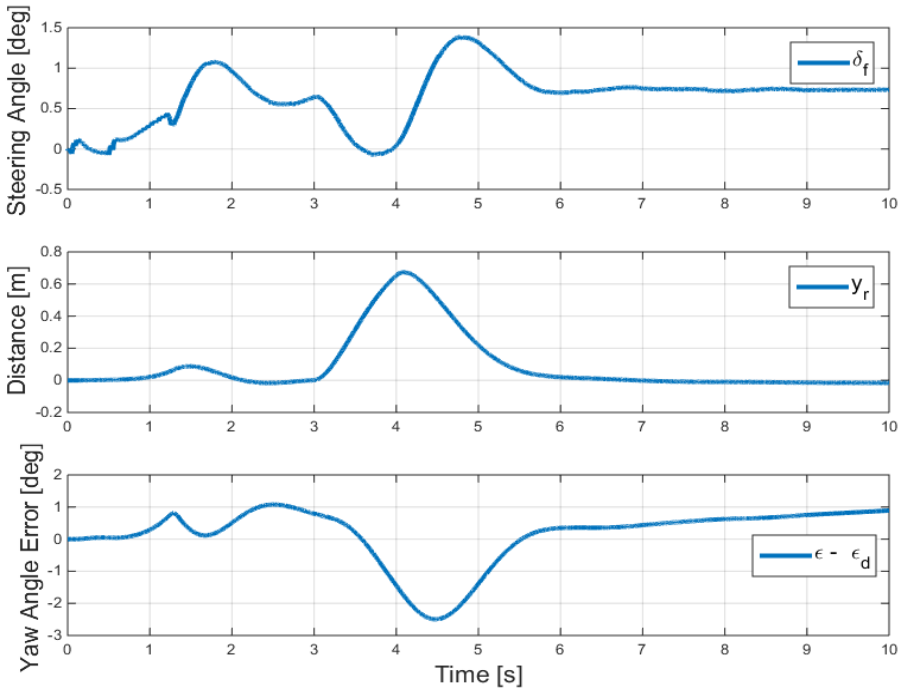

Figure 6-30: Simulation results for test scenario 10 (steering angle, lateral position, yaw angle error)

Chapter 7

Conclusions and Future Work

7-1 Conclusions

The vehicle model is constructed by using Matlab/Simulink, for the purpose of developing an Integrated Vehicle Dynamics Control (IVDC) system in different traffic scenarios. The two-wheeled model includes external resistance forces (aerodynamic drag resistance, rolling resistance, gravitational effects), load distribution, nonlinear longitudinal tire forces, linear lateral tire forces, the power train, brake and wheel dynamic effects.

The inputs of vehicle are characterized by the throttle, brake and steering actuator inputs. Acceleration, braking and steering performance of vehicle are investigated through simulations. Although the vehicle dynamics model is not validated against experimental data, the chosen parameters closely resemble an actual vehicle. Subjective evaluations are used to ascertain realistic driving.

In the scope longitudinal control, a control system that is prior to ensure safety and human-comfort in autonomous vehicles has been developed. The proposed longitudinal control system consists two levels of control such as the upper-level and low-level controllers.

The upper-level controller has been designed to achieve behavior of the host vehicle that would seem natural to a human driver in normal-driving situations and to achieve safe behavior in severe-braking situations in which large decelerations are necessary.

In the case of the radar does not detect any vehicle in the path of the host vehicle, proposed controller enables "Longitudinal Control Mode-0" and acts like the conventional Cruise Controller (CC). A Proportional-Derivative (PD) controller is designed so that the velocity of host vehicle converges to the user-set velocity.

When the radar detects a target vehicle in the ACC equipped vehicle's path, proposed longitudinal control system maintains a desired distance based on the velocity of the host vehicle and a user-specified time gap. Considering severe driving situations and to integrate the ACC and CA systems, the proposed algorithm makes the host vehicle operate in three modes: comfort, large-deceleration, and severe-braking. While in "comfort-mode (Longitudinal Control

Mode-1)", the control objective is to maintain the safety distance from the preceding vehicle while making the process seem natural to the driver. If the driving situation, based on indexes, is determined to be a "large- deceleration mode (Longitudinal Control Mode-2)", the ACC+CA system informs the driver by giving a warning signal and then decelerates. A linear optimal control method has been used for design of ACC and ACC+CA systems. In the case of a dangerous situation, the ACC+CA system switches to the "severe-braking mode (Longitudinal Control Mode-3)", and generates emergency-braking to completely avoid a rear-end collision in vehicle-following situations. The desired acceleration is computed by using nonlinear functions that map the indexes to the desired accelerations in severe-braking situations. To ensure driver acceptance and CA performance simultaneously, the threshold values for the warning index and inverse TTC for each control mode are used from manual-driving data, including those in normal-driving and severe-braking situations.

The low-level controller determines whether to apply braking control or throttle control so that the acceleration of the vehicle tracks a desired acceleration based on reverse dynamics. The longitudinal acceleration of host vehicle is limited in order not to cause ride comfort to deteriorate.

Simulations are conducted using a set of traffic scenarios which are likely to occur in reality, the results obtained from the simulated cases and their effects on the performance of the vehicle are examined and reported. The simulation results show that proposed controller in vehicle velocity and spacing control mode works in a satisfactory manner. It has been shown that the proposed controller can provide a natural following performance that is similar to human manual- driving at both high-speed driving and low-speed situations, and can prevent the vehicle-to-vehicle distance from dropping to an unsafe level in severe-braking situations. Seeing that the proposed system performs more adequate reactions in advance, it can be expected that the proposed system improves the driver acceptance and the safety.

Since driver acceptance of the proposed control system is crucial and to allow driver to personalize the control system in a desired manner, parameterization directly related to the key characteristics such as safety and comfort is included. The tuning parameters P_s and P_c which vary behavior of proposed control system are united in one design parameter P in order to allow driver to tune easily and intuitively.

Simulations have shown the proper functioning of the parameterized control system for a complete envelope of working conditions by changing the behavior of the system by adjusting the setting of the design parameter P. Thus, the overall longitudinal control can be a good solution for enhancing driver acceptance.

In the scope lateral control, a steering controller has been designed and synthesized by using algorithms which allowed for the inclusion of tracking performance, ride quality, and robustness specifications into the controller design.

A steering controller integrated with a desired speed determination function for autonomous vehicle path tracking by using GPS data has been presented. For lateral plane, the linearized model is used under several assumptions. The steering performance of vehicle model for simulation is examined and compared to real vehicle test data.

An optimal finite preview control method is used to develop a steering controller. The applied control algorithm manipulates not only the current error deviated from the desired path but also the prediction using a future information regarding road. The steering control input is

computed by taking into account the road information within preview distance. The speed determination module generates the desired speed command necessary to maintain a lateral acceleration limit and improve vehicle safety.

From the simulation results, it is found that the steering controller using finite preview optimal control produces satisfactory path tracking performance. Numerical results of simulations verify that the controller is able to steer the vehicle on a curved road for a wide range of operating conditions. Furthermore, the safety of the vehicle in lateral plane is improved by combining the steering controller with a desired speed determination function that maintains a lateral acceleration limit.

The current ACC systems automatically adjust speed to maintain a safe headway distance between the vehicles in the same lane by relying on a frontal radar. Major drawbacks resulting from this basic approach are the limited performance in high curvature environments and the inability to perform adequate reactions in advance. In order to obtain both lateral stability and safe clearance of autonomous driving vehicle, an IVDC strategy has been proposed. The proposed integrated control system has been implemented by interconnecting previously designed longitudinal and lateral controllers. The integrated control system, which addresses the complex interactions that emerge as a result of integrating these controllers, consists of 4 main layers such as Supervisor, Decision, Control Algorithm and Coordinator to create synergy and safe interaction between longitudinal and lateral controllers to ensure better performance overall.

The proposed control strategy is designed to optimally coordinate the throttle/brake and steering actuators simultaneously to obtain both lateral stability and longitudinal safety in various driving situations. Supervisor layer performs path planning and to determines desired vehicle motions. "Normal Driving", "Integrated Safety I", and "Integrated Safety II" modes have been defined in the index-based plane. In order to determine the current control mode, the longitudinal and lateral indexes are used. According to the selected control mode, the control algorithm layer respectively calculates a steering angle to track the desired path and improve vehicle lateral stability, a longitudinal acceleration to reach desired speed or to avoid rear-end collisions. From the control algorithm and the decision layers, the coordinator distributes actuator inputs optimally.

Simulations have been conducted to investigate the performance of the proposed IVDC system in various driving situations. From the simulations, it has been shown that the proposed system achieves lateral stability and prevents the vehicle to vehicle collision by optimal combination of computed throttle/brake and steering inputs. Especially the proposed control system improves the vehicle safety in severe driving situations in which both longitudinal and lateral motions are to be controlled simultaneously.

It has been shown that the integrated control system can provide natural following performance in a safe normal driving situation, and both the longitudinal and lateral acceleration of the host vehicle are within comfort limits. Furthermore, it can prevent the vehicle-to-vehicle distance from dropping to an unsafe level by using a severe braking or it can handle unstable lateral vehicle motion adequately and quickly depending on the driving situation. Simulation results show that the proposed integrated controller satisfies the performance in terms of autonomous driving and collision avoidance.

7-2 Future Work

In regards to future work, the focus will be on improvement of current work and development of system with new functions and technologies.

In the scope of improvement, the theoretical and experimental studies on vehicle model and integrated control will probably focus on the following issues.

High accuracy mathematical models that capture the dynamics of vehicle system are critical in this design task. An excellent means to determine such models is the use of system identification techniques. Therefore, vehicle model can be obtained from system identification methods.

More precise tire model which yields higher control precision is essential. The coupled longitudinal and lateral tire forces with non-linearities can be considered.

Further investigation is necessary on the details of weight distribution on tire forces and moments for vehicle stability control especially in cornering situations.

Currently used switching logic between Velocity Control (VC) and Spacing Control (SC) modes in longitudinal control system should be replaced with more sophisticated one in order to prevent unnecessary frequent switchings.

In the scope of development, new functions, algorithms and technologies can be integrated to vehicle and control systems.

Although assuming that friction coefficient is constant, the fact exists that friction coefficient changes slightly based on different road and weather conditions etc. Since friction coefficient is crucial for controlling of vehicle in both longitudinal and lateral planes, a function for friction coefficient estimation can be appended to control system.

Vehicle ride quality and handling performance can be improved through modification of vehicle dynamics in vertical directions and by integrating a suspension controller.

In general, a collision can be avoided either by decelerating to a full stop without hitting the obstacle, or by executing a timely lane-change maneuver. A lane change maneuver may be more desirable since it least disturbs the traffic flow and requires less deceleration. However, executing lane change maneuver may depend on the current traffic in the neighboring lanes, the vehicle speed, and its distance to the obstacle. If the traffic in the neighboring lane allows a lane change, then the host vehicle may execute a comfortable lane transition. More advanced algorithms for driving maneuvers such overtaking or lane change can be inserted into integrated control system.

General aim for future research is to study the possible interactions between multiple automotive control systems deployed together and formally define their interacting behavior as well as the impact on the overall system. This interacting behavior is important because there are possible cases where these systems can have conflicting objectives, and, hence, a clear understanding of their underlying interaction is crucial.

Future research will focus on the design of an integrated control system with different key characteristics, such as fuel economic driving or traffic flow efficiency. Furthermore, research will focus on extending the target-host vehicle to multiple vehicles. Taking vehicle-to-vehicle communication into account too, allows for the design of so-called cooperative ACC systems.

The communication provides additional information concerning the surrounding traffic in addition to the radar and GPS data, which can be very beneficial to the overall system behavior.

Future work will include further investigation into increasing the robustness of the integrated controller. Strategy tuning, control threshold value tuning, real-time implementation of integrated controller and experimental verification for different road conditions, are the future areas of research to extend the applicability of the proposed control method.

With the developments of sensor technology which is the way of control system obtaining data from a radar, GPS and camera; 3-D data and telematics technologies can used for data collection and sensor fusion. Thus, target vehicle selection can be performed more properly, even in cornering situations. Furthermore, pedestrian, cyclist or animal interactions also can be considered.

X-by-wire technology in the automotive industry is the use of electrical or electro-mechanical systems for performing vehicle functions traditionally achieved by mechanical linkages. Response time of IVDC incorporated with X-by-wire technology can be improved through elimination of mechanical linkages. Such incorporation may provide more design flexibility for vehicle dynamics control and integration.

A Lane Keeping Assist (LKA) mechanism can either reactively turn a vehicle back into the lane if it starts to leave or pro-actively keep the vehicle in the center of the lane. Lateral stability and path tracking performance of integrated controller can be improved by conjugating with LKA.

Appendix A

Parameters

A-1 Main File

```
%% MSc Thesis Project
% Title: Safe Interaction Between Lateral and Longitudinal
%        Adaptive Cruise Control in  Autonomous Vehicles
%
% A.F. Idriz - 4326962
% March 2015, TU Delft

%%%%%%%%%%%%%%%%%%%%%%%%%%%%%%%%%%%%%%%%%%%%%%%%%%%%%%%%%%%%%%%%%%%%%%%%%%%%%%%
clear
close all
clc;

%% Simulation Parameter
step_size = 1e-3;

%% Comfort and Safety Tuning Parameters
P = 0.5    % [0,1] Single-Tuning Parameter
Pc = P     % [0,1] Comfort Paramter
Ps = 1-Pc % [0,1] Safety Parameter

%% Load Parameters

% Load Vehicle Parameters
run('Vehicle_Parameters.m')

% Low-Level Controller Parameters
run('Low_Level_Controller_Parameters.m')

% Longitudinal Controller Parameters
run('Long_Controller_Parameters.m')
```

```
31
32 % Lateral Controller Parameters
33 run('Lat_Controller_Parameters.m')
34
35 %% Extraction of Road Information
36 run('pathplanning.m')
```

A-2 Vehicle Parameters

```
1  %%%%%%%%%%%%%%%%%%%%%%%%%%%%%%%%%%%%%%%%%%%%%%%%%%%%%%%%%%%%%%%%%%%%%%%%%%%%
2  % Vehicle Model Parameters
3  %%%%%%%%%%%%%%%%%%%%%%%%%%%%%%%%%%%%%%%%%%%%%%%%%%%%%%%%%%%%%%%%%%%%%%%%%%%%
4
5  %% Conversions
6  rad2deg=180/pi;
7  deg2rad=pi/180;
8  rad=1/deg2rad;
9  mile= 1.609344; %[km]
10 meter_per_second=3.6; % [km/h]
11 mps=2.237; % [mph]
12 radpersecond2rpm=60/(2*pi);
13
14 %% Environment
15 g = 9.806;% [m/s^2] Gravitational Acceleration
16 friction_mu= 0.9; % Friction coefficient (Dry Asphalt)
17 varrho= 1.225;% [kg/m^3] Atmospheric air density
18 theta= 0; % [deg] Inclination/slope of the road * Neglected *
19
20 %% Vehicle Data
21 m =1425 ;%[kg] Total mass of the vehicle (Toyota Prius)
22
23 CD= 0.25;% Drag factor (Toyota Prius)
24 Ah= 1.6 + 0.00056*(m-765); % Area of vehicle frontal projection
25 CR= 0.0136; % Coefficient of rolling resistance(Radial-ply passenger car)
26
27 lf=1.24;%[m] Distances of front wheel axle of the vehicle from CoG
28 lr=1.46;%[m] Distances of rear wheel axle of the vehicle from CoG
29 L=lf+lr;%[m] Distance between front and the rear wheel axle(Toyota Prius)
30 h= 0.6;% Height of center of gravity
31 W=1.745; % [m]
32 H=4.480; % [m]
33
34 % No Rear wheel steering angle
35 delta_r_des= 0;
36
37 Iz=(m*(W^2+H^2))/12 %[kg-m^2] Mass moment of inertia wrt a vertical axis
38
39 r= 0.3; % [m] Radius of wheels
40
41 % Static weight distribution
42 Fzf_static=m*g*((lr*cos(theta*deg2rad))/L +(h*sin(theta*deg2rad))/L)
43 Fzr_static=m*g*((lf*cos(theta*deg2rad))/L -(h*sin(theta*deg2rad))/L)
```

```
%% Tire Model

Cs= 0.16; % for 0.16/deg for radial ply tires
% (Fzf_static/2)
% Cornering stiffnesses front coefficient
Cyf= 0.5*Cs*Fzf_static*rad %[N/rad]
%Cornering stiffnesses rear coefficient
Cyr= 0.5*Cs*Fzr_static*rad %[N/rad]

% Coefficients of the Pacejka tire model for Longitudinal forces
Bp= 10; Cp= 1.9; Dp= 1; Ep= 0.97; % (Dry Tarmac)

%Kamm's Friction Circle
mu_Fz= m*g*friction_mu

%% Engine System
tau_e = 0.2; %[s] Engine lumped time lag
i_f =  3.23; % Final drive ratio

RPM=[800 1200 1600 2000 2400 2800 3200 3600 4000 4400 4800]';

alpha_throttle=[0 10 20  30 40 50 60 70 80 90 100];

% % % strictly monotonic increasing torque map
torque_map=[-40 -44 -49 -53 -57 -61 -65 -70 -74 -78 -82
             88  37  18   7  -6 -16 -27 -36 -44 -50 -57
            215 117  85  66  44  29  10  -2 -13 -22 -32
            245 208 178 148 122 104  85  66  48  33  18
            261 260 241 219 193 167 152 133 119  96  85
            262 279 282 275 260 238 223 208 189 171 152
            263 290 293 297 290 275 260 256 234 212 193
            264 297 305 305 305 301 293 282 267 249 226
            265 299 308 312 319 323 319 316 297 279 253
            266 300 311 318 326 327 327 327 312 293 267
            267 301 312 319 327 334 334 334 319 305 275];

Torque_MAX=max(max(torque_map));
Torque_MIN=min(min(torque_map));
RPM_MAX=max(max(RPM));
RPM_MIN=min(min(RPM));

%% Brake System
Kc = 1; % Pressure front and rear gain

extra   = 1.7;
Kbf     = 15 *extra;%[Nm/Bar] Pressure/torque conversion front constants
Kbr     = Kbf/3; %[Nm/Bar] Pressure/torque conversion rear constants

tau_b   = 0.2; %[s] Brake system lumped time lag

I_w = 1.4; %[kg-m^2] Moment of inertia of the wheels

%% Steering Dynamics
```

```
tau_delta = 0.2; %[s] Steering actuator dynamic time constant 0.15-0.25
delta_driver_wheel_ratio = 18; % range 16-19

%% Sensor Model
tau_r = 0.1; %[s]

%% Initial Velocity Conditions

% Vinital = 100/3.6 %[m/s] braking test
% Vinital = 2/3.6 %[m/s] %acceleration performance
% Vinital = 85/3.6 %[m/s] car following
% Vinital = 110/3.6 %[m/s] steering @ rho=580
  Vinital = 80/3.6 %[m/s] steering @ rho=220
% Vinital = 40/3.6 %[m/s] steering test

Vmax = 256/3.6; %[m/s]
```

A-3 Longitudinal Control Parameters

```
%%%%%%%%%%%%%%%%%%%%%%%%%%%%%%%%%%%%%%%%%%%%%%%%%%%%%%%%%%%%%%%%%%%%%%%%%%%%
% Longitudinal Controller Parameters
%%%%%%%%%%%%%%%%%%%%%%%%%%%%%%%%%%%%%%%%%%%%%%%%%%%%%%%%%%%%%%%%%%%%%%%%%%%%

% Acceleration constraints
ahx_min = -g*friction_mu; % [m/s^2]

ahx_ACC_CA = -4; % [m/s^2]
ahx_max =  2.25; % [m/s^2]

% Spacing Policy
d0 = 7.7; %[m] standstill distance
thw = 0.5 + 2* Ps % 0.5-2.5 [s]  desired headway time

tau_h = 0.675; %[s] Human delay


%% MODE-1 & 2 - Linear Quadratic Controller

% States
Ax = [0 -1; 0 0];
Bx = [0 -1]';

% weighting matrices at  speed region 0-40 km/h
qe =  0.2;
qvr = 0.75;
qah =2;

Qx = [qe*Ps 0 ; 0 qvr]
Rx = qah*Pc


% Velocity-dependent control gain at  speed region 0-40 km/h
```

```
for i=1:12
Kx(:,i) = lqr(Ax,Bx,Qx,Rx);
end

% weighting matrices at speed region > 40 km/h
qe =  2;
qvr = 2;
qah = 64;

Qx = [qe*Ps 0 ; 0 qvr]
Rx = qah*Pc

% Velocity-dependent control gain at speed region > 40 km/h
for i=13:50
Kx(:,i) = lqr(Ax,Bx,Qx,Rx);
end

%% Severe braking MODE-3 Controller
Velocity= 0:10:200;

% Weighting factors
W1=[1  1  1  1  1  0.66  0.33  0  0  0  0  0  0  0  0  0  0  0  0  0  0];
W2=[0  0  0  0  0  0.33  0.66  1  1  1  1  1  1  1  1  1  1  1  1  1  1];

% Threshold values for the inverse TTC
iT_threshold = [0  0.21  0.49  0.68  1.35 ];
deceleration_iT = [0 -2 -4 -6 ahx_min];

% Threshold values for the warning index
kappa_threshold =     [ 0.01  0.20  0.65  0.81  1.20   2];
deceleration_kappa = [  ahx_min    -8    -6    -4    -2   0];
```

A-4 Lateral Control Parameters

```
% %%%%%%%%%%%%%%%%%%%%%%%%%%%%%%%%%%%%%%%%%%%%%%%%%%%%%%%%%%%%%%%%%%%%%%%%%%%
% % Lateral Controller Parameters
% %%%%%%%%%%%%%%%%%%%%%%%%%%%%%%%%%%%%%%%%%%%%%%%%%%%%%%%%%%%%%%%%%%%%%%%%%%%

% Acceleration constraints
ahy_max = 7.2; % [m/s^2]
ahy_comfort = 3.6 ; % [m/s^2]

% Steering constraint
delta_f_0= 10;

%% State Space and Controller

% States
Ay1= -2*(Cyf+Cyr)/m;

Ay2= 2*(-lf*Cyf+lr*Cyr)/m;

```

```
19 Ay3= 2*(-lf*Cyf+lr*Cyr)/Iz;
20
21 Ay4= -2*((lf^2)*Cyf+(lr^2)*Cyr)/Iz;
22
23 By1= 2*Cyf/m;
24
25 By2= 2*Cyf*lf/Iz;
26
27 By = [ 0 By1 0 By2]';
28
29 Gamma_y = [ 0 0 ; 1 0 ; 0 0 ; 0 1];
30
31 Cy= [ 1 0 0 0; 0 1 0 0 ; 0 0 1 0 ; 0 1 0 0 ];
32
33
34 for i=1:50 % 0-50 [m/s]
35
36 Ay1_vel(i)=Ay1/i ;
37 Ay2_vel(i)=Ay2/i ;
38 Ay3_vel(i)=Ay3/i ;
39 Ay4_vel(i)=Ay4/i ;
40
41 end
42
43 % weighting matrices
44 Qy = [0.01 0 0 0; 0 0 0 0 ; 0 0 1 0 ; 0 0 0 0]
45 Ry = 5
46
47
48 for i=1:50;
49
50 Ay = [ 0 1 0 0 ;  0 Ay1_vel(i) -Ay1 Ay2_vel(i); 0 0 0 1 ; 0 Ay3_vel(i) -
       Ay3 Ay4_vel(i)];
51 %Observability
52 check(i)=(rank(obsv(Ay,Cy)));
53
54 Ay_vel{1,i}=Ay;
55
56 % Velocity-dependent control gain
57 [Ky(:,i),Pss{1,i}] = lqr(Ay,By,Qy,Ry);
58
59 end
60 min(check)
61
62 sim_Ay=cell2mat(Ay_vel);
63 sim_Pss=cell2mat(Pss);
```

A-5 Trajectory Generation and Extraction of Road Information

```
%%%%%%%%%%%%%%%%%%%%%%%%%%%%%%%%%%%%%%%%%%%%%%%%%%%%%%%%%%%%%%%%%%%%%%%%%%%%
% Trajectory Generation and Data extraction
%%%%%%%%%%%%%%%%%%%%%%%%%%%%%%%%%%%%%%%%%%%%%%%%%%%%%%%%%%%%%%%%%%%%%%%%%%%%

%% Test circuit generation

% % rho= 220  @ 80kmh
[xc1,yc1]=cercle(28.6,220,220);
X=[-lf:28  xc1  ];
Y=[0*(0:29) yc1 ];

% % rho= 580 @ 130 kmh
% [xc1,yc1]=cercle(28.6,580,580);
% X=[-lf:28  xc1 ];
% Y=[0*(0:29) yc1 ];


%% Extraction of road information

% Length of road
end_of_road=X(end)

%  Approximate Derivatives
x_d= diff(X);
x_d_d= diff(x_d);
y_d= diff(Y);
y_d_d= diff(y_d);

length_X=size(X,2);

% Curvature and radius of curvature
for i=1:length_X-2

    if ( x_d(i)==0 )
      x_d(i)=10^(-4);
    end

    if ( y_d(i)==0)
      y_d(i)=10^(-4);
    end

 % Curvature
 curvature(i)= (x_d(i)*y_d_d(i) - y_d(i)*x_d_d(i))/(x_d(i)^2 + y_d(i)^2)
     ^(3/2);

%  radius of curvature

    if curvature(i)==0

        rho(i)=10^4;
```

```
50      else
51
52          rho(i)=1/curvature(i);
53      end
54
55      if (rho(i)>10^4)
56
57          rho(i)=10^4;
58
59      elseif (rho(i)<-10^(4))
60                  rho(i)=-10^(4);
61      end
62
63      if i==size(X,2)-2
64         full=[rho rho(i) rho(i)];
65      end
66
67  end
68
69  % Tangent Vector
70  TangentVector=myfrenet(X,Y,0*X);
71
72  % Unit x-axis vector
73  unit= [1  0  0];
74
75  for i=1:length_X
76  Cos_varepsilon(i)= dot(unit,TangentVector(i,:))/(norm(unit)*norm(
        TangentVector(i,:)));
77
78  % Desired yaw angle
79  varepsilon_des(i)= sign(TangentVector(i,1))*sign(TangentVector(i,2))*acos
        (Cos_varepsilon(i))*180/pi;
80
81  % Maximum allowable speed in the curve
82  Vlimit(i)= sqrt(abs(full(i))*g*friction_mu);
83  end
```

Appendix B

Overview of Implementation

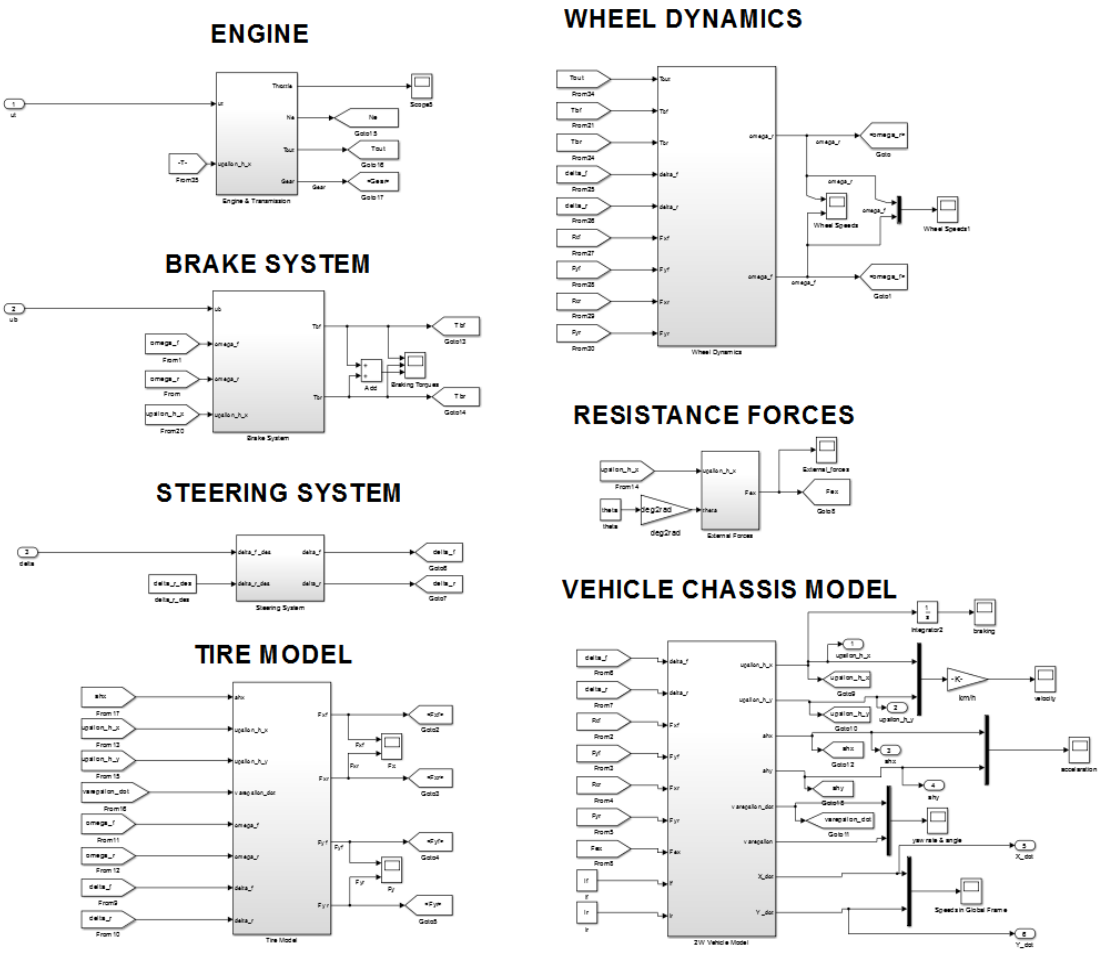

Figure B-1: Vehicle model

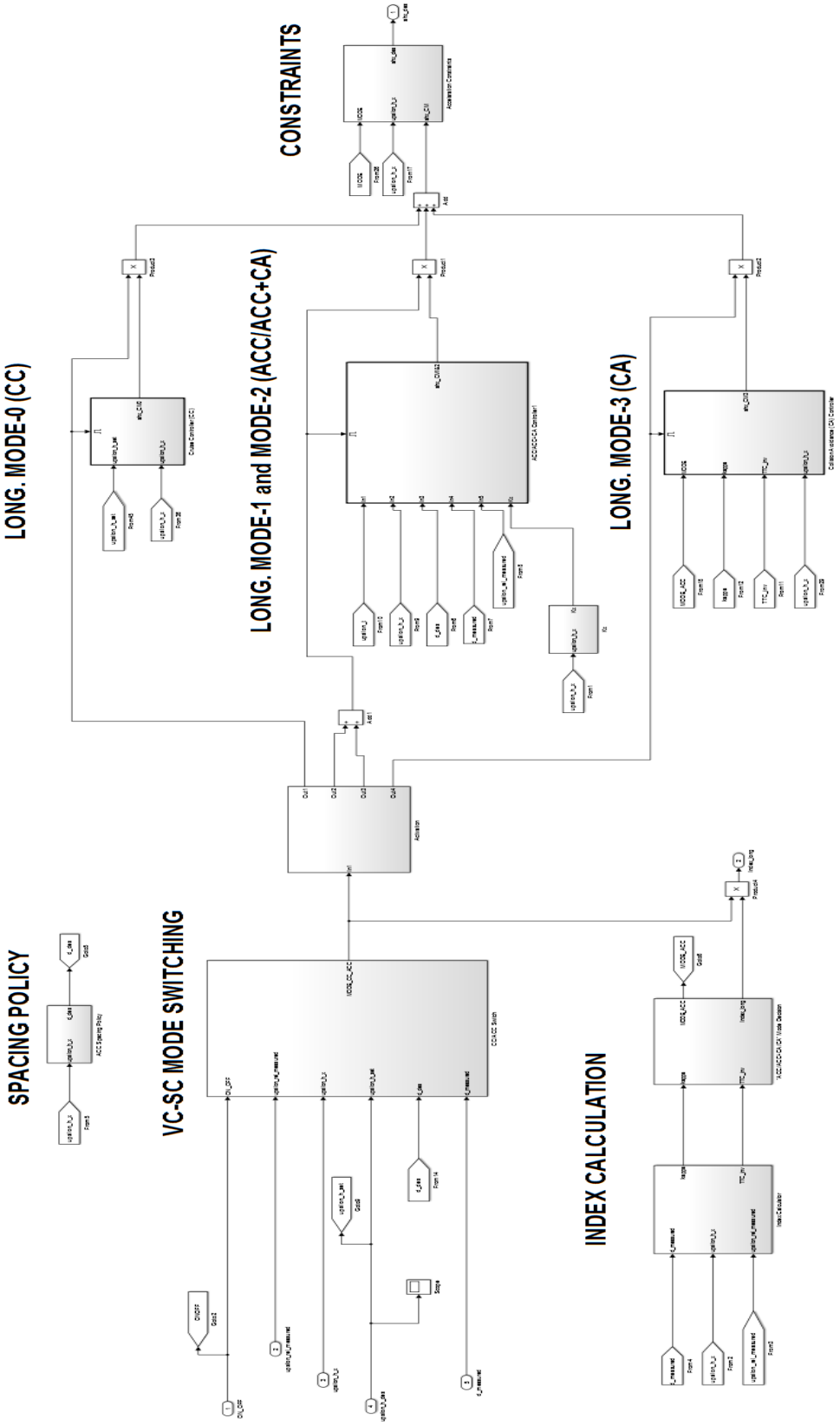

Figure B-2: Longitudinal upper-level controller

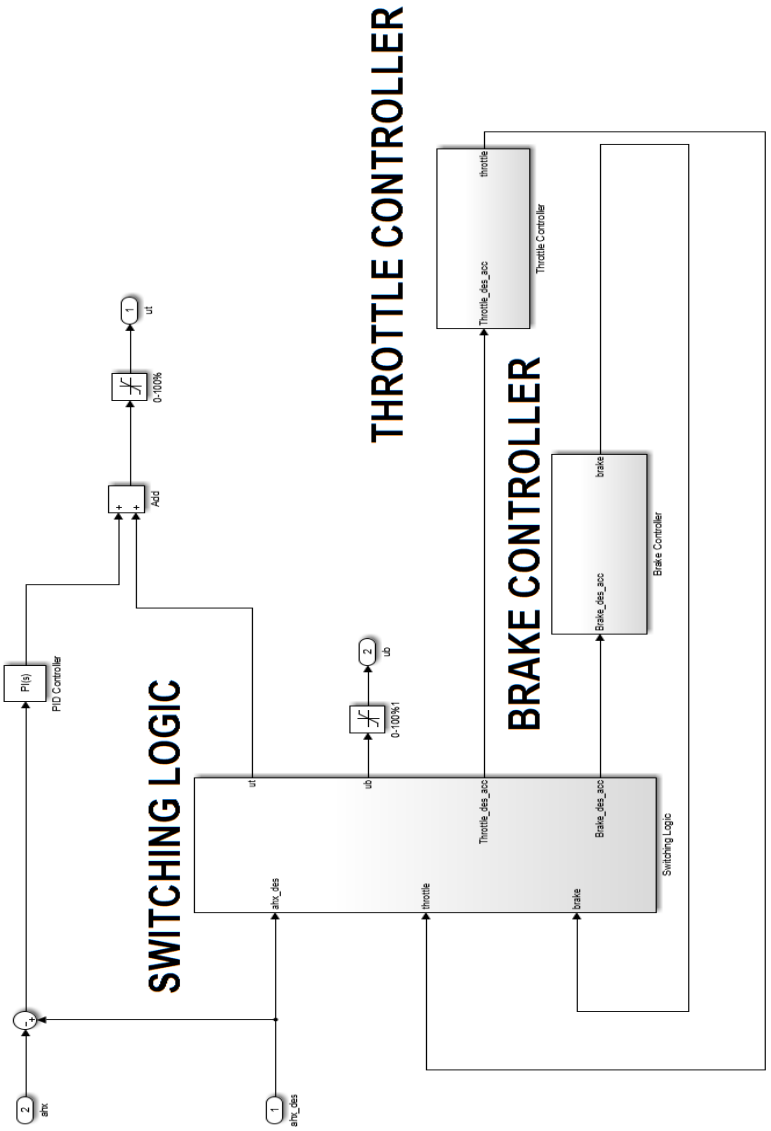

Figure B-3: Longitudinal low-level controller

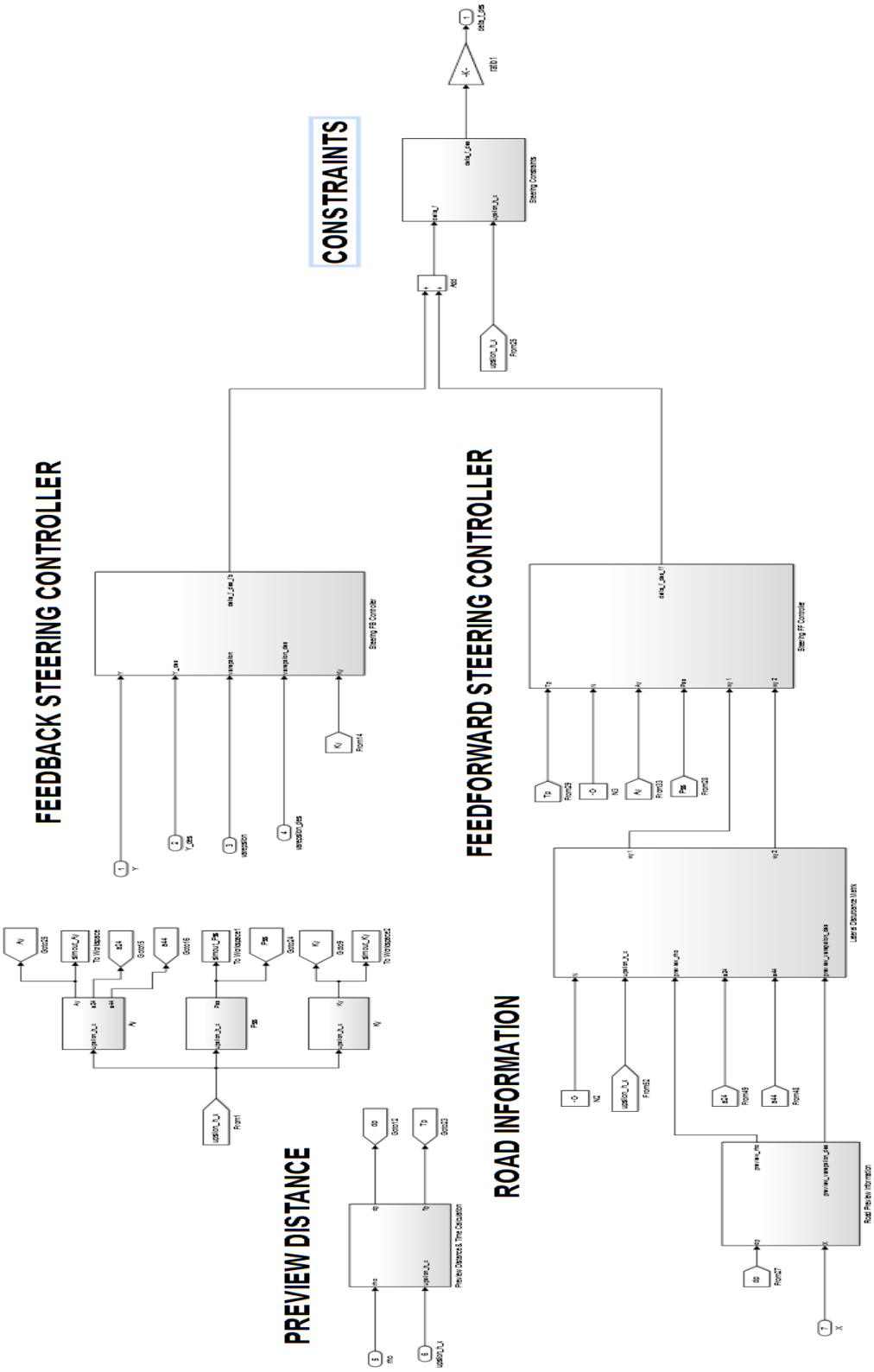

Figure B-4: Steering controller

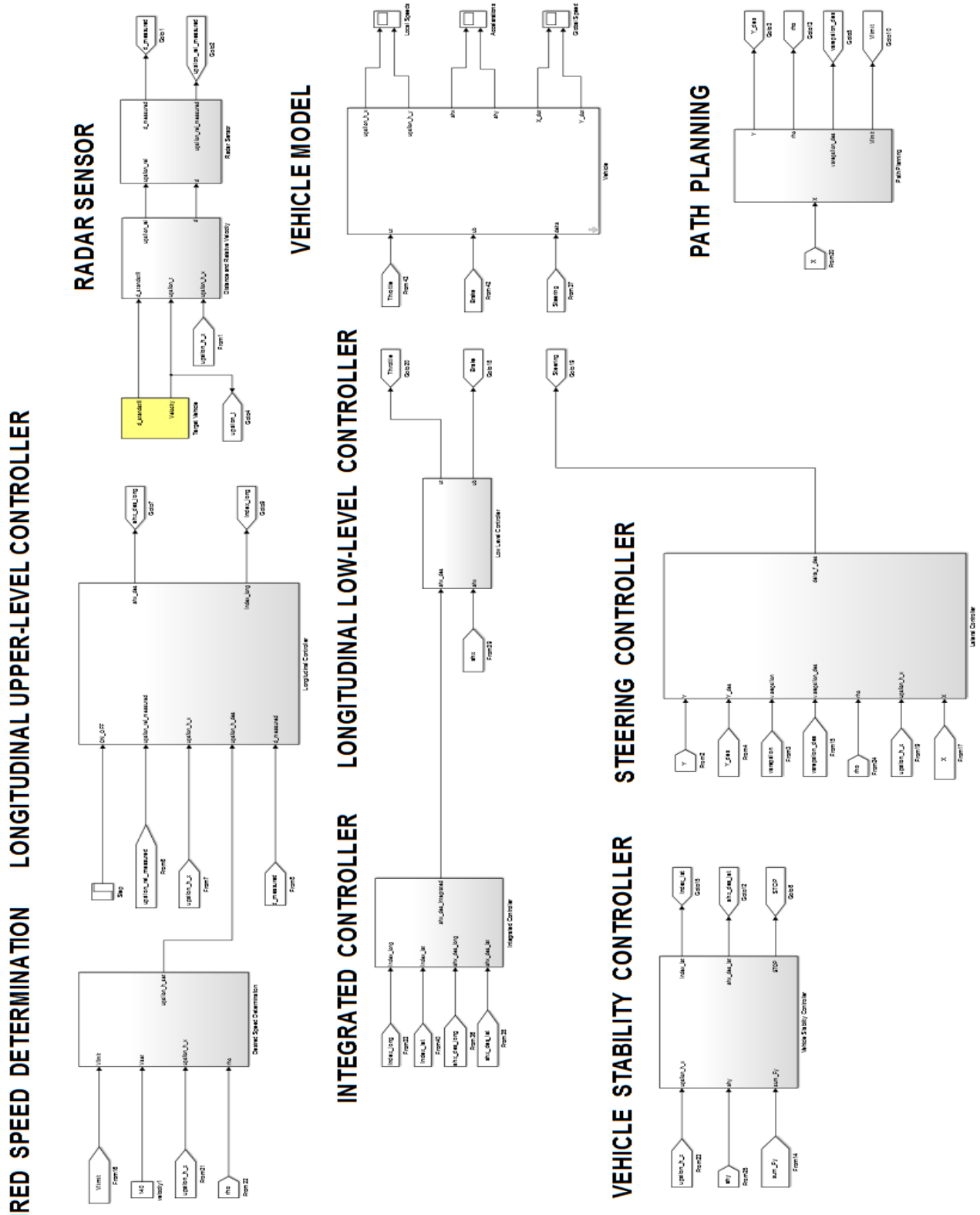

Figure B-5: Overall implementation with integrated controller

Bibliography

[1] R. Hoogendoorn, B. van Arem, R. Happee, M.M. Espinoza and D. Kotiadis, *Towards Safe and Efficient Driving through Vehicle Automation: The Dutch Automated Vehicle Initiative*, 2013.

[2] O. Gietelink, J. Ploeg, B. De Schutter, and M. Verhaegen, *Development of advanced driver assistance systems with vehicle hardware-in-the-loop simulations*, Vehicle System Dynamics, vol. 44, no. 7, pp. 569-590, 2006.

[3] J. Xu, K. Yang, Y.Shao, and G. Lu, *An Experimental Study on Lateral Acceleration of Cars in Different Environments in Sichuan, Southwest China*, Hindawi Publishing Corporation Discrete Dynamics in Nature and Society Volume 2015, Article ID 494130, 2014.

[4] P. Shakouri, A. Ordys, M. Askari, D. S. Laila, *Longitudinal vehicle dynamics using Simulink/Matlab*, 2008.

[5] A. Tautkus, *Lecture notes- Longitudinal and lateral dynamics*, 2011

[6] J. Kang, R.Y. Hindiyeh, S. Moon, J.C. Gerdes, K. Yi, *Design and Testing of a Controller for Autonomous Vehicle Path Tracking Using GPS/INS Sensors*, Proceedings of the 17th World Congress The International Federation of Automatic Control Seoul, Korea, July 6-11, 2008

[7] B. A. Guvenc and E. Kural, *A Low-Cost, Multiple-Driver-In-The-Loop Adaptive Cruise Control Simulator*, IEEE Control Systems Magazine, 2006.

[8] A. Katriniok, J.P. Maschuw, F. Christen, L. Eckstein and D. Abel, *Optimal Vehicle Dynamics Control for Combined Longitudinal and Lateral Autonomous Vehicle Guidance*, 2013 European Control Conference (ECC) July 17-19, 2013.

[9] F. Borrelli, P. Falcone, T. Keviczky, J. Asgari and D. Hrovat, *MPC-Based Approach to Active Steering for Autonomous Vehicle Systems*, 2005.

[10] B. Ganji, A. Z. Kouzani, S. Y. Khoo, M. Shams-Zahraei, *Adaptive cruise control of a HEV using sliding mode control*,Science Direct Expert Systems with Applications, 2013.

[11] M. Short, M.J. Pont and Q. Huang *Technical Report ESL 04-01 Simulation of Vehicle Longitudinal Dynamics*, 2004.

[12] E. Eyisi, Z. Zhang, X. Koutsoukos, J. Porter, G. Karsai, and J. Sztipanovits, *Model-Based Control Design and Integration of Cyberphysical Systems: An Adaptive Cruise Control Case Study* , Hindawi Publishing Corporation Journal of Control Science and Engineering Volume 2013, Article ID 678016, 2012.

[13] P. Shakouri, A. Ordys, *Nonlinear Model Predictive Control approach in design of Adaptive Cruise Control with automated switching to cruise control*, Science Direct Control Engineering Practice 26, 2014.

[14] J. G. Fernandez, *A Vehicle Dynamics Model for Driving Simulators*, Master's Thesis, Chalmers University of Technology, 2012

[15] R. T. O'Brien, P. A. Iglesias, and T. J. Urban, *Vehicle Lateral Control for Automated Highway Systems*, IEEE Transactions on Control Systems Technology, Vol. 4, No. 3, 1996.

[16] mathworks.com/help/simulink/examples/modeling-an-automatic-transmission-controller

[17] K Yi, S. Lee and Y. D. Kwon, *An investigation of intelligent cruise control laws for passenger vehicles*, 2000.

[18] R. Rajamani, *Vehicle Dynamics and Control*, 2006.

[19] D. Katzourakis, J.C.F. de Winter, S. de Groot, R. Happee, *Driving simulator parameterization using double-lane change steering metrics as recorded on five modern cars*, Science Direct Simulation Modelling Practice and Theory 26, 2012.

[20] G.J.L. Naus, J.Ploeg, M.J.G. Van de Molengraft, W.P.M.H. Heemels, M.Steinbuch, *Design and implementation of parameterized adaptive cruise control:An explicit model predictive control approach*, Science Direct Control Engineering Practice 18, 2010.

[21] S. Moona, I. Moon , K. Yi, *Design, tuning, and evaluation of a full-range adaptive cruise control system with collision avoidance*, Science Direct Control Engineering Practice 17, 2009.

[22] M. H. Lee, H. G. Park, S. H. Lee, K. S. Yoon, and K.S. Lee, *An Adaptive Cruise Control System for Autonomous Vehicles*, International Journal of Precision Engineering and Manufacturing Vol. 14, No. 3, pp. 373-380, 2013.

[23] P. Shakouri, J. Czeczot, and A. Ordys, *Adaptive Cruise Control System Using Balance-Based Adaptive Control Technique*, IEEE, 2012.

[24] A. Eliasson, *A controller for autonomous intelligent cruise control -a preliminary design*, IEEE Vehicle Navigation and Information Systems, 1992.

[25] P. Falcone, F. Borrelli, J. Asgariy, H. E. Tsengy, D. Hrovat, *A Model Predictive Control Approach for Combined Braking and Steering in Autonomous Vehicles*, 2007.

[26] E. Kreyszig, *Principal Normal, Curvature, Osculating Circle*, Differential Geometry, New York: Dover, pp. 34-36, 1991.

[27] D. Kim, S. Moon, J. Park, H.J. Kim and K. Yi, *Design of an Adaptive Cruise Control / Collision Avoidance with Lane Change Support for Vehicle Autonomous Driving*, ICROS-SICE International Joint Conference, 2009.

[28] K. Noh, D. Jung and H. Choi, and K. Yi, *Development of Ergonomic Driver Model Considering Human Factors*, 2007.

[29] H. Peng and M. Tomizuka, *Vehicle Lateral Control for Highway Automation*, 1990.

[30] W. Cho, H. Heo, K. Yi , S. Moon and C. Lee, *Design and Evaluation of an Integrated Vehicle Safety System for Longitudinal Safety and Lateral Stability*, 2009.

[31] F. Yu, D. Li, D.A. Crolla, *Integrated Vehicle Dynamics Control-State-of-the Art Review*, IEEE Vehicle Power and Propulsion Conference (VPPC), September 3-5, 2008.

[32] I. Bae, J. Moon, J. Cha, and S. Kim, *Integrated Lateral and Longitudinal Control System for Autonomous Vehicles*, IEEE 17th International Conference on Intelligent Transportation Systems (ITSC) October 8-11, 2014.

[33] D. Kim, J. Kang, and K. Yi, *Control Strategy for High-Speed Autonomous Driving in Structured Road*, 14th International IEEE Conference on Intelligent Transportation Systems, October 5-7, 2011.

[34] W. Cho, H. Heo, and K. Yi, *An Investigation into Unified Chassis Control for Agility, Maneuverability and Lateral stability*, 14th International IEEE Conference on Intelligent Transportation Systems, October 5-7, 2011.

[35] Anders Wikstrom, *Yaw Rate and Lateral Acceleration Sensor Plausibilisation in an Active Front Steering Vehicle*, Master's thesis, Linkopings Universitet, 2006.

[36] A.D.C. GmbH, *ARS 30XX Long Range Radar*, Data-sheet, Continental Corporation, 2009.

[37] Nicholas D. Smith, *Understanding Parameters Influencing Tire Modeling*, Colorado State University, Formula SAE Platform, 2004.

[38] A. S. Kilinc and T. Baybura, *Determination of Minimum Horizontal Curve Radius Used in the Design of Transportation Structures, Depending on the Limit Value of Comfort Criterion Lateral Jerk*, FIG Working Week, Rome, Italy, 2012.

[39] en.wikipedia.org/wiki/Speed_limits_by_country

Glossary

List of Acronyms

ADAS	Advanced Driver Assistance System
IVDC	Integrated Vehicle Dynamics Control
CC	Cruise Control
ACC	Adaptive Cruise Control
CA	Collision Avoidance
CW	Collision Warning
SG	Stop and Go
LKA	Lane Keeping Assist
VSC	Vehicle Stability Control
VC	Velocity Control
SC	Spacing Control
CoG	Center of Gravity
DOF	Degree of Freedom
TTC	Time to Collision

Nomenclature

F_C	Centripetal force
v_h	Absolute velocity of the host vehicle
m	Total mass of the vehicle
ρ	Radius of curvature
v_{h_x}, v_{h_y}	Longitudinal and lateral velocity of the host vehicle
g	Gravitational acceleration
μ	Friction coefficient
$v_{h,limit}$	The maximum allowable velocity of the host vehicle in curve
F_D	Drag force
v_{wind}	Wind speed
C_D	Drag factor
A_h	Area of vehicle frontal projection
ϱ	Atmospheric air density
F_g	Gravitational force
θ	Inclination/slope of the road
F_R	Rolling resistance force
C_R	Coefficient of rolling resistance
F_{z_f}, F_{z_r}	Front and rear vertical forces
l_f, l_r	Distances of front and rear wheel axle of the vehicle from center of gravity
L	Distance between the front and the rear wheel axle of the vehicle
h	Height of center of gravity
a_{h_x}, a_{h_y}	Longitudinal and lateral acceleration of the host vehicle
F_{x_f}, F_{x_r}	Longitudinal tire forces for front and rear wheels
F_{y_f}, F_{y_r}	Lateral tire forces for front and rear wheels
δ_f, δ_r	Front and rear wheel steering angles
I_z	Mass moment of inertia with respect to a vertical axis
M_z	Z-axis moment
ε	Yaw angle of the host vehicle
$\dot{\varepsilon}$	Yaw rate of the host vehicle
X, Y	Absolute vehicle position in inertial coordinates

α_f, α_r	Front and rear tire slip angle
υ_f, υ_r	Front and rear tire speed
$\upsilon_{x_f}, \upsilon_{y_f}$	Front tire speed along x-axis and y-axis
$\upsilon_{x_r}, \upsilon_{y_r}$	Rear tire speed along x-axis and y-axis
s_f, s_r	Front and rear wheel-slip ratio
r	Radius of wheels
ω_f, ω_r	Front and rear tire angular velocities
B_P, C_P, D_P, E_P	Coefficients of the Pacejka model
C_{y_f}, C_{y_r}	Cornering stiffnesses
C_s	Cornering stiffness coefficient
T_e	Engine torque
T_{ec}	Engine torque subject to control
τ_e	Engine lumped time lag
N_e	Engine speed
u_t	Throttle input
I_{ei}	Summation of engine and impeller moment of inertia
T_i	Impeller torque
C_{sr}, C_{tr}	Speed and torque ratios
K_{tc}	Capacity factor
N_i	Impeller speed
T_t	Turbine torque
N_t	Turbine angular velocity
T_{in}, T_{out}	Transmission input and output torques
N_{out}, N_{in}	Transmission output and input speeds
i_f	Final drive ratio
i_g	Current gear ratio
T_w	Wheel torque
P_{b_f}, P_{b_r}	Brake line pressures
K_{c_f}, K_{c_r}	Pressure gains
u_b	Brake input
τ_b	Brake system lumped time lag
T_{b_f}, T_{b_r}	Braking torques
K_{b_f}, K_{b_r}	Pressure/torque conversion constants
I_w	Moment of inertia of the wheels
$\dot{\omega}_f, \dot{\omega}_r$	Angular acceleration of the wheel
τ_δ	Steering actuator dynamic time constant
K_δ	Ratio of steering wheel to wheel
$\delta_{f_{des}}$	Desired wheel steering angle
δ_{SW}	Steering wheel angle
$d_{measured}$	Sensed distance between the host and target vehicles by the radar
$\upsilon_{rel,measured}$	Relative velocity measured between the host and target vehicles by the radar
τ_r	Radar model time constant
υ_{rel}	Relative velocity
d	Actual distance between vehicles
a_x, a_y	Longitudinal and lateral acceleration
P, P_s, P_c	Driver's desirable safe and comfortable settings
$a_{h_{x,des}}$	Desired longitudinal acceleration of the host vehicle

$v_{h,set}$	User-set velocity of the host vehicle
$v_{h,error}$	Velocity error of the host vehicle
K_P, K_D	Proportional and derivative control gains
d_{des}	Desired distance
d_{error}	Distance error
d_0	Desired distance at standstill
t_{hw}	Desired headway time
v_{t_x}	Velocity of the target vehicle
a_{t_x}	Longitudinal acceleration of target vehicle
v_{t_x}	Longitudinal velocity of target vehicle
x_t	Displacement of target vehicle
x_h	Displacement of the host vehicle
κ	Warning index
d_{brc}	Braking-critical distance
d_{wc}	Warning-critical distance
τ_s	System delay
τ_h	Delay in human response
χ_x	Longitudinal states for the host and target vehicles
A_x, B_x, Γ_x	Longitudinal state-space matrices
w_x	Longitudinal disturbance
J_x	Longitudinal cost function
Q_x, R_x	Longitudinal weighting matrices
K_x	Longitudinal state-feedback gain
P_x	Longitudinal steady-state solution of the Riccati equation
W_1, W_2	Weighting factors
$a_{h,min}$	Minimum acceleration
h_b	Boundary layer
$T_{e,des}$	Desired engine net torque
$T_{b,des}$	Desired brake torque
Υ	Curvature
ϕ	Tangential angle
s	Arc length
y_r	Lateral position error
C_{path}	Centerline of the desired path
ε_d	Desired yaw angle
$\dot{\varepsilon}_d$	Desired yaw rate
A_y, B_y, Γ_y	Lateral state-space matrices
w_y	Lateral disturbance
χ_y	Lateral states for the host vehicle
J_y	Lateral cost function
Q_y, R_y	Lateral weighting matrices
P_y	Lateral steady-state solution of the Riccati equation
K_y	Lateral optimal state-feedback gain
d_p	Preview distance
T_p	Preview time
λ	Lagrange multiplier
H	Feed-Forward control term
M	Finite preview control term

$v_{h,comfort}$	Velocity of the host vehicle in the terms of comfort
$a_{h_{y,des}}$	Desired lateral acceleration of the host vehicle
$v_{h,des}$	Desired velocity of the host vehicle
$I_{longitudinal}$	Longitudinal index
$I_{lateral}$	Lateral index
β	Vehicle body side slip angle
a_{ymax}	Maximum value of lateral acceleration